NUCLEAR STRUCTURE OF ^{70}Ga

NUCLEAR STRUCTURE OF ^{70}Ga

By

DONALD ALBERT DOHAN, B.Sc., M.Sc.

A Thesis
Submitted to the School of Graduate Studies
in Partial Fulfilment of the Requirements
for the Degree
Doctor of Philosophy

McMaster University
July 1972

DOCTOR OF PHILOSOPHY (1972)
(Physics)

McMASTER UNIVERSITY
Hamilton, Ontario

TITLE: Nuclear Structure of ^{70}Ga

AUTHOR: Donald Albert Dohan, B.Sc., M.Sc. (Manitoba)

SUPERVISOR: Professor R. G. Summers-Gill

NUMBER OF PAGES: ix, 134

SCOPE AND CONTENTS:

The nuclear properties of ^{70}Ga have been investigated by several methods. High resolution studies of the reactions ^{69}Ga(d,p)^{70}Ga and ^{71}Ga(d,t)^{70}Ga show that 7 levels exist below 1 MeV excitation, with a large gap of 508 keV separating the first two. Between 1 and 2 MeV, 42 additional levels are observed. Parities and spectroscopic factors for the low lying levels were extracted by DWBA analysis of the proton and triton angular distributions.

Electromagnetic decay properties of the levels of ^{70}Ga were investigated by means of the ^{70}Zn(p,nγ)^{70}Ga reaction. Gamma ray angular distribution and linear polarization measurements were used to elucidate spins of low lying levels and mixing ratios of the transitions. Gamma-ray yields as a function of energy are shown to depend markedly on the spin of the level, in agreement with Hauser-Feshbach calculations for the (p,n) cross section. Analysis of the decay of the low lying levels indicates the existence of remarkably few E1 transitions.

A theoretical calculation of the energy levels of ^{70}Ga is presented in the light of the shell model. Both the zero range and surface delta interactions were used as the residual interaction between the nucleons. The surface delta interaction is shown to reproduce the energy levels much better than the zero range force, but fails to predict the large energy gap between the first two levels.

ACKNOWLEDGEMENTS

A great number of people have been instrumental in making this work possible. I would especially like to thank the following:

Professor R.G. Summers-Gill, my supervisor, for his insight, technique, and thoroughness,

The other members of my Supervisory Committee, Professors D.G. Burke and G.L. Keech for their interest and support,

Hamish Robertson, for his companionship and perception,

Professor J.A. Kuehner for his approach to physics,

Past and present members of the group, Konrad Aniol, Sherali Hussein, Aquila Islam, Malcolm Macphail, Tony Pierce, Terry Taylor, and Jim Waddington, for their help during long accelerator nights.

Brian Cook and Geoff Frank, comrades to the nineteenth hole, and Aadu Pilt, a good sparring partner,

Jack Tippett for his concept of physics,

Phil Ashbaugh and the staff of the Tandem Accelerator,

Mrs. Helen Kennelly, for her efforts in typing this thesis,

And the National Research Council of Canada, who supported the research financially through grants to the group.

To my wife Marge

TABLE OF CONTENTS

LIST OF FIGURES

LIST OF TABLES

INTRODUCTION

The continuing effort by physicists to understand the diverse properties of nuclei has involved the utilization of many, highly sophisticated, experimental techniques. Of particular value in this effort is the study of nuclei with odd numbers of protons and neutrons. Whereas the energy levels of even-even nuclei are mainly determined by the pairing interaction, in which pairs of nuclei are coupled to $J = 0$, and $T = 1$; odd-odd nuclei are more sensitive to the nucleon-nucleon interaction for $J > 0$, $T = 1$ and for $T = 0$.

Because of the much higher density of states, odd-odd nuclei have been more difficult to study experimentally. Aided by recent advances in experimental technique and by the development of sophisticated computer programs for performing complex theoretical calculations, researchers have begun to investigate odd-odd nuclei in the s-d shell, and more recently, in the f-p shell.

This work is an experimental study of the structure of ^{70}Ga. Situated well into the f-p shell, with 3 protons and 11 neutrons outside the ^{56}Ni core occupying the $p_{3/2}$, $f_{5/2}$, $p_{1/2}$ and $g_{9/2}$ orbits, this nucleus provides a test for shell model predictions further away from closed shells.

When this work was initiated the known data on ^{70}Ga were few. Morozov et al (1959) and Glagolev et al (1959) had attributed to ^{70}Ga a 20 ms isomer which de-excited with a $\sim$ 180 keV γ-ray. This identification was later confirmed by Meyers and Schats (1966). Rester et al (1966) had observed conversion electrons corresponding to a 188 keV transition and used a NaI detector to detect gamma rays following the reaction $^{70}Zn(p,n)^{70}Ga$. They placed levels at 0.188, 0.448, 1.03 and 1.66 MeV. Since ^{70}Ga is located between two stable isobars, it has not been studied by β-decay.

In order to enlarge upon this information, this investigation was undertaken. The first study, to determine the locations, parities, and spectroscopic factors of the levels, used the $^{69}Ga(d,p)^{70}Ga$ reaction. This was followed by an investigation of the $^{71}Ga(d,t)^{70}Ga$ reaction to see if additional levels would be populated.

In order to learn about the electromagnetic transitions that occur between the levels in ^{70}Ga, an in-beam study of the $^{70}Zn(p,n\gamma)^{70}Ga$ was undertaken. Gamma-rays were placed in the decay scheme with the aid of singles data, excitation functions and coincidence measurements described in Chapter III. During the course of these investigations, several other studies of ^{70}Ga were published. These include the results of the $^{69}Ga(n,\gamma)^{70}Ga$ experiments of Vervier and Bolotin (1971) and of Linusson et al (1970). These experiments, and the neutron time-of-flight measurements in the $^{70}Zn(p,n)^{70}Ga$

reaction by Finckh et al (1970) and Tanaka et al (1970) essentially agreed on the locations of levels in ^{70}Ga. Studies of the decay of levels in ^{70}Ga include the work of Linusson et al (1970) who measured the low energy γ-ray spectrum from ^{69}Ga$(n,\gamma)^{70}$Ga, and Arnell et al (1970) who studied γ-rays produced in the ^{70}Zn(p,n) ^{70}Ga, ^{67}Zn$(\alpha,p)^{70}$Ga and ^{69}Ga(d,p) ^{70}Ga reactions. It should also be pointed out that preliminary accounts of the present work have already been reported at two conferences (Dohan and Summers-Gill 1970, 1972).

In spite of all these data which establish the levels up to $\sim$ 2MeV, there was still a need for definite spin information. Accordingly, the angular distributions of many of the γ-rays were determined, as well as the linear polarization of two of the γ-rays. These measurements are also described in Chapter III.

As the information on ^{70}Ga accumulated, the interpretation of the levels became increasingly a challenge. For clarity, however, all of these considerations are deferred to Chapter IV.

CHAPTER I

NUCLEAR THEORY

1.1 Nuclear Shell Theory

1.1a The Individual Particle Model

One of the main objectives of the study of nuclear physics is the understanding of the structure of nuclei. Mathematically, the complete description of nuclear structure is contained in the correct total wave functions of the nucleus, which consists of A strongly interacting particles or nucleons. The exact form for the nucleon-nucleon interaction is not known, however. Even if the mutual interactions are completely specified, there is no exact solution to the quantum mechanical many body problem. The progress made so far in understanding many features of nuclear structure has been due to the use of models. Among these, the shell model, or more precisely, the individual particle model, has been very successful in explaining and predicting a vast amount of experimental data.

Shell models are characterized by the assumption that each member of a system of interacting particles moves, almost independently of the others, in its own closed orbit. To a first approximation, the interaction of any nucleon with the rest of the nucleus is described by an average single particle potential U(r). Following Goeppert Mayer (1948, 1949) and Haxel, Jensen and Suess (1948, 1949), the mean potential is a sum of central and spin-orbit terms.

$$U = U(r) + \xi \, \vec{\ell} \cdot \vec{s} \; .$$

The Hamiltonian of this independent particle version of the shell model is thus

$$\mathcal{H}_o = \sum_{i=1}^{A} H_o(i)$$

$$H_o(i) = T_i + U_i$$

where T_i and U_i are the kinetic and potential energies of the i^{th} nucleon and the sum embraces all A constitutents of the nucleus.

The shape and depth of U(r) and the strength of the spin-orbit potential can now be adjusted in such a way that the spectrum of $\mathcal{H}_o$ reproduces the observed single particle level systematics. In practice, for a given nucleus, a harmonic oscillator well is assumed with the well parameter chosen to produce agreement with the r.m.s. radius of the nucleus. The eigenfunctions of $\mathcal{H}_o$ constitute a complete set $\{\psi^{n\ell jm}\}$ of single particle states, each characterized by its principal quantum number n, orbital quantum number ℓ, and total spin quantum number j with z-projection m. Within the identical nucleon framework, or the isospin formalism, each nucleon is assigned an additional quantum number t, known as the isospin, with z component t_z, which is related to the charge of the nucleon:

$$\text{charge} = (\frac{1}{2} - t_z)e \quad .$$

Nuclear ground states in the independent particle model are made by filling single particle levels in accordance with the Pauli principle and in order of increasing energy. Wave functions for the system are then Slater determinants of the A single particle functions. In the extreme single particle model of an odd mass nucleus, all but one of the nucleons are paired off to form an inert core. There is only one active nucleon, and it alone determines the spin and electromagnetic moments of the nucleus in the ground state.

1.1b Configuration Mixing

To discuss any other properties of the nucleus, more than one valence nucleon must be given an active role. In order to keep the problem tractable, however, only a few nucleons can be liberated from the inert core and these valence nucleons can be allowed to enter only a few of the available orbits. In any given physical situation most of the basic single particle states are assumed to be completely filled or completely empty. Thus in a shell model calculation a few 'active' nucleons populate a small number of single particle orbits around the Fermi surface of the nucleus.

The active nucleons in this treatment are not truly independent. The shell model Hamiltonian must be extended to allow a residual two-body interaction between nucleons;

$$H = H_o + \sum_{i<j}^{A} v_{ij} \ .$$

The calculation is then carried out in three stages. First, a complete set of antisymmetric wavefunctions is constructed for n valence nucleons in a finite number of single particle orbits. Each such wavefunction has a definite value of angular momentum J and isospin T, formed by vector coupling the individual j's and t's of the nucleons (de Shalit and Talmi, 1963). Second, the matrix of the Hamiltonian operator is computed in this basis. One important property of this basis is that any matrix element

$$H_{pq} = \langle\psi_p|\Sigma v_{ij}|\psi_q\rangle$$

in the Hamiltonian matrix reduces to two-body matrix elements only, and that ψ_p and ψ_q can differ in the quantum numbers of, at most, two particles. This is because v_{ij} can only act on the co-ordinates of particles i and j, and all others must integrate out. Third, the energy matrix is diagonalized, yielding eigenvalues which correspond to the allowed energies of the system, and eigenvectors or wavefunctions which may be used to compute moments and transition rates. This entire operation necessarily starts with an act of truncation, and the main focus of attention in shell model physics then is on the realistic application of approximation techniques. A more detailed account of the mechanics of shell model calculations, based on the second quantized formalism of French is described in the excellent review article (French et al, 1969).

1.1c Residual Interaction

To obtain the two-body matrix elements of the effective Hamiltonian operator, three methods are used most often at present. One of these methods involves the calculation of the two-body matrix elements from free nucleon-nucleon interactions by reaction matrix methods. Most calculations of this type in the literature (eg. Kuo and Brown 1966, 1967) are aimed at obtaining the effective interaction for two particles (or two holes) outside an inert core. Important renormalization effects arising from relatively low-lying core excitations are taken into account in these calculations. These effects, such as core polarization, effectively change the single particle orbits in which the nucleons move, thereby changing their interaction with the other valence nucleons. Such calculations do not, however, take into account effects due to partially filled shells, and hence are not usually applicable for nuclei further away from closed shells.

A second popular method of obtaining effective interactions is to treat the two-body matrix elements as free parameters (Talmi 1962, Glaudemans et al 1964), these being determined so as to give a best fit between calculated eigenvalues and observed level energies. Within the scope of the ^{70}Ga problem, there are 120 two-body matrix elements, far more than the number of known energy levels, spins, and parities in this region to accurately determine such a large number of parameters.

For nuclei not near closed shells, it is necessary to resort to the third method, which is to perform a model calculation for the interaction. The interaction is treated as a phenomenological quantity whose parameters are determined by optimizing the correlation between experimental data and theory. An example of a model interaction which has been used extensively in the past is the zero-range force with spin exchange:

$$v_{ij} = -V_o\{\alpha + (1-\alpha)\ \bar{\sigma}_i\cdot\bar{\sigma}_j\}\delta(\vec{r}_i-\vec{r}_j)$$

where V_o is the strength of the interaction and α determines the spin exchange component.

Another interaction which has recently enjoyed considerable success in the s-d shell and for nuclei with 82 neutrons (eg. Halbert et al, 1971) is the surface delta interaction (SDI). This interaction,

$$V_{ij}^{SDI} = -4\pi\ A_T\ \delta(\Omega_{ij})\delta(r_i-R)\delta(r_j-R)$$

where Ω_{ij} is the angle between the radius vectors of the interacting pair and R is the nuclear radius, represents the simplest density dependent interaction and has received qualitative theoretical justification (Glaudemans 1970). In this model, the interaction takes place only if both nucleons are at the same place on the nuclear surface . The 4π is introduced for convenience. It is assumed that the single particle radial wavefunctions of the active shells have the same absolute value at the nuclear surface; that is, v_{ij} does not depend on ℓ (Arvieu and Moszkowski 1966). The interaction strength A_T depends only on the isospin of the interacting pair. Direct calculation of the matrix elements yields:

$$<j_a j_b|v_{ij}^{SDI}|j_c j_d>_{J,T} =$$

$$\frac{A_T}{2(2J+1)}\left[\frac{(2j_a+1)(2j_b+1)(2j_c+1)(2j_d+1)}{(1+\delta_{ab})(1+\delta_{cd})}\right]^{1/2}$$

$$[(-1)^{\ell_a+\ell_c+j_b+j_d} <j_a\ \tfrac{1}{2}\ j_b -\tfrac{1}{2}|J0><j_c\ \tfrac{1}{2}\ j_d\ -\tfrac{1}{2}|J0>\{1+(-1)^{\ell_c+\ell_d+J+T}\}$$

$$-<j_a\ \tfrac{1}{2}\ j_b\ \tfrac{1}{2}|J1><j_c\ \tfrac{1}{2}\ j_d\ \tfrac{1}{2}\ J1>\{1+(-1)^T\}]$$

1.1d Nuclear Isospin

Throughout this discussion it is assumed the basis set of multi-particle wavefunctions ψ_{JT} can be characterized by the quantum numbers J and T. The quantum number J (total angular momentum) follows from the invariance of the nuclear system under rotations. The goodness of the quantum number T implies an invariance under rotation in T space, which corresponds to a change in the charge of a given A nucleon system. This implies that a mathematical description of a nucleus should apply for all isobars of the nucleus. From nucleon-nucleon interaction data it is found that the nuclear interaction between nucleons is very nearly charge independent. However, the proton also has a charge so that in nuclear systems protons arrange themselves in a shell structure slightly different from that of neutrons. The most important part of the Coulomb interaction is the isovector part (Soper 1969, Glaudemans 1970). For nuclei with N=Z, the isospin mixing in the ground state caused by such a potential rises to about 2% in ^{40}Ca, and would continue to rise. Stable nuclei, however develop a neutron excess beyond this point which acts to prevent further increase in the impurity. Under these influences the admixture actually drops with increasing A, to about 1% in ^{208}Pb.

In this work it is assumed that isospin mixing is small and that in fact wavefunctions for ^{70}Ga can be characterized with the quantum T. Only the lowest possible T is considered (T=4) since the T=5 states are expected to lie much higher in energy.

1.2 Direct Nuclear Reactions

In a nuclear reaction, as the incident projectile, or nucleon, enters the nucleus, it feels the nuclear force field of the other A nucleons. In the ensuing collisions between the target nucleons and the projectiles, the distribution of energy among them is determined by the free nucleon-nucleon interactions and by the nuclear density, which in effect determines the single-particle potential seen by the projectile. The projectile can collide with a target nucleon and excite it above the Fermi sea, thereby producing a compound state. Two alternatives are now possible: at least one of the nucleons (or group of nucleons) has energy greater than its separation energy, or neither has. In the former case, the nucleon(s) may leave the nucleus without further interaction. This is generally referred to as a direct reaction,which is primarily a surface phenomenon, and which occurs within a time interval which is comparable to the transit time of the projectile over a distance equal to a nuclear diameter. The motion of the incident and emitted nucleons is highly correlated. In the case in which none of the nucleons has energy greater than that required for separation, each nucleon will undergo further collisions,gradually spreading its excitation energy over the entire nucleus. A state of statistical equilibrium is reached in the configuration involved in this energy sharing. A certain fraction of the state consists of configurations in which sufficient energy is concentrated on one (or more) nucleons so that it may escape from the nucleus. A process such as this takes place on a much longer time scale and is called a compound nucleus reaction, which will be discussed in more detail in the next section.

In the shell model description of a nucleus, the properties of the low lying levels are determined by the interactions between the valence nucleons which occupy a relatively small configuration space. The active particles in adjacent nuclei occupy the same model space and therefore the properties of the low lying levels of these nuclei are expected to be related. Direct reactions, wherein the coordinates of only a small number of nucleons are affected can therefore be used to study similarities and correlations between the nuclear properties of neighbouring nuclei. The reactions studied in this work are of the class of single nucleon transfer reactions, in particular the neutron stripping and pickup reactions, (d,p) and (d,t).

Let us consider for the moment, the stripping reaction

$$A + a \rightarrow B + b$$

where $A + x = B$, $a = b + x$, and x is the stripped nucleon. The cross section for a direct reaction of this type separates naturally into two parts. One of these is a measure of the probability that the nucleons in the initial state will find themselves in an arrangement corresponding to the final state. This "spectroscopic factor" depends only on the wavefunctions of the nuclear states involved and provides a useful basis for comparison between experiment and theory. The second factor measures the probability that, when the overlap above occurs, the reaction actually takes place. This factor contains the interaction strength and the usual kinematical and phase space factors.

The cross section for the reaction can be expressed as

$$\sigma_{exp}(\theta) = \frac{2J_B+1}{2J_A+1}\,\sigma^{(\theta)}_{KIN}\,\langle T_A T_{Az}\,\tfrac{1}{2}\,t_z|T_B T_{Bz}\rangle^2\,S$$

In this equation, $2J_B+1$ and $2J_A+1$ are statistical factors (the cross section is averaged over initial and summed over final magnetic sub-states), σ_{KIN} is the theoretical kinematical cross section, $\langle T_A T_{Az}\,\frac{1}{2}\,t_z|T_B T_{Bz}\rangle^2$ is the isospin Clebsch-Gordan coefficient which determines the probability that the isospin of the stripped nucleon will couple to the initial isospin to produce T_B, the isospin of the final state.

The spectroscopic factor S is the overlap between the initial and final states

$$S = [\langle\psi_A \otimes \psi_{\substack{\text{Transferred}\\ \text{particle}}}|\psi_B\rangle^2$$

where ψ_A and ψ_B are the wavefunctions of the target and residual nuclei, respectively. The $\otimes$ indicates that the wavefunction of the transferred particle is vector coupled to the target wavefunction. The wavefunctions ψ_B can be expressed in terms of a complete set of (A+1)-nucleon basis wavefunctions

$$\psi_B = \sum_q b_q\,\psi^q_{J_B M_B}\,.$$

Each of these in turn can be expressed in terms of the complete set of A-nucleon wavefunctions, ψ_{JM}, vector coupled to a single nucleon wavefunction with orbital and total angular momenta ℓ and j:

$$\psi^q_{J_B M_B} = \sum_{\substack{J,M\\ r,p,j}} \alpha_{qpr}\langle JjMM_B-M|J_B M_B\rangle\psi^p_{JM}\phi^r_{j,M_B-M}\,.$$

In the summation over terms involving ϕ_j^r, j embraces the values of angular momentum corresponding to those of the active shells (de Shalit and Talmi, 1963). It is found experimentally that the differential cross section for the transfer of a nucleon with angular momenta ℓ and j exhibits a pattern which is characteristic of the orbital angular momentum of the nucleon but nearly independent of j.

The cross section for the stripping reaction A(d,p)B, corresponding to the transfer of a neutron with orbital angular momentum ℓ, in which the i^{th} state of spin J_B is populated, is then

$$\sigma^{\ell}_{\text{stripping}}(i,\theta)=1.53\left(\frac{\sigma^{\ell j}_{DW}}{2j+1}\right)C^2\left[\frac{2J_B+1}{2J_A+1}\sum_{j=\ell-\frac{1}{2}}^{\ell+\frac{1}{2}} S_{\ell j}(i,J_B)\right] .$$

The quantity 1.53 is a normalization constant peculiar to the (d,p) reaction (Bassel 1966). For the (d,t) reaction this constant is 3.37. The theoretical cross section, $\left(\frac{\sigma^{\ell j}_{DW}}{2j+1}\right)$, is calculated in the distorted wave Born approximation (DWBA) and is nearly independent of j. Details of this calculation are given in a number of works (Satchler 1964, 1965 and Robertson 1971). Several computer programs have been written to calculate DWBA cross sections, and that used for the present work (called DWUCK) originated at the University of Colorado and was supplied to McMaster University through the kindness of Dr. P. D. Kunz.

For the (d,p) reaction, the isospin coupling coefficient

$C^2 = 1$ since the addition of a neutron with $t_z = \frac{1}{2}$ to a nucleus with $T_0 = T_{0z}$ can only make states with $T = T_0 + \frac{1}{2}$.

The quantity in the square brackets which is derived from the experimental cross section is commonly called the "strength". It obeys the sum rules (Robertson and Summers-Gill, 1971)

$$\sum_{i,J_B} [\sum_j S_{\ell j}(i,J_B) \frac{2J_B+1}{2J_A+1}] = N_\ell^h \quad \text{(stripping)}$$

where N_ℓ^h represents the number of neutron holes of type ℓ in the target. If the wavefunctions of the levels of the resultant nucleus can be described well by the coupling of an ℓ,j neutron to the target configuration, then the summed spectroscopic factor for levels of a given J_B

$$\sum_i S_{\ell j}(i,J_B) = S_{\ell j}(J_B)$$

is the same for all spins J_B. The strengths then have the familiar $2J_B+1$ dependence.

For the pickup reaction, A(d,t)B, the principle of detailed balance may be applied to the above formalism. The cross section becomes

$$\sigma^\ell_{\text{pickup}}(i,\theta) = 3.37(\frac{\sigma^{\ell j}_{DW}}{2j+1})C^2[\sum_{j=\ell-\frac{1}{2}}^{\ell+\frac{1}{2}} S_{\ell j}\ (i,J_B)].$$

The sum rule obeyed by the strengths is then

$$\sum_{i,J_B} [\sum_j S_{\ell j}\ (i,J_B)] = N_\ell \quad \text{(pickup)}$$

where N_ℓ represents the number of neutrons in the target in the shell with orbital angular momentum ℓ. In this expression there appears to be no explicit $2J_B+1$ dependence. The reason is that the quantity $S_{\ell j}$ defined previously is a stripping spectroscopic factor. The relevant stripping reaction in the present case corresponds to stripping to an odd nucleus from an odd-odd nucleus. The $2J_B+1$ factor is still present, but concealed in the expression for the spectroscopic factor. Under the simplifying assumptions made above, this $2J_B+1$ dependence is then

$$\sum_i S_{\ell j}(i, J_B) = \frac{2J_B+1}{(2J_A+1)(2j+1)} N_\ell \qquad \text{(pickup)}.$$

When the neutrons are not in the lowest seniority states, significant deviations from the $(2J_B+1)$ rule can occur.

1.3 Electromagnetic Transitions in Nuclei

1.3a Transition Rates

The theory of electromagnetic interactions in nuclei is well documented in the literature. Only needed results are quoted here.

The two types of transitions that occur in nuclei, electric and magnetic, are related to the distributions of nuclear charge and currents respectively. The probability of emission per unit time of a γ quantum of energy $\hbar\omega$ and multipolarity L, projection M, (Blatt and Weisskopf 1952) is

$$T^{\pi}_{(L,M)} = \frac{4(L+1)}{L[(2L+1)!!]^2} \frac{k^{2L+1}}{\hbar} |\langle f|\Omega_L^{M\pi}|i\rangle|^2$$

Here $k = \frac{\omega}{c} = \frac{E_\gamma(\mathrm{MeV})}{197} 10^{13}\ \mathrm{cm}^{-1}$ is the wave number. The quantity

$$|\langle f|\Omega_L^{M\pi}|i\rangle|^2$$

is the reduced transition rate between states $|i\rangle$ and $|f\rangle$, and can usefully be described in the isospin formalism. The operator $\Omega_M^{L\pi}$, of multipolarity L and parity $(-1)^\pi$ (π=0 for electric transitions, 1 for magnetic transitions) can be expanded as

$$\Omega_M^{L\pi} = S_M^{L\pi}\cdot \underline{\underline{I}} - V_M^{L\pi}\cdot \tau_o{}^1$$

where $S_M^{L\pi}$ = isoscalar part

$V_M^{L\pi}$ = isovector part

$\underline{\underline{I}}$ = identity operator

(tensorial rank zero).

$\tau_o{}^1 = \tau_3$ = the charge operator

(tensorial rank one and projection zero). The operators S and V operate in J-space while $\underline{\underline{I}}$ and τ_3 operate in T-space.

For electric transitions, these operators are related to the distribution of charge in the nucleus:

$$S_M^{L0} = \sum_{i=1}^{A} \frac{e_p(i)+(-)e_n(i)}{2} r_i{}^L Y_M{}^L(\hat{r})$$

where e_p and e_n are the charges of the proton and neutron respectively. For the electric isovector part, V_M^{L0}, the negative sign is used in the above equation.

The operators for magnetic transitions depend on the g-factors of the neutrons (g_n) and protons (g_p):

$$S_M^{L1} = \sum_{i=1}^{A} [\nabla r_i^L Y_M^L(r_i)] \cdot \{ (g_p^\ell(i) + (-) g_n^\ell(i)) \frac{2\vec{\ell}_i}{L+1} + (g_p^s(i) + (-) g_n^s(i)) \vec{s}_i \} \frac{e\hbar}{2M_p C} .$$

The superscripts ℓ and s on the g factors indicate whether it is the orbital or spin angular momentum, respectively, which is involved. For the isovector magnetic operator, V_M^{L1}, the negative signs in the above equation are used.

Both the neutrons and protons through nuclear interaction affect the charge and current distributions in the core. For this reason, in the refined theory, the operators $S_M^{L\pi}$ and $V_M^{L\pi}$ contain "effective" values for the charge and g factors for the neutrons and protons.

From the form of these operators, it can be seen that an electric 2^ℓ-pole corresponds to a spherical harmonic of order ℓ and a magnetic 2^ℓ-pole to a spherical harmonic of order ℓ-1 multiplied by the operator μ_ℓ, which in itself carries unit angular momentum. Thus any 2^ℓ-pole carries orbital angular momentum ℓ in units of $\hbar$. However, the parity of an ℓ^{th} order spherical harmonic is $(-1)^\ell$, while that of μ_ℓ, which is an axial vector, is even. Thus, an electric 2^ℓ-pole has parity $(-1)^\ell$ while a magnetic one has parity $(-1)^{\ell-1}$ so that electric and magnetic multipole transitions of the same order cannot interfere with one another.

The dependence of the transition probability on the initial and final spins J_i and J_f may be separated out by means of the Wigner-Eckhart theorem. If all the magnetic substates M_i are populated equally, then the reduced transition probability, commonly referred to as B(L), is found by taking the average over initial states and the sum over possible final magnetic sub-states M_f for the transition. The final result is

$$B(L) = \frac{1}{(2J_i+1)(2T_f+1)} [\langle J_f T_f ||| S^L \underline{\underline{I}} ||| J_i T_i \rangle \delta_{T_i T_f}$$

$$- \langle T_i T_{iz} 1, 0 | T_f T_{fz} \rangle \langle J_f T_f ||| V^L \tau_o^1 ||| J_i T_i \rangle]^2 .$$

The triple bar indicates that the matrix element is reduced in isospin space as well as spin space. From the reduced matrix elements it is seen that the limitations on the multipole order L for a given transition $J_1 \rightarrow J_2$ are

$$|J_1 - J_2| \leq L \leq J_1 + J_2 \ .$$

Selection rules may also be imposed on the allowed values of T. For the isoscalar part

$$\Delta T = 0 \ .$$

For the isovector part

$$\Delta T = 0, \text{ or } 1$$

but not

$$T = 0 \rightarrow T = 0.$$

Further, if $\Delta T = 0$, then the Clebsch-Gordon coefficient becomes

$$\frac{T_z}{\sqrt{T(T+1)}}$$

so that $\Delta T = 0$ can occur only for $T_z \neq 0$.

The width $\Gamma(L)$ of a state is related to the transition probability $T(L)$ by the uncertainty relation

$$\Delta E \ \Delta t \simeq \hbar .$$

Thus

$$\Gamma(L) = \frac{8\pi(L+1)}{L[(2L+1)!!]^2} k^{2L+1} B(L).$$

1.3b Weisskopf Units

The Weisskopf units or estimates give a crude idea about the expected magnitude for the width of a transition. Actual widths are usually expressed as multiples of these estimates. The estimates are based on a simple model which assumes that

1) The nucleus consists of an inert core and one proton.
2) The final state has $\ell=0$, the initial $\ell=L$.
3) The spin wave functions are not changed in the transition.
4) The radial parts of the initial and final wave functions are both given by

$$U(r) = \text{constant} \quad (r < R)$$
$$U(r) = 0 \quad (r > R)$$

With $R = 1.2\ A^{1/3}$, the Weisskopf width may be expressed as a function of E_γ(MeV) and A for the different multipolarities:

$$\Gamma_W(E1) = 6.8\times10^{-2}\ A^{2/3}\ E^3\ \text{eV}$$
$$\Gamma_W(E2) = 4.9\times10^{-8}\ A^{4/3}\ E^5\ \text{eV}$$

$$\Gamma_W(M1) = 2.1\times10^{-2} \quad E^3 \text{ eV}$$
$$\Gamma_W(M2) = 1.5\times10^{-8} A^{2/3} E^5 \text{ eV} .$$

From these estimates it can be seen that transitions of the same type diminish rapidly with L, so that it is usually sufficient to consider the lowest L of each type. Furthermore, M(L) and E(L+1) transitions are competitive, whereas E(L) and M(L+1) transitions are not.

1.3c Gamma Ray Angular Distributions

Rose and Brink (1967) have developed the theory of the angular distribution of γ-rays emitted from aligned states. A summary is given here, in which their formalism is adopted.

Consider the reaction A(a,b)B*, where neither the target nucleus A nor the beam of particles a is polarized. The axis of quantization is defined along the beam direction. The residual nucleus B*, in an excited state $|J,m\rangle$ with definite parity is said to be aligned if the population parameters $P(m_1)$ for the ensemble satisfy the relation

$$P(m_1) = P(-m_1)$$

and

$$P(m_1) \neq \frac{1}{2J_1+1} .$$

Here $P(m)$ is the probability that the m^{th} substate is populated, and $\sum_{m=-J}^{J} P(m) = 1$. If all $P(m) = \frac{1}{2J+1}$ then there is no preferred axis and the decay of the nucleus B^* will be isotropic.

Consider the state $|J_1m_1\rangle$ decaying to a state $|J_2m_2\rangle$. If q defines the circular polarization ($q = \pm 1$) and $\vec{k}$ is the wave vector of the gamma ray, the probability amplitude for such a transition may be represented by

$$A^q_{m_1m_2}(\vec{k}) = -\sqrt{\frac{k}{\hbar}} \sum_{LM\pi} q^\pi \langle J_1m_1|T^{L\pi}_M|J_2m_2\rangle D^L_{Mq}(R)$$

where $D^L_{Mq}(R)$ is the rotation matrix which takes the beam axis Z into the direction $\vec{k}$. $T^{L\pi}_M$ is defined in the previous section.

If the orientation of the spin J_2 of the final state is not observed, then the probability of transition from the state $|J_1m_1\rangle$ to any substate of J_2 by the emission of a photon is

$$\sum_{m_2} |A^q_{m_1m_2}(\vec{k})|^2 .$$

The total transition probability is then equal to the sum of the above weighted according to the relative population of each initial substate $|J_1m_1\rangle$:

$$\sum_{m_1} P(m_1) \sum_{m_2} |A^q_{m_1m_2}(\vec{k})|^2.$$

Evaluating this expression by the techniques of Racah algebra yields, for the angular distribution of circularly polarized gamma rays,

$$W(\theta, J_1 \to J_2; q) = \frac{k}{\hbar} \sum_{\substack{KLL' \\ \pi\pi'}} B_K(J_1) P_K(\cos\theta)$$

$$\cdot (-1)^{q+J_1-J_2+L'-L-K} \sqrt{2J_1+1} \langle LL'q-q|K0\rangle$$

$$\cdot W(J_1J_1LL';KJ_2) q^{\pi+\pi'} \langle J_1||T^{L\pi}||J_2\rangle \langle J_1||T^{L'\pi'}||J_2\rangle$$

in which

$$B_K(J_1) = \sum_{m_1} P(m_1)(-1)^{J_1-m_1}\sqrt{2J_1+1}\ \langle J_1 m_1 J_1 -m_1 | K0\rangle .$$

In the summation, assuming $L' \geq L$, K is limited to the even integer $\leq$ min $(2L', 2J_1)$ because of the Racah coefficient and the assumption that $P(m_1) = P(-m_1)$.

As shown in the previous section, it is sufficient to consider the lowest two multipole orders L and L'. The multipole mixing ratio is then defined as

$$\delta = \frac{\langle J_1 || T^{L'\pi'} || J_2\rangle}{\langle J_1 || T^{L\pi} || J_2\rangle} \ \frac{2L'+1}{2L+1} \ ; \quad L' = L+1 \quad .$$

If polarization is not observed, then the incoherent sum over the circular polarization index q is taken, and the angular distribution formula is then

$$W(\theta) = \sum_K A_K\, P_K(\cos\theta)$$

where

$$A_K = B_K(J_1)\ \frac{R_K(LLJ_1J_2) + 2\delta R_K(LL'J_1J_2) + \delta^2 R_K(L'L'J_1J_2)}{1+\delta^2}$$

and

$$R_K(LL'J_1J_2) = (-1)^{1+J_1-J_2+L'-L-K}\sqrt{(2J_1+1)(2L+1)(2L'+1)}$$

$$\cdot\ \langle L1L'-1|K0\rangle\ W(J_1J_1LL';KJ_2) \ .$$

In this expression, $B_K(J_1)$ contains all the information on the alignment of the initial state $|J_1 m_1\rangle$. The R_K terms depend specifically on the geometry of the $J_1 \to J_2$ cascade and are tabulated for spins $\leq$ 10 by Rose and Brink. The internal nuclear properties appear through the mixing ratio δ.

Since A_o is proportional to the intensity of the γ-ray, it is customary to quote the normalized angular distribution coefficients

$$a_2 = A_2/A_o$$

$$a_4 = A_4/A_o \ .$$

Experimentally, a finite detector is used to measure $W(\theta)$, and hence the theoretical distribution must be averaged over the subtended solid angle. For a cylindrical detector, the effect is that the $P_K(\cos\theta)$ are replaced by $Q_K P_K(\cos\theta)$. The coefficients $Q_K (Q_o=1)$ have been tabulated for standard size detectors (Smith 1962).

Angular distributions may also be attenuated by extra-nuclear perturbations. If the excited nuclear state lives for a significant length of time, the population parameters at the moment of decay are not the same as those which were applicable when the excitation was produced. In effect, the nuclei are subject to torques due to the interaction of either the magnetic dipole moment μ with an extra-nuclear magnetic field B, or the electric quadrupole moment Q with electric field gradients $\frac{\partial^2 V}{\partial x^2}$, $\frac{\partial^2 V}{\partial y^2}$ and $\frac{\partial^2 V}{\partial z^2}$. If the external fields are not static then it is more appropriate to think of the interactions causing transitions among the magnetic substates m_I. When the fields are randomly oriented, the effect on the angular distribution can be expressed by replacing A_K by $G_K A_K$. The theory is summarized and formulae for the G_K are given by Frauenfelder and Steffen (1964). The magnitude of the interaction and the nuclear lifetime are parameters in the theory.

The magnetic and electric interaction between the nucleus and its environment has been studied in a variety of experimental conditions. The attenuation coefficients G_K for most of these experiments are in satisfactory agreement with theory.

1.3d Linear Polarization of Gamma Rays

As described in the previous section, the probability of emission of a γ-ray with circular polarization q and wave vector $\vec{k}$ from a state $|J_1 m_1>$ to a state with spin J_2 is proportional to

$$\sum_{m_2} |A^{q}_{m_1 m_2} (\vec{k})|^2$$

If the linear polarization of the γ-ray is measured, one must take a coherent superposition of the $q = \pm 1$ terms. Thus

$$\sum_{m_2} \left| \frac{A^{q=-1}_{m_1 m_2} + (-)\, A^{q=+1}_{m_1 m_2}}{\sqrt{2}} \right|^2$$

describes the emission of linearly polarized photons with the plane of polarization perpendicular (parallel) to the x direction as shown in the following diagram:

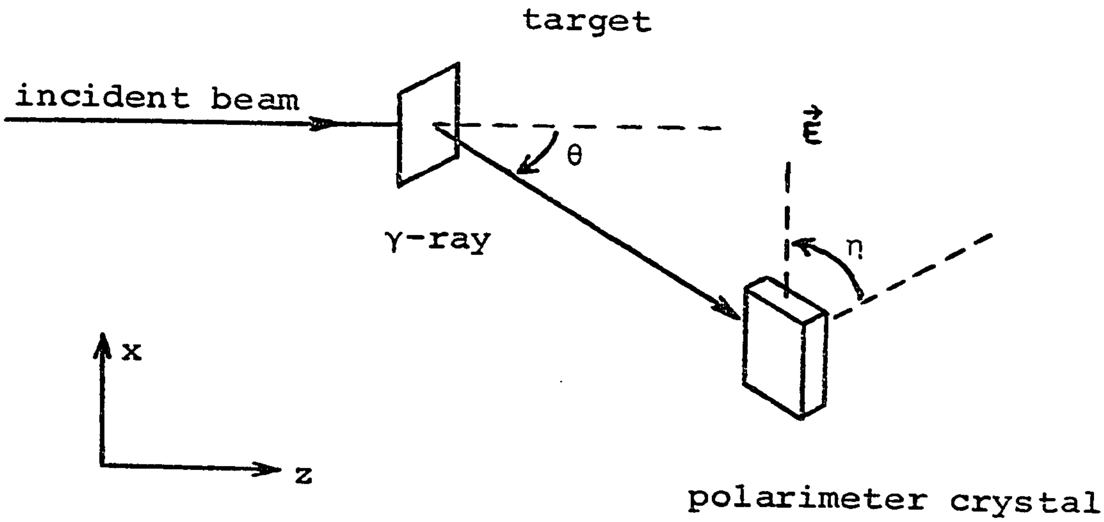

Following Poletti et al (1967) we define the probability of emission of a γ-ray as $W(\theta,\eta)$ where θ is the angle of emission and η is the angle which the electric vector makes with plane defined by the beam and the emitted γ-ray. It is then customary to define the degree of polarization at an angle θ by

$$P(\theta) = \frac{W(\theta,\eta=0°)-W(\theta,\eta=90°)}{W(\theta,\eta=0°)+W(\theta,\eta=90°)} .$$

Specific expressions may be written down for $P(\theta)$. For a mixed quadrupole/dipole transition

$$P(\theta) = \pm \frac{\frac{1}{2}(a_2+b_2)P_2^{(2)}(\cos\theta) - \frac{1}{12} a_4 P_4^{(2)} \cos(\theta)]}{1 + a_2P_2(\cos\theta)+a_4P_4(\cos\theta)} .$$

The plus sign is to be taken for E2/M1 mixtures, the minus sign for M2/E1 mixtures. In this equation,

$$b_2 = \frac{8a_2\ \delta\ R_2(12\ J_1J_2)}{3[R_2(11\ J_1J_2)+2\delta R_2(12\ J_1J_2)+\delta^2 R_2(22\ J_1J_2)]}$$

and $P_K^{(2)}$ are associated Legendre functions. The quantities $R_K(LL'J_1J_2)$, δ, and a_K were defined in the previous section.

For any spin sequence $J_1 \rightarrow J_2$ there are, in general, two values of the mixing ratio δ for which the denominator in the expression for b_2 vanishes. Since the same geometrical factor is also contained in a_2, the resulting indeterminate form is then better expressed as

$$b_2 = \frac{8}{3} \sum_{m_1} P(m_1)\rho_2(J_1m_1)R_2(12\ J_1J_2)\ \frac{\delta}{1+\delta^2}\ .$$

The statistical tensor coefficients $\rho_K(J_1m_1)$ are tabulated by Rose and Brink (1967). It is important to note that even if $a_2 = a_4 = 0$, the polarization may be non-zero, depending on the specific substate populations.

CHAPTER II

DIRECT NUCLEAR REACTION STUDIES

2.1 Introduction

The nucleus ^{70}Ga, with 31 protons and 39 neutrons, lies well into the f-p shell. Treating ^{56}Ni as a closed core, the 3 active protons and 11 active neutrons occupy the $2p_{3/2}$, $1f_{5/2}$, $2p_{1/2}$, $1g_{9/2}$ and, at higher excitation, the $2d_{5/2}$ and $3s_{1/2}$ orbits. In the simplest picture of lowest seniority, states in ^{70}Ga are then formed by coupling the last odd proton and neutron.

The known information on the level structure of ^{70}Ga at the start of this investigation was very sparse. In order to locate levels in ^{70}Ga, and to obtain structural information about these levels, a study was made of the neutron transfer reactions, ^{69}Ga(d,p)^{70}Ga and ^{71}Ga(d,t)^{70}Ga. Both ^{69}Ga and ^{71}Ga have even numbers of neutrons, while the 3 protons in each of these targets couple to spin 3/2, with negative parity. The neutrons in these transfer reactions can therefore take on ℓ-values of 1, 3, or 4 at low excitation. States in ^{70}Ga will in general be populated with mixtures of ℓ-values of the same parity .

2.2 The $^{69}Ga(d,p)^{70}Ga$ Experiment

Targets of Ga_2O_3 enriched to 99.8% in ^{69}Ga were prepared by vacuum evaporation onto backings of 30 μg cm^{-2} carbon. Target thicknesses varied between 10 and 30 μg cm^{-2}.

In the $^{69}Ga(d,p)^{70}Ga$ experiments 10 MeV deuterons from the McMaster University FN tandem accelerator were used. The protons were momentum analyzed in an Enge split-pole magnetic spectrograph (Spencer and Enge 1967) and detected with 50 micron thick photographic emulsions* placed in the focal plane of the spectrograph. A .020" thick aluminum foil was placed over the emulsion to absorb all other particles with the same magnetic rigidity as the protons (in particular, the inelastic deuterons from the target and backing materials). This has the additional advantage that the proton energies are reduced, resulting in denser tracks in the emulsion. Since the photographic plates are located outside the magnetic field of the spectrograph this energy degradation does not affect the position of the protons.

A proton spectrum taken at 30° is shown in Figure 2.1. Spectra such as this one are obtained by scanning the photographic plates under a microscope and counting the number of tracks in 1/4 mm. strips, which for the proton exposures corresponds to approximately 3.4 keV. The dispersion of the

---

*KODAK NTB-50 Nuclear Emulsions

Figure 2.1

Experimental proton spectrum from $^{69}Ga(d,p)^{70}Ga$ taken with E_d = 10 MeV.

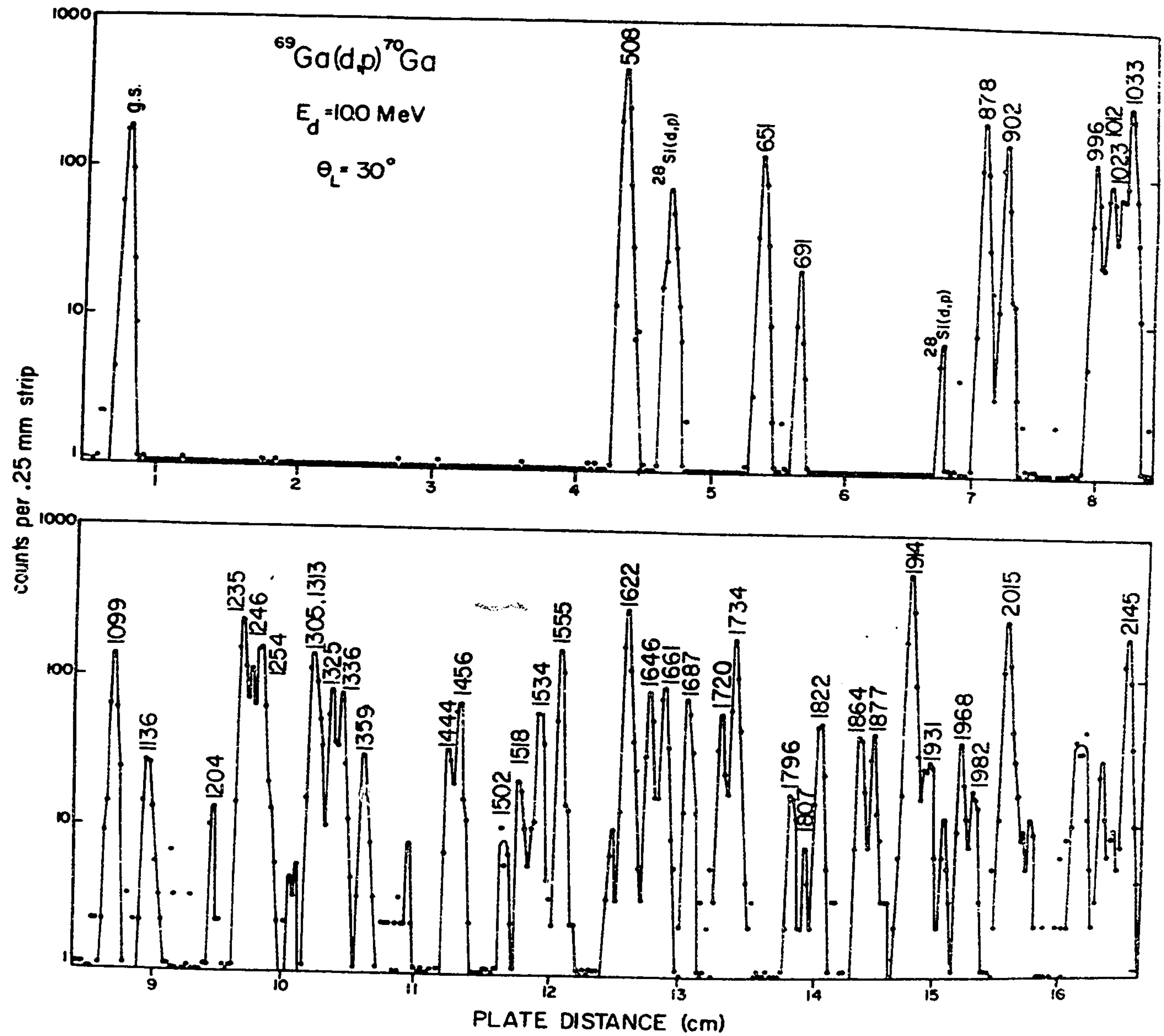

$^{69}Ga(d,p)^{70}Ga$
E_d = 10.0 MeV
θ_L = 30°
counts per .25 mm strip
PLATE DISTANCE (cm)
g.s.
508
$^{28}Si(d,p)$
651
691
878
902
996
1012
1023
1033
1099
1136
1204
1235
1246
1254
1305, 1313
1325
1336
1359
1444
1456
1502
1518
1534
1555
1622
1646
1661
1687
1720
1734
1796
1807
1822
1864
1877
1914
1931
1968
1982
2015
2145

magnet had been previously established (Burke 1969) by measurements of the positions of alpha groups of known energies from a ThC' source, for various field settings. Excitation energies in ^{70}Ga were then obtained by measuring the positions of peaks relative to the edge of the photographic plate. Because the location of the plate within the spectrograph is uncertain, energies were determined relative to the ground state, and no attempt was made to measure the ground state Q value of the reactions which is known to be 5.418±.007 MeV (Mattauch et al 1965). Energies were obtained with the Enge at five different angles in which the energy resolution varied from 7-11 keV. The average energies obtained in this way are listed in Table 2.1. The errors are based on the reproducibility, and are calculated such that each independent measurement agrees, within the quoted error, with the average value. The proton energies are in good agreement with the energies obtained independently in the (n,γ) and (p,n) experiments recently carried out at other laboratories.

The γ-ray measurements of Arnell et al (1971) and work to be described in the next chapter indicate that closely spaced levels exist at 1009.6 and 1015.1 keV. This prompted a re-examination of the plates in the region from 990-1040 keV using a finer scan width (1/8 mm). This region of the proton spectra, obtained at lab angles of 15° and 35°, is shown in Fig. 2.2. In each of these spectra, it can be seen that the peak in the region of 1012 keV is noticeably broader than the

Table 2.1

Energy Levels in ^{70}Ga

^{69}Ga(n,γ)		^{70}Zn(p,n)		^{69}Ga(d,p)	^{71}Ga(d,t)	^{70}Zn(p,nγ)
Ref. 1	Ref. 2	Ref. 3	Ref. 4	This Work*		
0	0	0	0	0	0	0
507	508	509	508	508(1)	507(1)	508.1(3)
652	651	651	651	651(1)	649(2)	651.1(2)
692	691	692	692	691(2)		690.9(2)
		877		878(3)	876(2)	878.5(4)
		902	900	902(1)	899(2)	901.3(4)
995	996	995	1000	996(2)	995(2)	995.7(2)
		1012		1010(2)	1010(2)	1009.7(3)
				1015(3)	1014(2)	1015.1(3)
1022	1025	1024	1020	1023(3)	1023(2)	1024.1(3)
				1033(2)	1035(4)	1033.2(4)
				1099(4)	1098(4)	1101.6(3)
		1138	1137	1136(4)	1138(4)	1135.4(2)
1141	1141					1140.4(2)
1202	1204	1203	1205	1204(4)	1202(3)	1203.5(2)
				1235(4)	1231(3)	1234 (2)
		1245	1248	1246(4)		1244.5(2)
1250				1254(3)	1250(4)	1252.8(5)
1260	1264	1260	1261	1262(4)	1262(4)	1263.2(2)
						1286.5(5)
1305				1305(4)	1306(2)	1306.8(3)
1310	1309		1312	1313(4)	1313(4)	1311.9(2)
				1325(3)		1325.9(3)
			1336	1336(3)		1336.6(4)
1358	1361		1360	1359(3)	1357(3)	1359.9(5)
1412	1414	1414	1415			1413.0(3)
1444	1447	1446		1444(3)	1443(4)	1445.9(2)
1455	1457	1457	1453	1456(4)	1455(2)	1454.7(2)
		1503		1502(4)	1498(4)	1502.0(2)
1516	1519	1518	1521	1518(4)	1517(2)	1518.3(2)
1531	1535	1535		1534(3)	1532(2)	1533.0(2)
1553	1555	1556	1560	1555(3)	1554(3)	1552.8(2)
		1598				
1620		1620		1622(2)	1620(3)	1621.0(2)
1631		1633	1635			1633.4(2)
				1646(2)		1646.1(6)
				1661(2)		
1690	1692	1694	1694	1687(3)		
1718				1720(3)	1718(3)	1720.2(3)
1724	1725	1726				1725.0(6)
1733		1738	1734	1734(3)†		
					1734(3)	
1792		1795	1800	1796(3)	1793(3)	1794.2(2)
		1809		1807(4)	1805(3)	1808.0(2)

(continued next page)

Table 2.1 (continued)

^{69}Ga(n,γ) Ref. 1	^{69}Ga(n,γ) Ref. 2	^{70}Zn(p,n) Ref. 3	^{70}Zn(p,n) Ref. 4	^{69}Ga(d,p)	^{71}Ga(d,t) This Work*	^{70}Zn(p,nγ)
1822		1827	1830	1822(2) †		1824.1(6)
					1823(3)	
1844						
1864		1870	1867	1864(3)	1865(3)	1864.7(4)
				1877(3)		
1904					1906(3)	1905.5(5)
		1912	1912	1914(2)		
1928				1931(4)	1928(3)	1931(1)
1935		1936	1935		1937(3)	
1968		1971		1968(3)	1968(2)	
1982		1984		1982(4)		1981.9(9)
2014		2019		2015(2)	2012(4)	

* The numbers in the parentheses in this and the other tables indicate the uncertainty in the last digit.

Ref. 1 Vervier and Bolotin (1971). The uncertainties were typically 1-2 keV.

Ref. 2 Linusson et al. (1969). The uncertainties were typically 2-3 keV.

Ref. 3 Tanaka et al (1970). The uncertainties were typcially 3-4 keV.

Ref. 4 Finckh et al (1970). The uncertainties were typcially 5-10 keV.

† There are two levels at 1734 keV (and also at ∿1822 keV) with opposite parities as revealed by the (d,p) and (d,t) angular distributions.

Figure 2.2

Proton and triton spectra from $^{69}Ga(d,p)^{70}Ga$ and $^{71}Ga(d,t)^{70}Ga$ in the region from 990 - 1040 keV. For these, the plates were scanned in 1/8 mm. strips. The peak due to the 508 keV level is shown on the left for comparison purposes. The dotted lines indicate the expected level positions from the $^{70}Zn(p,n\gamma)^{70}Ga$ reaction. One division on the ordinate corresponds to 50 counts per scan.

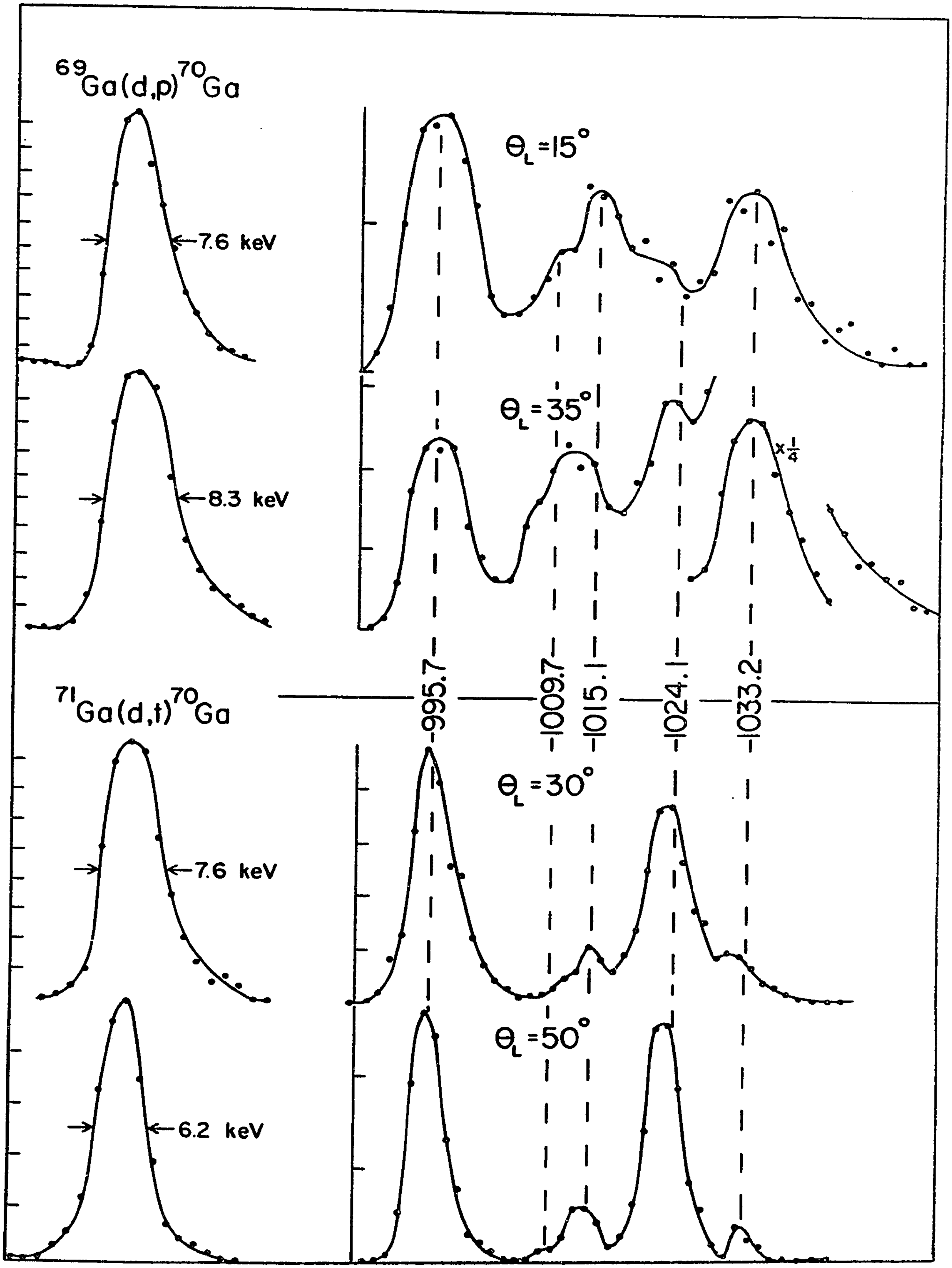

$^{69}Ga(d,p)^{70}Ga$
7.6 keV
8.3 keV
$\Theta_L=15°$
$\Theta_L=35°$
x 1/4
995.7
1009.7
1015.1
1024.1
1033.2
$^{71}Ga(d,t)^{70}Ga$
7.6 keV
6.2 keV
$\Theta_L=30°$
$\Theta_L=50°$

neighbouring peaks (e.g. 995.7 keV), supporting the existence of two levels rather than just one.

For the proton angular distribution, data were taken at laboratory angles ranging from 10 to 90 degrees in 5 degree steps at the smaller angles and in 10 degree steps beyond 50 degrees. The exposures were initially monitored with a Faraday cup and a Si(Li) counter at 90° detecting elastically scattered deuterons. Due to the short lifetime of the counters, however, the Faraday cup alone was used subsequently. Effects due to target non-uniformity were shown to be less than 10%, which is the uncertainty adopted in the relative normalization. The experimental proton angular distributions are shown in Fig. 2.3. Absolute values of the cross sections were obtained by the method described in section 2.4.

Only two impurities were identified in the spectra. The ^{13}C in the backing produced a very broad peak (due to the fact that the plates were not in the correct focal plane for such a light target). In addition, two peaks due to $^{28}Si(d,p)^{29}Si$ (corresponding to the levels at 1.28 and 2.03 MeV in ^{29}Si) were observed at several angles. A check of the expected positions for other levels in ^{29}Si and in ^{30}Si and ^{31}Si showed that they would not make significant contributions at any angle.

2.3 The $^{71}Ga(d,t)^{70}Ga$ Experiment

Targets of Ga_2O_3 enriched to 99.6% in ^{71}Ga were prepared by vacuum evaporation onto backings of 30 μgm cm^{-2} carbon.

Figure 2.3

Proton angular distributions from $^{69}Ga(d,p)\ ^{70}Ga$. The solid curves are admixtures of empirical line shapes of von Ehrenstein and Schiffer (1967), least squares fitted to the data. The dotted lines on the unfitted distributions are included to guide the eye.

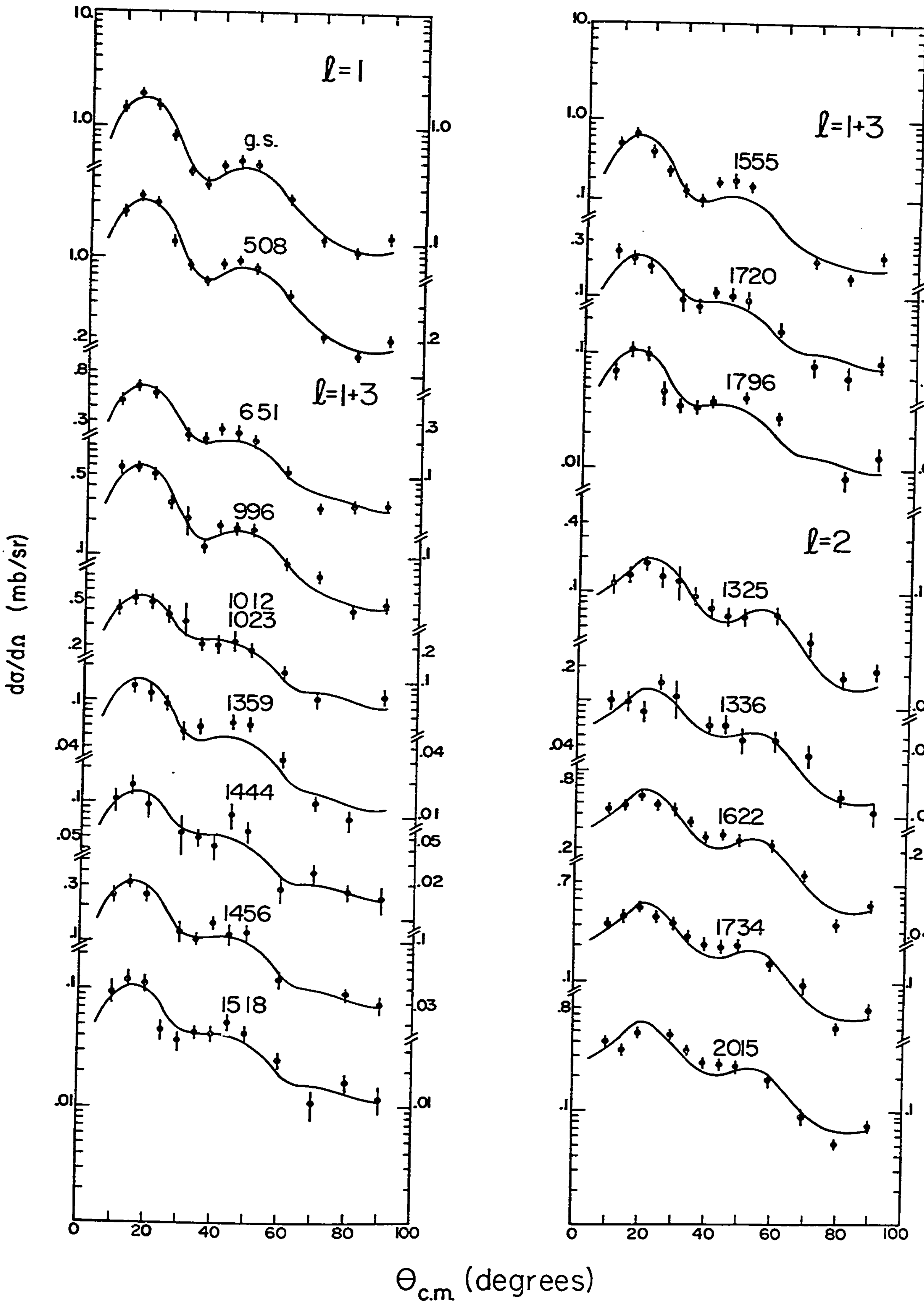

ℓ=1
g.s.
508
ℓ=1+3
651
996
1012
1023
1359
1444
1456
1518
ℓ=1+3
1555
1720
1796
ℓ=2
1325
1336
1622
1734
2015
dσ/dΩ (mb/sr)
Θc.m. (degrees)

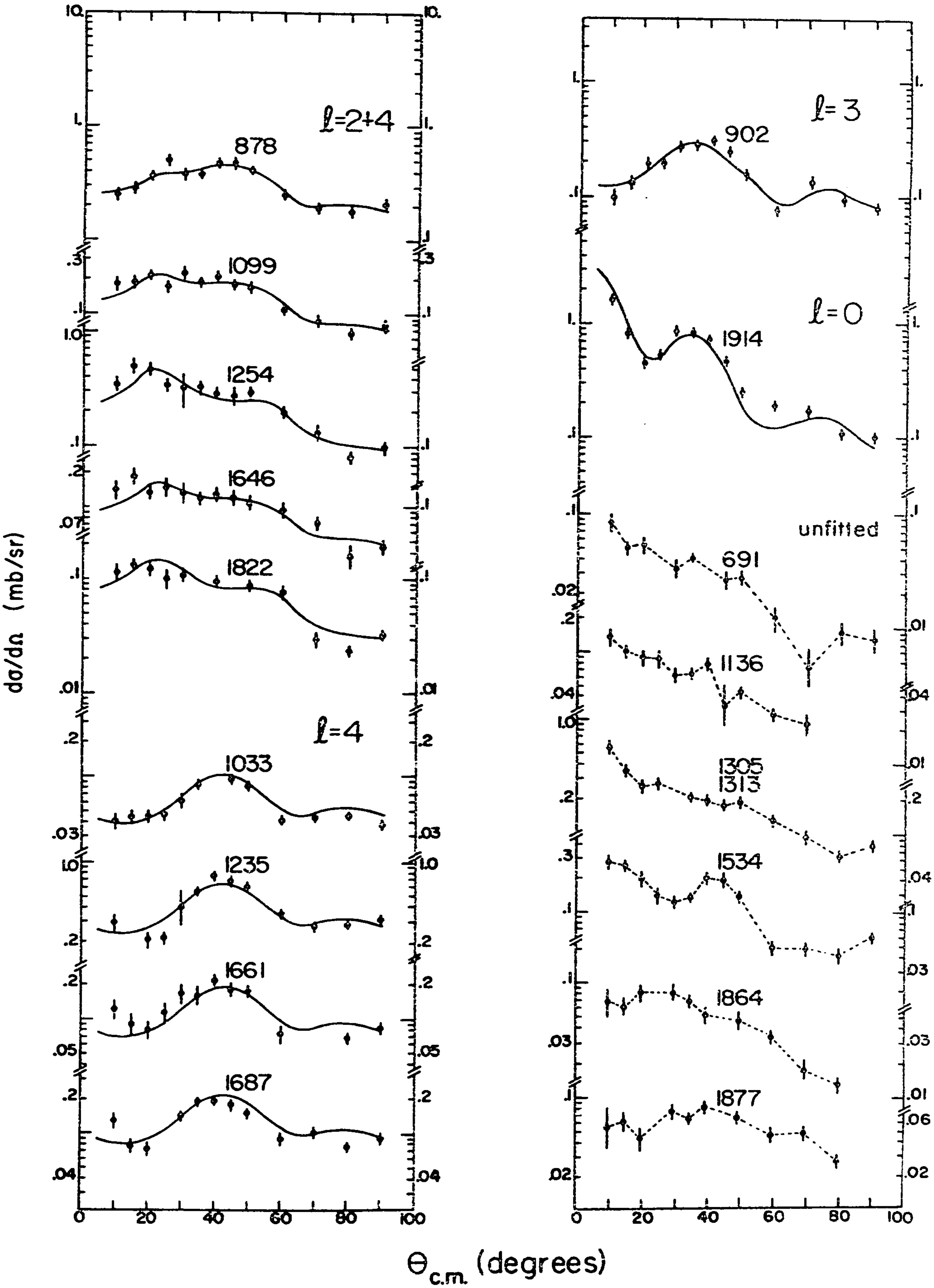

ℓ=2+4
878
1099
1254
1646
1822
ℓ=4
1033
1235
1661
1687
ℓ=3
902
ℓ=0
1914
unfitted
691
1136
1305
1313
1534
1864
1877
dσ/dΩ (mb/sr)
Θc.m. (degrees)

Target thicknesses varied between 10 and 30 μgm cm^{-2}.

In the $^{71}Ga(d,t)^{70}Ga$ experiment, 16 MeV deuterons were used. In a magnetic spectrograph, particles having the same magnetic rigidity

$$B\rho = \frac{\sqrt{2mE}}{q}$$

where B is the magnetic field, ρ is the instantaneous radius of curvature, and m, q and E are the mass, charge, and energy of the particle, respectively, will follow the same paths. Elastically scattered deuterons will follow the same paths as tritons with energy $E_T \approx \frac{2}{3} E_d$. Since the Q-value for this reaction is -3.052±.007 MeV (Mattauch et al 1965), it is then possible to observe tritons corresponding to 2 MeV excitation or less in ^{70}Ga without interference from the elastically scattered deuterons by using a beam energy of 16 MeV. Tritons were detected with 50 micron thick photographic emulsions*, without an absorber. Figure 2.4 shows a triton spectrum at 35 degrees, obtained by scanning the plate in 1/4 mm. scans, corresponding to 2.8 keV. A broad peak due to the $^{13}C(d,t)$ reaction was observed.

Triton energies were obtained relative to the ground state from the positions of the peaks as in the (d,p) experi-

---

*Ilford K-1 nuclear emulsions. These emulsions are much less sensitive than the Kodak NTB-50 plates, which enabled the plate scanners to discriminate against background deuteron tracks.

Figure 2.4

Experimental triton spectrum from $^{71}Ga(d,t)^{70}Ga$ taken with E_d = 16 MeV.

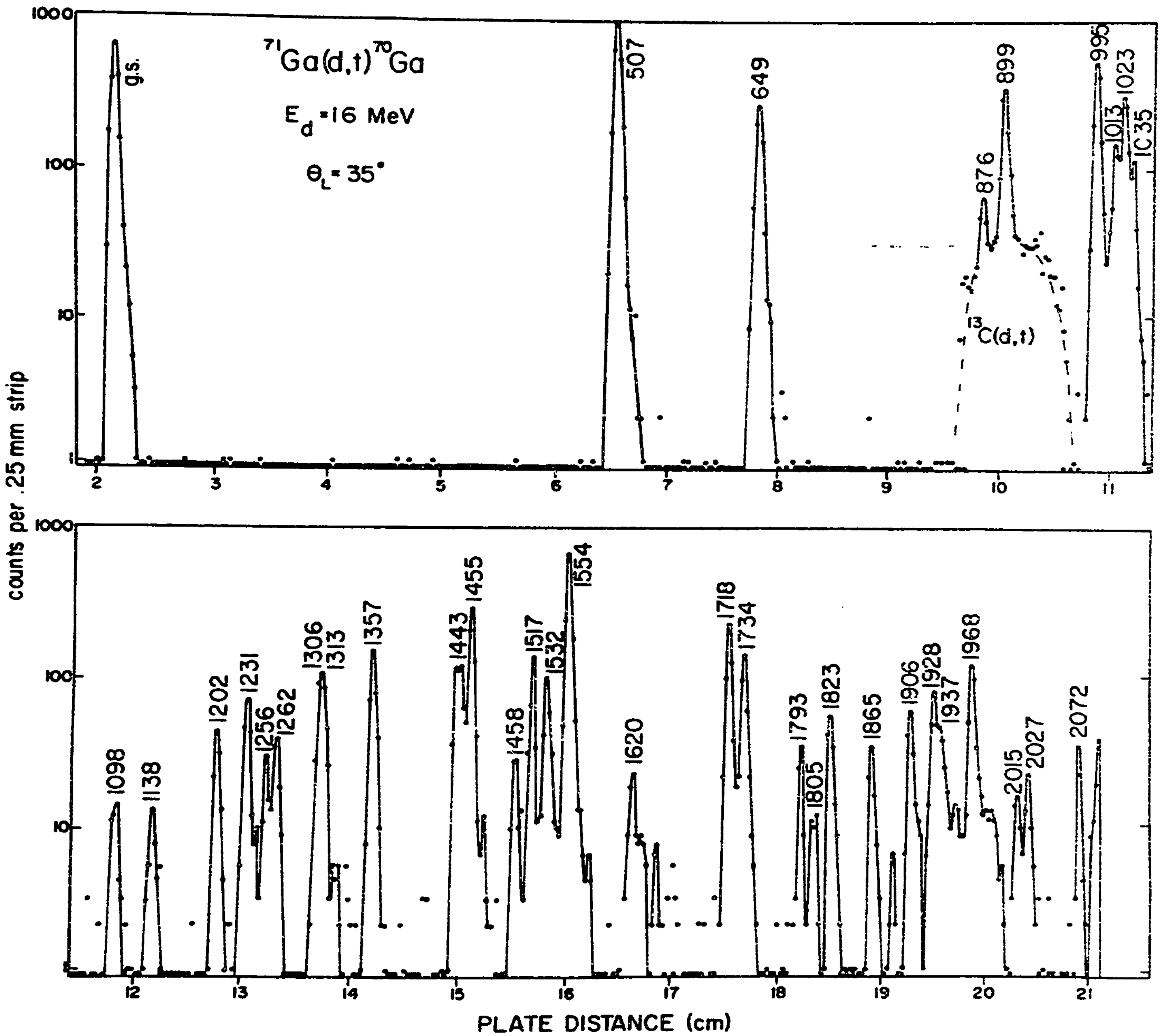

$^{71}Ga(d,t)^{70}Ga$
$E_d = 16$ MeV
$\theta_L = 35°$
g.s.
507
649
876
899
995
1013
1023
1035
$^{13}C(d,t)$
1098
1138
1202
1231
1256
1262
1306
1313
1357
1443
1455
1458
1517
1532
1554
1620
1718
1734
1793
1805
1823
1865
1906
1928
1937
1968
2015
2027
2072
counts per .25 mm strip
PLATE DISTANCE (cm)

ment. The triton energies obtained in this way at five different angles were averaged and the results are given in Table 2.1. Figure 2.2 shows the region of the triton spectrum between 990 and 1040 keV, taken at $\theta=30°$ and $50°$; using 1/8 mm scans. The evidence for the existence of 2 levels at $E_x \stackrel{\sim}{\sim} 1013$ keV is quite convincing in this case.

Angular distributions in the ^{71}Ga(d,t)^{70}Ga reaction were measured from 15 to 85 degrees in steps of 5 degrees. The relative normalization was carried out by monitoring the integrated current in the Faraday cup. Typical exposures involved integrated currents of 2000 μ Coulombs. However, levels populated by $\ell=4$ still suffered from poor statistics. The experimental results are shown in Figure 2.5. Absolute cross sections were obtained by the method described in the next section.

2.4 Absolute Normalization of the Cross Sections

Absolute cross sections were obtained by the well known technique of comparing the reaction yield to the Rutherford elastic scattering cross section. By using a gallium target of natural isotopic abundance the absolute normalization for both reactions was determined with the same target. This is possible because the (d,p) and (d,t) Q values for ^{69}Ga and ^{71}Ga are such that the particle groups leading to the ^{70}Ga ground state are the most energetic in both the proton and triton spectra. In fact, all the states up to $\stackrel{\sim}{\sim}$ 1 MeV excitation can be seen without interference from the other isotope.

Figure 2.5

Triton angular distributions from $^{71}Ga(d,t)^{70}Ga$. The solid curves are admixtures of theoretical DWBA curves least squares fitted to the data. The dotted lines on the unfitted distributions are included to guide the eye.

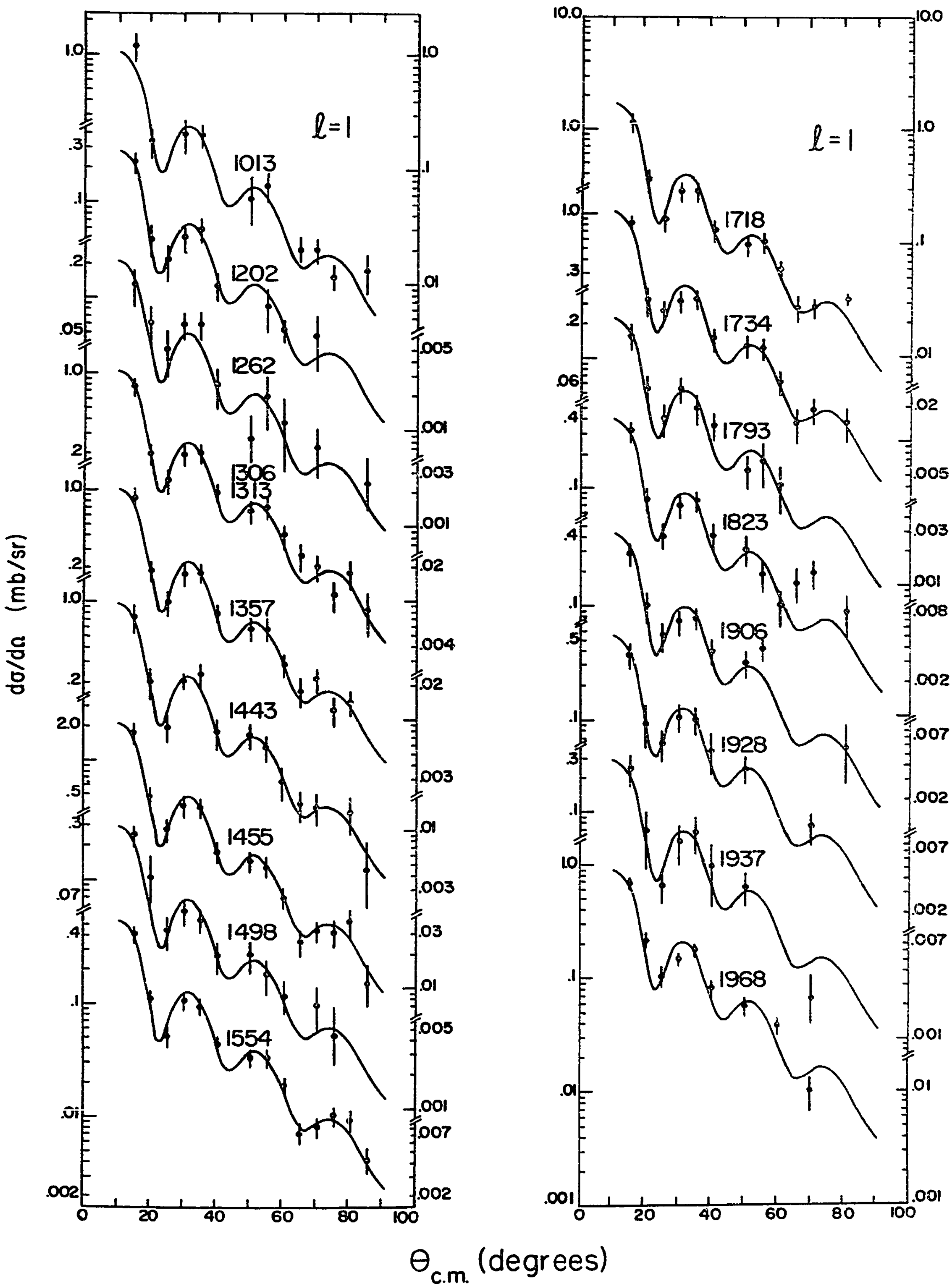

$\ell=1$
1013
1202
1262
1306
1313
1357
1443
1455
1498
1554
$\ell=1$
1718
1734
1793
1823
1906
1928
1937
1968
$d\sigma/d\Omega$ (mb/sr)
$\Theta_{c.m.}$ (degrees)

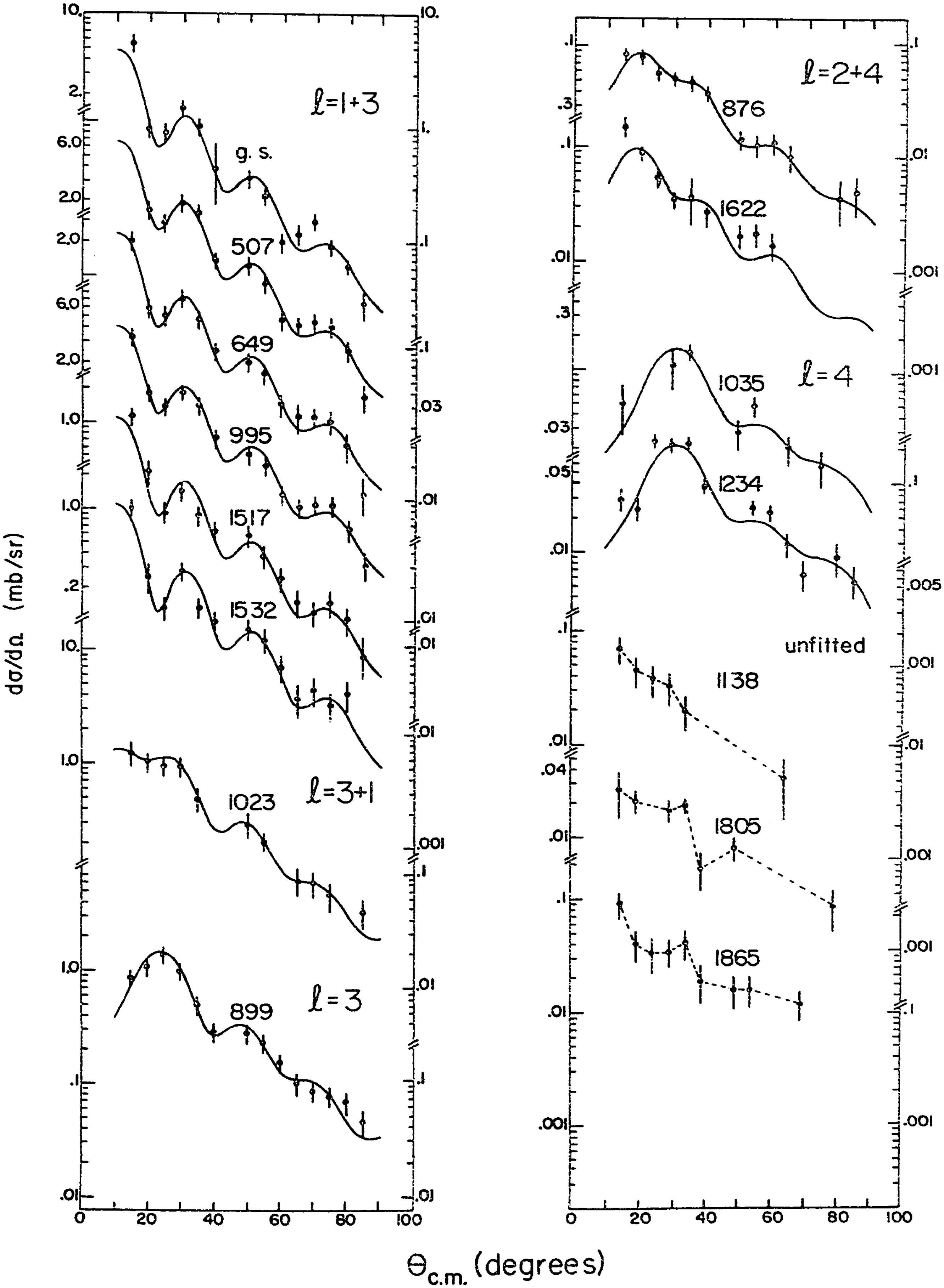

ℓ=1+3
g. s.
507
649
995
1517
1532
1023
ℓ=3+1
899
ℓ=3
ℓ=2+4
876
1622
1035
ℓ=4
1234
unfitted
1138
1805
1865
dσ/dΩ (mb/sr)
Θc.m. (degrees)

The elastic scattering of 10 MeV deuterons was measured at 15 degrees and compared with the Rutherford formula

$$\frac{d\sigma}{d\Omega}(\theta) = \left(\frac{Z_1 Z_2 e^2}{2E_d}\right)^2 \frac{1}{\sin^4(\frac{\theta}{2})} \quad \frac{cm^2}{sr}$$

$$= \quad 1.30 \left(\frac{Z_1 Z_2}{E_d}\right)^2 \mathrm{cosec}^4(\tfrac{\theta}{2}) \ \mathrm{mb\ sr^{-1}} \quad (E_d \text{ in MeV})$$

after conversion of θ and Ω to center of mass. Observations at 1 degree intervals between 12 and 15 degrees showed the expected angular dependence and thus provided a check on the assumption that the scattering was purely Rutherford. This assumption was also borne out by optical model calculations of the scattering. The $^{69}Ga(d,p)^{70}Ga$ cross sections were then obtained by simply comparing the yield of protons for a known integrated beam current with the elastic deuteron yield. For the normalization of the (d,t) reaction, the yield for $^{71}Ga(d,t)^{70}Ga$ with E_d = 16 MeV was compared with the 10 MeV elastic deuteron yield. Checks were made to ensure the target thickness did not change with time. From the reproduc ibility of the data, a 15% uncertainty is adopted in the absolute cross sections.

2.5 Theoretical Analysis

The theoretical (d,p) angular distributions were computed using a zero range DWBA calculation. The optical model parameters used in these calculations are from Perey et al (1968) for the protons, and Perey and Perey (1963) for the deuterons, and are listed in Table 2.2. In order to obtain agreement with the experimentally observed angular distributions, it was necessary to assume incoherent sums of either ℓ = 1+3 or ℓ = 2+4 transfers. Because the cross sections for ℓ = 1 and 2 are so much larger than for ℓ = 3 and 4, respectively, the ℓ = 3 (or 4) strengths obtained in the analysis are very sensitive to the exact shape of a pure ℓ = 1 (or 2) distribution. Although the calculations were in acceptable agreement with the observed distributions, it was felt that more reliable determinations of ℓ-value admixtures would be obtained if empirically determined (d,p) curves were used in the comparison. The curves chosen as standards were those of Von Ehrenstein and Schiffer (1967) who used 10 MeV deuterons in the ^{68}Zn(d,p)^{69}Zn reaction. In this reaction the target and product nuclei have the same numbers of neutrons as in the ^{69}Ga(d,p)^{70}Ga reaction. The absolute cross sections at the first maxima (except for ℓ=0, in which case the second maximum is used) of these curves were obtained from the DWBA calculation, which was performed for excitations in ^{70}Ga from 0 to 2 MeV in .5 MeV steps in order to extract the Q-value dependence.

The results are represented by the solid curves in Fig. 2.3. The mixtures of ℓ-transfers were extracted by least squares analysis, and the corresponding strengths are listed in Table 2.3. In Figure 2.3 levels are grouped into the following categories:

Table 2.2

Optical Model Parameters Used for the $^{69}Ga(d,p)^{70}Ga$ and $^{71}Ga(d,t)^{70}Ga$ Calculations

$^{69}Ga(d,p)^{70}Ga$

	V_S	W_S	r_{OS}	a_S	r_{OI}	a_I	$4W_D$
Deuterons[a]	94	0	1.15	.81	1.34	.68	76
Protons[a]	53.5	0	1.25	.65	1.25	.47	56
Neutrons[b]	44.3	0	1.25	.65	0	0	

$^{71}Ga(d,t)^{70}Ga$

	V_S	W_S	r_{OS}	a_S	r_{OI}	a_I	$4W_D$
Deuterons[a]	91.6	0	1.15	.74	1.29	.72	68.4
Tritons[a]	127	22.4	1.15	.79	1.51	.80	0
Neutrons[c]	46.9	0	1.25	.65	0	0	0

[a] $V(r) = U_C(r) - V_S(1+e^{x})^{-1} - iW_S(i+e^{x'})^{-1} + i4W_D \frac{d}{dx'}(1+e^{x'})^{-1}$

where $x = a_S^{-1}(r - r_{OS}A^{1/3})$

$x' = a_I^{-1}(r - r_{OI}A^{1/3})$

V_S, W_S, and W_D are in MeV

r_{OS}, a_S, r_{OI} and a_I are in Fermi .

[b] V_S adjusted to give 7.642 MeV separation energy

[c] V_S adjusted to give 9.309 MeV separation energy.

Table 2.3

Spectroscopic Factors for ^{69}Ga(d,p)^{70}Ga and ^{71}Ga(d,t)^{70}Ga

^{69}Ga(d,p)^{70}Ga at 10 MeV						^{71}Ga(d,t)^{70}Ga at 16 MeV				
	Spectroscopic Factor						Spectroscopic Factor			
Energy	ℓ=0	1	2	3	4	Energy	ℓ=1	2	3	4
0		0.34				0	0.30		0.19	
508		0.57				507	0.50		0.46	
651		0.10		0.15		649	0.18		0.15	
691										
878			0.07		1.60	876		0.02		0.11
902				0.41		899			1.38	
996		0.09		0.05		995	0.37		0.36	
1012 }		0.07		0.19		1013	0.10			
1023 }						1023	0.09		1.03	
1033					4.14	1035				0.50
1099			0.05		0.57	1098				
1136						1138				
1204						1202	0.03			
1235					2.45	1231				0.33
1246										
1254			0.13		0.54	1250				
1262						1262	0.02			
1305						1306 }	0.11			
1313						1313 }				
1325			0.06							
1336			0.05							
1359		0.02		0.03		1357	0.11			
1444		0.02		0.04		1443	0.11			
1456		0.05		0.06		1455	0.23			
1502						1498	0.03			
1518		0.01		0.03		1517	0.13		0.06	

(continued next page)

Table 2.3 (continued)

$^{69}Ga(d,p)^{70}Ga$ at 10 MeV	Spectroscopic Factor					$^{71}Ga(d,t)^{70}Ga$ at 16 MeV	Spectroscopic Factor			
Energy	$\ell=0$	1	2	3	4	Energy	$\ell=1$	2	3	4
1534						1532	0.12		0.03	
1555		0.11		0.08		1554	0.63			
1622			0.21			1620		0.03		0.08
1646			0.04		0.32					
1661					0.68					
1687					0.79					
1720		0.03		0.06		1718	0.20			
1734			0.15							
						1734	0.14			
1796		0.01		0.02		1793	0.03			
1807						1865				
1822			0.04		0.17					
						1823	0.06			
1864						1865				
1877										
						1906	0.06			
1914	0.08									
1931						1928	0.08			
						1937	0.04			
1968						1968	0.12			
1982										
2015			0.21			2012				

$\ell=1$ meaning essentially pure $\ell=1$. The ground state and 508 keV state are the only levels that fit into this category. The least squares analysis favoured a small amount of $\ell=3$ for both these levels but the resulting fit was not significantly altered with this admixture. The pure $\ell=1$ spectroscopic strengths are quoted in Table 2.3.

$\ell=1+3$ indicating a definite admixture of $\ell=3$ with $\ell=1$. All the remaining even parity levels are of this type, except for the 902 keV level.

$\ell=2$ meaning essentially pure $\ell=2$. The least squares analysis favoured a small amount of $\ell=4$ in the five levels of this type. This was considered to be a defect in the fitting analysis, possibly due to the fact that the data is fitted at discrete points.

$\ell=2+4$ indicating mixed $\ell= 2+4$

$\ell=4$ meaning essentially pure $\ell=4$

$\ell=3$ meaning essentially pure $\ell=3$

$\ell=0$ meaning essentially pure $\ell=0$

unfitted indicating that the angular distribution cannot be fitted into any of the above categories. Angular distributions in this category are either unresolved doublets possibly consisting of levels of the opposite parity, or, in the case of weakly populated levels, may contain contributions from compound nuclear processes.

DWBA predictions for the (d,t) reaction were calculated using the triton parameters of Haefele, as given by Daehnick (1969), and the deuteron parameters of Perey and Perey (1963). These are listed in Table 2.2. The solid curves in Fig. 2.5 are the best fitting ℓ admixtures obtained by least squares analysis. The spectroscopic strengths obtained in this analysis are given in Table 2.3. The levels are categorized with respect to ℓ value as in the (d,p) with the addition of a new category, ℓ=3+1, indicating predominantly ℓ=3 but a definite mixture of ℓ=1. In the (d,p) experiment, the level in this category, at 1024 keV, was not resolved from the doublet at $\sim$1012 keV.

2.6 Discussion

2.6a The Total Spectroscopic Strength

The total observed strengths in the neutron transfer reactions may be compared with the expected values of 12 (holes) in ^{69}Ga and 12 (particles) in ^{71}Ga. The observed strengths are given in Table 2.4. The division of the $\ell=1$ strengths into $p_{1/2}$ and $p_{3/2}$ in this table is discussed in the next section. From the isospin coupling coefficient C^2 for the ^{71}Ga(d,t)^{70}Ga reaction, only .9 of the total (d,t) strength is expected to occur for the low lying T = 4 states in ^{70}Ga. For this reason, an extra column is given in Table 2.4 in which the individual (d,t) strengths have been divided by this factor.

From the comparison of the observed and expected strengths, it can be seen that the agreement is acceptable considering the inaccuracies in both the cross section determination and the DWBA calculations. It is concluded from these data that essentially all of the ℓ = 1, 3 and 4 strength has been observed below 2 MeV excitation in both (d,p) and (d,t). It is somewhat disturbing that the apparent occupation numbers for the $p_{3/2}$ and $f_{5/2}$ orbits decreases from ^{69}Ga to ^{70}Ga. This is probably due to errors in the (d,t) experiment, where the strengths are difficult to extract at higher excitation. Such a comparison is not possible for the $\ell=4$ strength where the (d,p) has exceeded the total possible strength for the $g_{9/2}$ orbit.

Table 2.4

Neutron Occupation Numbers for ^{69}Ga and ^{71}Ga

	^{69}Ga(d,p)		^{71}Ga(d,t)	
	N_h^{ℓ}	N^{ℓ} *	$N^{\ell}C^2$	N^{ℓ}
$p_{1/2}$	1.17	.83	1.54	1.71
$f_{5/2}$	1.12	4.88	3.66	4.07
$p_{3/2}$	.25	3.75	2.34	2.60
$g_{9/2}$	11.26	-	1.02	1.13
Total	13.8	-		9.51
Expected	12.0	10.0		12.0

* $N^{\ell} = (2j+1) - N_h^{\ell}$.

2.6b The ℓ=1 Spectroscopic Strength

The ℓ=1 strengths reflect both $p_{1/2}$ and $p_{3/2}$ neutron transfer. Since the $p_{3/2}$ neutron shell is expected to be nearly filled in both ^{69}Ga and ^{71}Ga, the $p_{3/2}$ strength should show up more strongly in (d,t) than in (d,p). This is because it is relatively easier to take a particle from a nearly filled shell than to put one into it. Fig. 2.6 shows a plot of the distribution of ℓ=1 strength. It can be seen that the (d,p) strength falls off above $\sim$ 1000 keV while in the (d,t) it falls to low values between 1000 keV and 1300 keV and then rises again. This suggests that the $p_{3/2}$ strength is mainly concentrated above 1300 keV and that the $p_{1/2}$ strength is contained at most in five levels - 0, 509, 651, 996 and 1015 keV.

The protons in ^{70}Ga are expected to occupy the $p_{3/2}$ orbital as is indicated by the spin 3/2 ground states of both ^{69}Ga and ^{71}Ga. When these couple with a neutron configuration containing an unpaired $p_{1/2}$ particle one obtains spins 1^+ and 2^+. In the simplest picture, there should be two levels with spectroscopic strengths in the ratio 3 to 5, following the 2J+1 rule. The ground state is spin 1^+ and so one might deduce, from the (d,p) and (d,t) data, that the 509 keV level is 2^+. However, if mixing occurs, the strength will be split among additional levels. This will be discussed further in section 4.3.

Figure 2.6

Distribution of $\ell = 1$ strengths in $^{69}Ga(d,p)^{70}Ga$ and $^{71}Ga(d,t)^{70}Ga$.

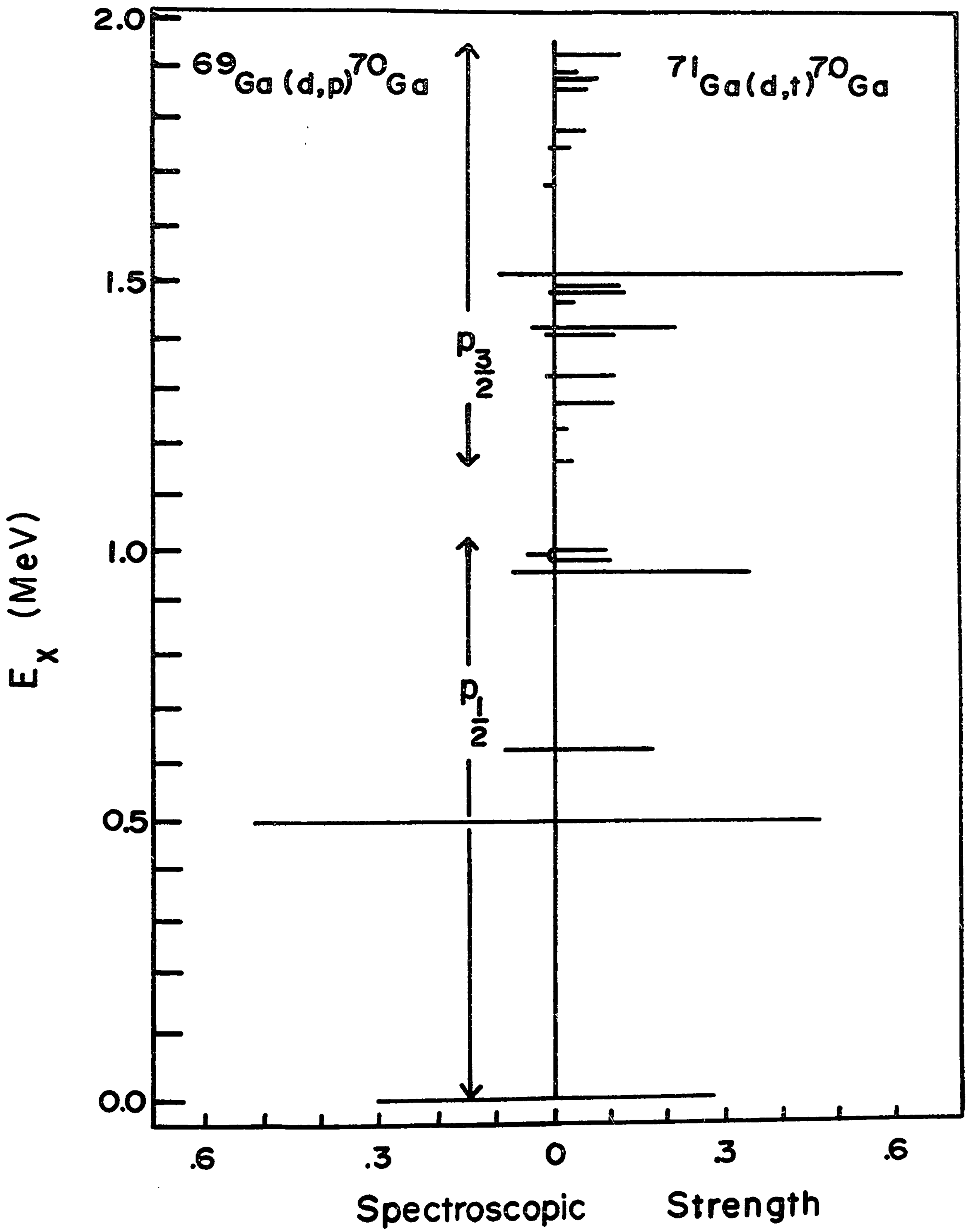

$^{69}Ga(d,p)^{70}Ga$
$^{71}Ga(d,t)^{70}Ga$
$p_{\frac{3}{2}}$
$p_{\frac{1}{2}}$
E_x (MeV)
2.0
1.5
1.0
0.5
0.0
.6
.3
0
.3
.6
Spectroscopic Strength

The $p_{3/2}$ strength is so fractioned that little can usefully be said. The coupling of the $p_{3/2}$ proton configuration with the $p_{3/2}$ neutron configuration should lead to states of $J^{\pi} = 0^{+}, 1^{+}, 2^{+}$ and 3^{+}. The 1555 keV state carries so much of the experimental strength that it may well be 3^{+}.

2.6c The ℓ=3 Spectroscopic Strength

For the ℓ=3 strengths, the situation is not as clear. States with $J^{\pi} = 1^{+}, 2^{+}, 3^{+}$ and 4^{+} are formed by coupling the $p_{3/2}$ proton configuration with an $f_{5/2}$ neutron. The total strength may be used to yield the sum rule prediction which favours spin 3^{+} for the 1023 keV level and 4^{+} for the 902 keV state. These spins could be interchanged, however, and still give acceptable agreement. However, the (d,t) distribution for the 1023 level has an $\ell = 1$ contribution which excludes the $J = 4$ possibility for it. The ground state is 1^{+}, and on the basis of the $\ell = 1$ strengths, the 508 keV level is 2^{+}. The two remaining levels strong in (d,t) — at 651 and 996 keV — could be 1^{+} and 2^{+}.

2.6d The ℓ=4 Spectroscopic Strengths

States with $J^{\pi} = 3^{-}, 4^{-}, 5^{-}$ and 6^{-} are formed by the transfer of a $g_{9/2}$ neutron. The total observed ℓ=4 spectroscopic strength in (d,p), 11.3, exceeds the maximum possible value of 10 for $g_{9/2}$ alone. According to the

2J+1 rule, assuming the $g_{9/2}$ strength is exhausted by the observed levels, the strength is expected to be distributed in the ratio 3.7:3.1:2.5:2.0 for J = 6, 5, 4 and 3 respectively. The levels seen with an admixture of $\ell=2$ cannot have spin values of 5 or 6 so that only the four levels at 1034, 1234, 1660 and 1685 keV may be 5^- or 6^-. On this basis, it is concluded that the 1034 keV level has $J^\pi = 6^-$ and the 1234 and one of the 1660 or 1685 keV levels has $J^\pi = 5^-$. The other levels cannot be assigned spins on this basis.

For the (d,t) reaction, the agreement with the 2J+1 rule is not as good. Here, even a very small cross section translates into a significant $\ell=4$ strength so that the strengths have to be regarded as quite uncertain.

Dividing the 1.1 units of observed strength (which is not an unreasonable occupancy for $g_{9/2}$ in ^{71}Ga - one has to allow also for the unobserved T = 5 strength) according to 2J+1, it must still be concluded that the 1034 keV level has spin 6^-, the 1234 keV level spin 5^-, and the 879 keV level spin 3^- or 4^-.

2.3e The ℓ = 0, 2 and Unfitted Distributions

Since only a fraction of the $\ell=0$ and 2 strength has been observed, little can usefully be said here. The spins which can be made with these ℓ-transfers are $J^\pi = 1^-$ or 2^- for $\ell = 0$ $(3s_{1/2})$ and $J^\pi = 1^-, 2^-, 3^-$ or 4^- for $\ell = 2$ $(2d_{5/2})$.

In the unfitted category, the level at 691 keV is of particular interest. This level is populated very weakly in (d,p) and is seen at only one angle in (d,t) suggesting either a proton excitation or a higher seniority configuration. The possibility of a compound nuclear component in the cross sections cannot be neglected for levels in this category.

The unresolved levels at 1305 and 1313 keV in the (d,p) are not necessarily of the same parity and hence the doublet may correspond, in general, to any mixture of ℓ values.

CHAPTER III

THE $^{70}Zn(p,n\gamma)^{70}Ga$ REACTION

3.1 Introduction

In order to complement the information obtained in the particle transfer work, an in-beam study was undertaken of the γ-rays produced in the $^{70}Zn(p,n\gamma)^{70}Ga$ reaction. The investigation, which included yield function determinations, coincidence measurements, γ-ray angular distributions and linear polarization measurements, has provided valuable information on the spins and electromagnetic decay properties of the levels of ^{70}Ga. In this chapter will be discussed the experimental aspects of this reaction.

3.2 γ-Ray Singles Spectra

Oxide targets of both natural and enriched ^{70}Zn (enrichment 67.5%) were prepared by glueing the oxide powder onto .020" tantalum backings. Target thicknesses were determined by weighing and were estimated to be between 2 and 4 mg/cm^2. The glue, which consisted of polystyrene dissolved in benzene, contained the elements C and H which did not produce background γ-rays in the region of interest (E_γ = 0-2 MeV). The Ta backings were mounted on copper cooling bars and placed inside a small target chamber with .020" stainless steel walls.

The Q-value for the $^{70}Zn(p,n\gamma)^{70}Ga$ reaction is -1.435 ± .009 MeV (Mattauch et al 1965). In the first experiment, a 3.5

MeV proton beam was used to bombard both the enriched and natural Zn targets, and the resultant gamma rays were detected with Ge(Li) detectors placed at 135° to the beam. The signals from the preamplifiers were shaped by Tennelec 203 BLR linear amplifiers, and sent through base line restorers to Nuclear Data analog-to-digital converters (ADC's). Spectra of 4096 channels were accumulated in a Nuclear Data 3300 multichannel analyzer, and then dumped on magnetic tape. For the 3.5 MeV runs, a beam current of $\sim$ 100 nA was used and the spectra were accumulated for $\sim$ 3 hours. In a later experiment in which the γ-rays from ^{70}Ga were observed at various angles with a high resolution detector, no net Doppler shift was observed. Figure 3.1 shows the spectrum obtained with a 40 cm^3 volume Ortec detector. Since ^{70}Zn is present with an abundance of .62% in natural Zn, only the gamma rays which appear in the enriched run but very weakly or not at all in the natural run were accepted as possible candidates in the decay of ^{70}Ga levels. In this way, the most common impurity lines are excluded. Recognized impurity lines were ascribed to ^{19}F, ^{23}Na, ^{27}Al, ^{58}Fe and ^{181}Ta. The only ^{70}Ga gamma rays present in both runs were lines at 508.1, 651.1, and 690.9 keV, which are the strongest lines by far in the spectrum of the enriched sample.

Table 3.1 contains the energies and intensities of the γ-rays satisfying the above criteria. The lines at 318.7 and

Figure 3.1

Gamma rays from $^{70}Zn(p,n\gamma)^{70}Ga$, with $E_p = 3.5$ MeV, observed with a 40 cm^3 Ge(Li) detector. One division on the abscissa is 100 channels. Impurity peaks and weak γ-rays from ^{70}Ga are not labelled.

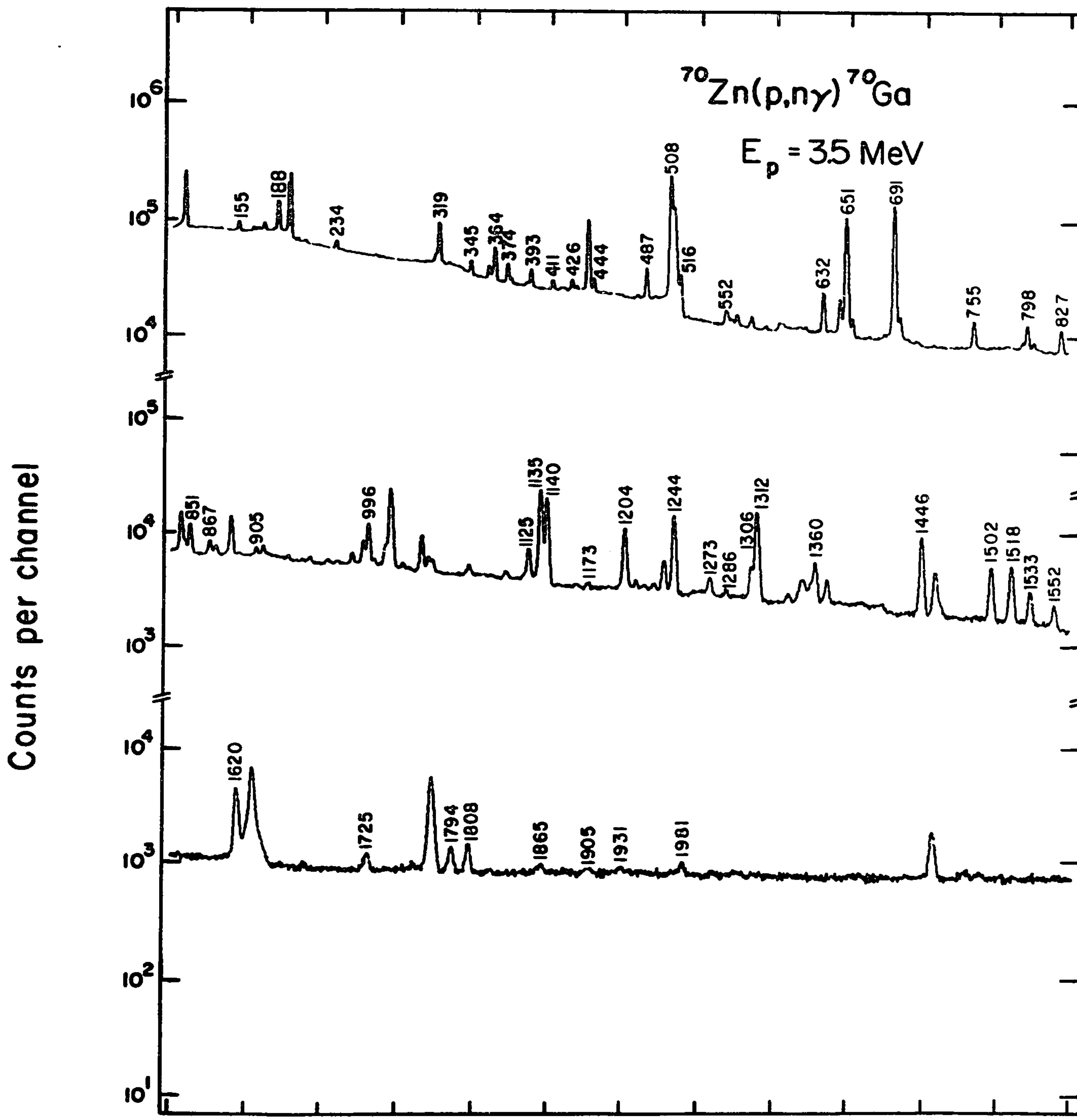

$^{70}Zn(p,n\gamma)^{70}Ga$
$E_p = 3.5$ MeV
Counts per channel
10^6
10^5
10^4
10^5
10^4
10^3
10^4
10^3
10^2
10^1
155
188
234
319
345
364
374
393
411
426
444
487
508
516
552
632
651
691
755
798
827
851
867
905
996
1125
1135
1140
1173
1204
1244
1273
1286
1306
1312
1360
1446
1502
1518
1533
1552
1620
1725
1794
1808
1865
1905
1931
1981

Table 3.1

Energies and Relative Intensities of γ-rays from $^{70}Zn(p,n\gamma)^{70}Ga$

E_γ (keV)	I_γ	E_i (keV)	E_f (keV)	Comments
139.7(2)	.29	1135.4	995.7	
154.7(2)	2.2	1033.2	878.5	
170.8(3)	3.4			fits 1306.8 → 1135.4 or 1311.9 → 1140.4
187.6(3)	9.8	878.5	690.9	
201 (2)		1234	1033.2	observed only in coincidence
209.6(2)	.51	1413.0	1203.5	
234.8(2)	1.3	1244.5	1009.7	
238.8(3)	.26	1263.2	1024.1	
245.4(2)	.23			
267.6(3)	.13	1263.2	995.7	
292.5(3)	.08			
316.2(2)	1.7	1325.9	1009.7	
318.7(2)	15.5	1009.7	690.9	contains unresolved impurity
326.7(2)	.33			
344.6(2)	3.0	995.7	651.1	
364.0(2)	10.1	1015.1	651.1	
374.3(3)	4.5	1252.8	878.5	
377.6(3)	.75			
393.2(2)	3.6	901.3	508.1	
410.7(2)	1.8	1101.6	690.9	
417.4(3)	.50	1552.8	1135.4	
426.8(2)	2.6			fits 1661 → 1234 or 1734 → 1306.8
430.5(2)	.83	1454.7	1024.1	
444.5(2)	.32	1135.4	690.9	
450.0(2)	.62			
487.5(2)	9.2	995.7	508.1	contains unresolved impurity
508.1(3)	83.2	508.1	0	
516.1(2)	10.3	1024.1	508.1	
520.4(9)	.21	1621.0	1101.6	
527.7(3)	.12	1864.7	1336.6	
532.6(6)	.13			
554.3(6)	1.88			
572.1(4)	.40			
585.1(2)	.63			
596.1(10)	1.24	1286.5	690.9	
598.6(10)	.96	1621.0	1024.1	
612.9(4)	.39	1646.1	1033.2	
617.5(2)	.43			

(continued next page)

Table 3.1 (continued)

E_γ(keV)	I_γ	E_i(keV)	E_f(keV)	Comments
632.2(2)	9.4	1140.4	508.1	
636.7(3)	.22			
645.7(3)	7.66	1336.6	690.9	
651.1(2)	75.6	651.1	0	
655.8(3)	2.97	1306.8	651.1	
669.3(6)	.27	1359.9	690.9	
681.9(5)	.28			
690.9(2)	100	690.9	0	
708.7(9)	.22			
722.5(2)	.25			
755.0(2)	5.4	1263.2	508.1	also fits 1445.9→690.9
794.8(3)	.80	1445.9	651.1	
798.6(3)	4.4	1306.8	508.1	
803.7(2)	.79	1311.9	508.1	also fits 1454. → 651.1
827.4(1)	4.6	1518.3	690.9	
851.0(2)	3.9	1502.0	651.1	
867.1(3)	7.4	1518.3	651.1	
881.7(3)	.43	1533.0	651.1	also fits 1905.5 → 1024.1
904.8(2)	.74	1413.0	508.1	
930.8(3)	.53			
948.3(3)	.66			
962.4(5)	.69			
970.1(6)	.42	1621.0	651.1	
982.3(2)	1.32	1633.4	651.1	
995.7(2)	8.26	995.7	0	
1000.6(3)	.23			
1010.2(10)	2.79	1009.7	0	
1023.8(6)	.65	1024.1	0	
1044.6(3)	2.02	1552.8	508.1	
1047.7(3)	1.6			
1125.4(2)	5.0	1633.4	508.1	
1135.3(2)	30.8	1135.4	0	
1140.4(2)	25.8	1140.4	0	
1173.0(6)	.46	1824.1	651.1	
1203.5(2)	12.5	1203.5	0	
1212.1(2)	13.0	1720.2	508.1	
1227.9(5)	5.1			
1244.5(2)	19.0	1244.5	0	
1286.2(6)	.61	1286.5	0	
1307.0(5)	4.6	1306.8	0	
1312.0(3)	23.0	1311.9	0	
1359.7(10)	2.7	1359.9	0	
1445.9(2)	16.0	1445.9	0	

(continued next page)

Table 3.1 (continued)

E_γ(keV)	I_γ	E_i(keV)	E_f(keV)	Comments
1502.0(2)	7.2	1502.0	0	
1518.3(2)	7.1	1518.3	0	
1533.1(2)	3.1	1533.0	0	
1552.9(2)	1.9	1552.8	0	
1620.9(2)	10.8	1621.0	0	
1725.0(6)	1.1	1725.0	0	
1794.2(2)	1.9	1794.2	0	
1808.0(2)	2.0	1808.0	0	
1865.3(9)	.53	1864.7	0	
1905.0(9)	.43	1905.5	0	
1931.0(10)	.85	1931.0	0	
1981.9(9)	.12	1981.9	0	

487.5 keV appeared strongly in both runs but are included in this list because they are observed in coincidence with γ-rays from ^{70}Ga as described in the next section. Evidently they are present both in ^{70}Ga and as impurities. To obtain the energies of the gamma rays, calibration spectra were accumulated immediately before and after the experiment, to check for electronic drifts. Count rates similar to those of the actual run were used to avoid count rate dependent gain shifts. The line intensities are given in Table 3.1 relative to the 690.9 keV line, which is normalized to 100. The relative efficiency of the counter as a function of γ-ray energy was obtained from measurements of R.G.H. Robertson who used γ-rays of known relative intensities from thin sources of ^{60}Co, ^{143}Ce, ^{160}Tb and ^{182}Ta.

At a later time, the laboratory acquired a small volume (0.9 cm^3) Ortec Ge(Li) detector with very good resolution (570 eV at 112 keV). The gamma ray spectrum was re-examined at various proton energies with this detector. The improved resolution resulted in the complete separation of lines at 508.1(.2) and 516.0(.2) keV from the broad 511 keV positron annihilation line. Fig. 3.2 shows the spectrum obtained with this counter in the energy range E_γ = 0-700 keV.

3.3 γ-γ Coincidences

In order to definitely place γ-rays from complex spectra into the decay scheme of a nucleus, a coincidence experiment

Figure 3.2

Gamma rays from $^{70}Zn(p,n\gamma)^{70}Ga$ (E_p = 2.75 MeV) observed with a 0.9 cm^3 Ge(Li) detector. One division on the abscissa is 100 channels.

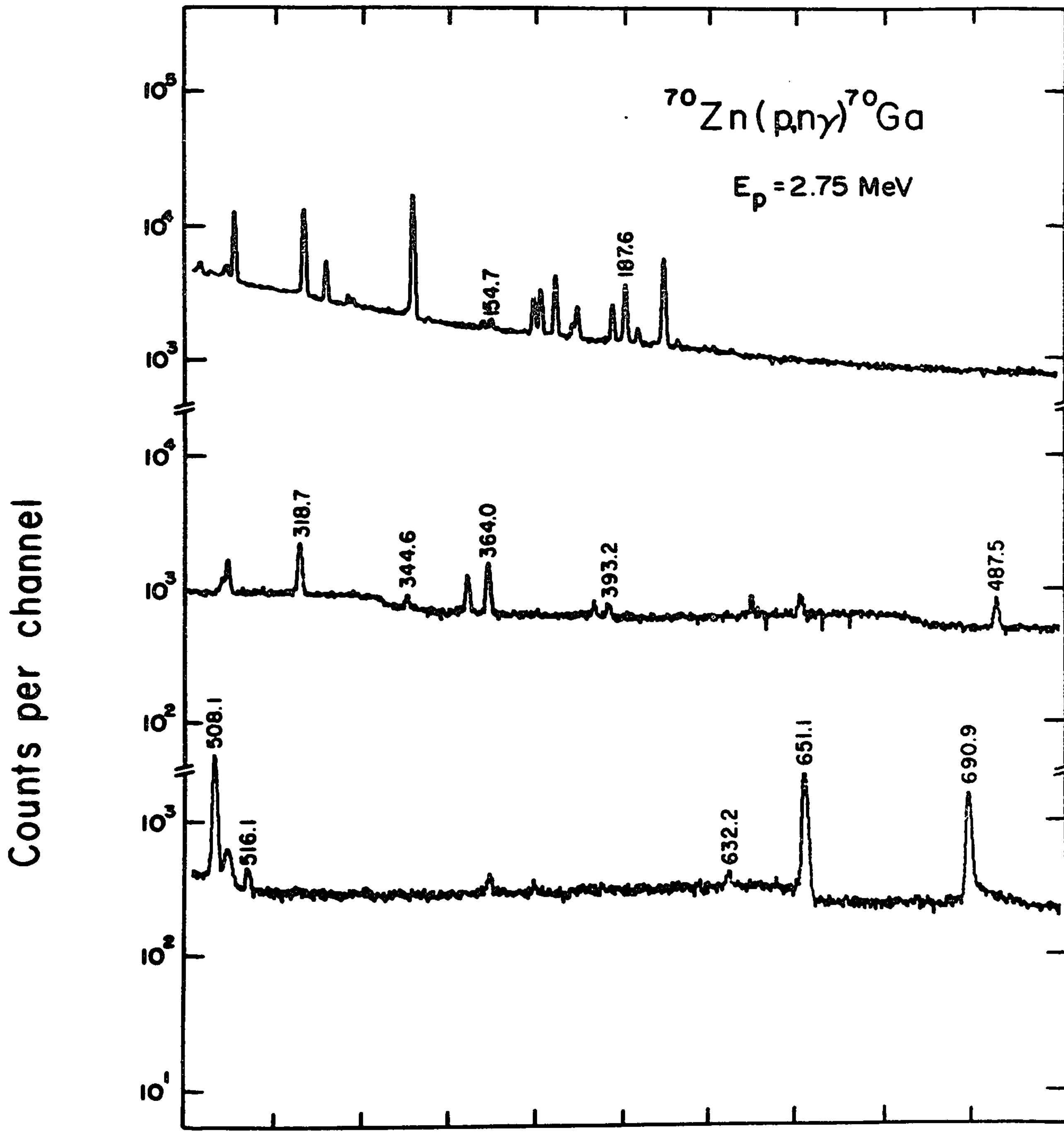

$^{70}Zn(p,n\gamma)^{70}Ga$
$E_p = 2.75$ MeV
Counts per channel
10^5
10^4
10^3
10^4
10^3
10^2
10^3
10^2
10^1
154.7
187.6
318.7
344.6
364.0
393.2
487.5
508.1
516.1
632.2
651.1
690.9

is essential. The method used here was the address recording technique in which every coincident event is stored as a pair of addresses on magnetic tape. In this way, optimum use is made of beam time, and of available analyzer storage. The magnetic tape can be played back in parts on an off-line computer, effectively making the system into a 16 million (4096×4096) channel analyzer.

Coincident γ-rays were observed with two large Ge(Li) detectors (12 cm^3 and 40 cm^3 in volume) using an enriched ^{70}Zn target and scattering chamber arrangement as in the singles run. The counters were arranged at ±135° to the beam with both counters and the target in one plane and were shielded as much as possible from one another with lead to prevent γ-rays Compton scattered in one counter from entering the other. Such events would produce a serious background in the coincidence spectrum.

A block diagram of the electronics used in the experiment is shown in Fig. 3.3. Pulses from the detector preamplifiers were shaped by Tennelec 203BLR linear amplifiers and delayed as necessary for a coincidence decision to be made. They were then sent through Tennelec base-line restorers to Nuclear Data 4096 channel ADC's for later processing by a PDP-9 computer. On the 40 cm^3 side, timing pulses for the start input of a time-to-amplitude converter (TAC) were generated by an Ortec type 453 constant fraction timing discriminator, while leading edge

Figure 3.3

Block diagram of the electronics used to measure coincidences in $^{70}Zn(p,n\gamma)^{70}Ga$. AMP: Amplifier. BLR: Base-Line Restorer ADC: Analog-to-Digital Converter. SCA: Single Channel Analyzer. TAC: Time-to-Amplitude Converter. CFTD: Constant Fraction Timing Discriminator. TFA: Timing Filter Amplifier. LSD: Logic Shaper and Delay.

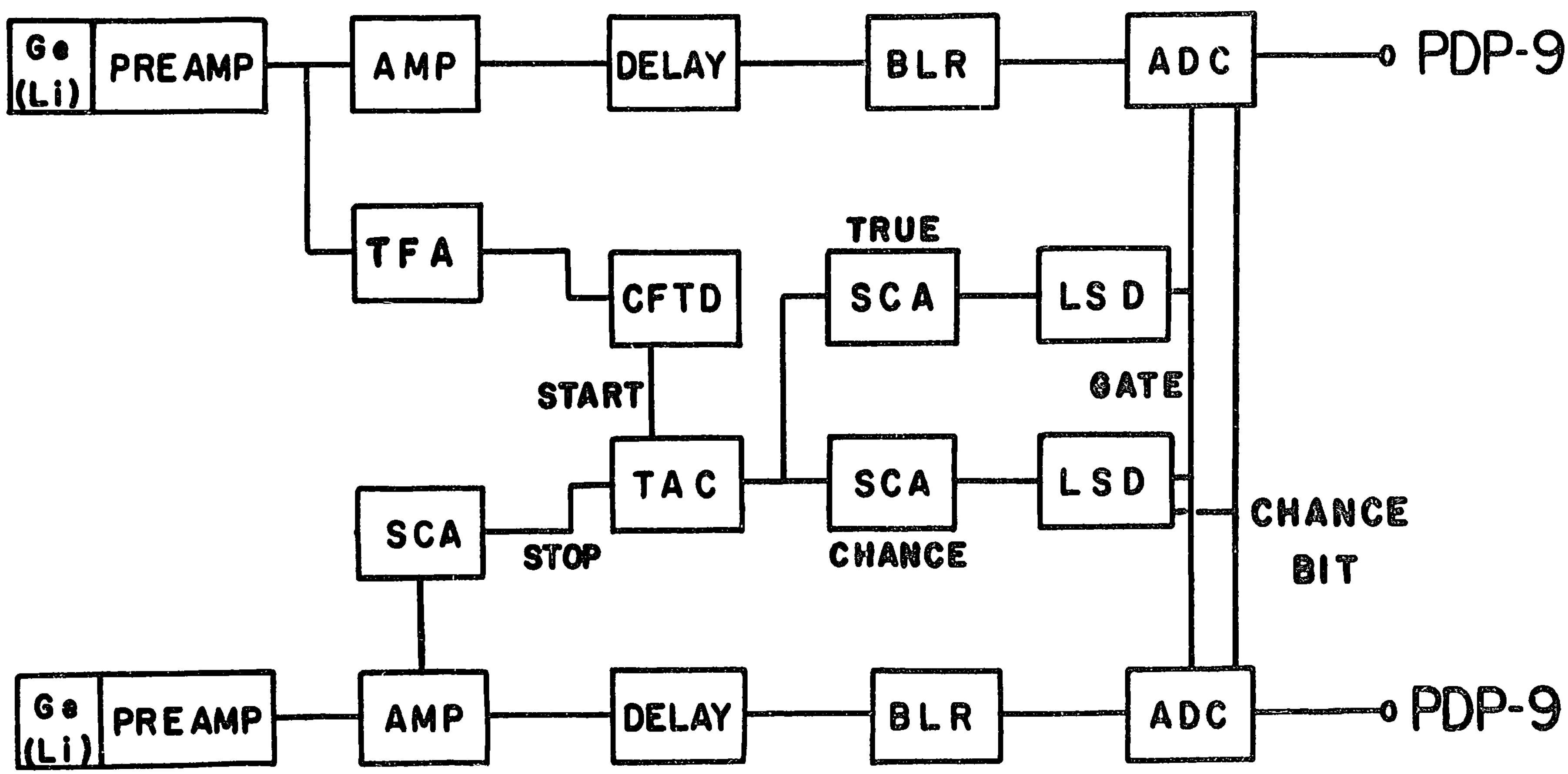
Ge (Li)
PREAMP
AMP
DELAY
BLR
ADC
PDP-9
TFA
CFTD
START
TAC
STOP
SCA
TRUE
SCA
LSD
GATE
SCA
CHANCE
LSD
CHANCE BIT
Ge (Li)
PREAMP
AMP
DELAY
BLR
ADC
PDP-9

timing was used on the 12 cm^3 side to provide the stop pulse. Two windows of equal width were set on the linear output of the TAC, corresponding to the "true + chance" and "chance" events. Their width corresponded to 120 nsec, the observed time resolution of the system. If an event occurred within either window, the linear gates on the ADC's were opened to allow processing of the energy signals from the linear amplifiers. The pulses from the "chance" window single channel analyzer, after being shaped into logic pulses, were also routed to a connection on the back of the ADC's, causing a "chance" bit to be set in each ADC register. For each coincident event, the contents of the ADC's and the chance bits were read and stored in two 18 bit words, along with a time sequence bit which identified alternate pairs of words. These data sequentially filled one of two 1000-word buffers. When one buffer was filled its contents were written onto magnetic tape, while data collection continued in the other.

The singles count rate in the counters was adjusted to maintain a true-to-chance ratio between 8:1 and 10:1. The tape was later read at the McMaster University CDC 6400 computer which unpacked the data and sorted it onto digital windows set on the 12 cm^3 axis. For each window, the chance events were collected in a separate area of core then later subtracted from the "true+chance" spectrum. Windows of equal width were set on peaks of interest and on background areas as close as possible to those peaks. The spectra in the background windows were then subtracted from those in the peak windows, while the statistical errors incurred in these subtractions were computed and stored.

Figure 3.4 shows the spectra resulting from the above process. The gamma rays appearing in coincidence with each gate are tabulated in Table 3.2.

3.4 Yield Functions

By measuring the yield functions of γ-rays too weak to be observed in a coincidence experiment, it is possible, in some cases, to place these γ-rays in the decay scheme of the nucleus. In an experiment of this type, in which the γ-ray yield, or production cross section is measured as a function of the beam energy, an upper limit can be placed on the excitation energy of the level from which the γ-ray is emitted. Also, if a level decays by more than one γ-ray, the branching ratios of the γ-rays must remain constant with beam energy. This is true except near threshold in which case the nucleus may be aligned, causing anisotropies in the angular distributions which are in general different for each γ-ray.

The experimental set up for the yield function measurements was identical to that of the singles run (section 3.2). Proton energies of 2.1, 2.4, 2.6, 2.8, 3.2, 3.6, 3.8, 4.2, 4.4 and 5.0 MeV were used. The 2 mg/cm^2 targets corresponded to an energy loss of $\sim$ 100 keV for the 5 MeV protons and $\sim$ 200 keV

Figure 3.4

Ge(Li)-Ge(Li) coincidence spectra

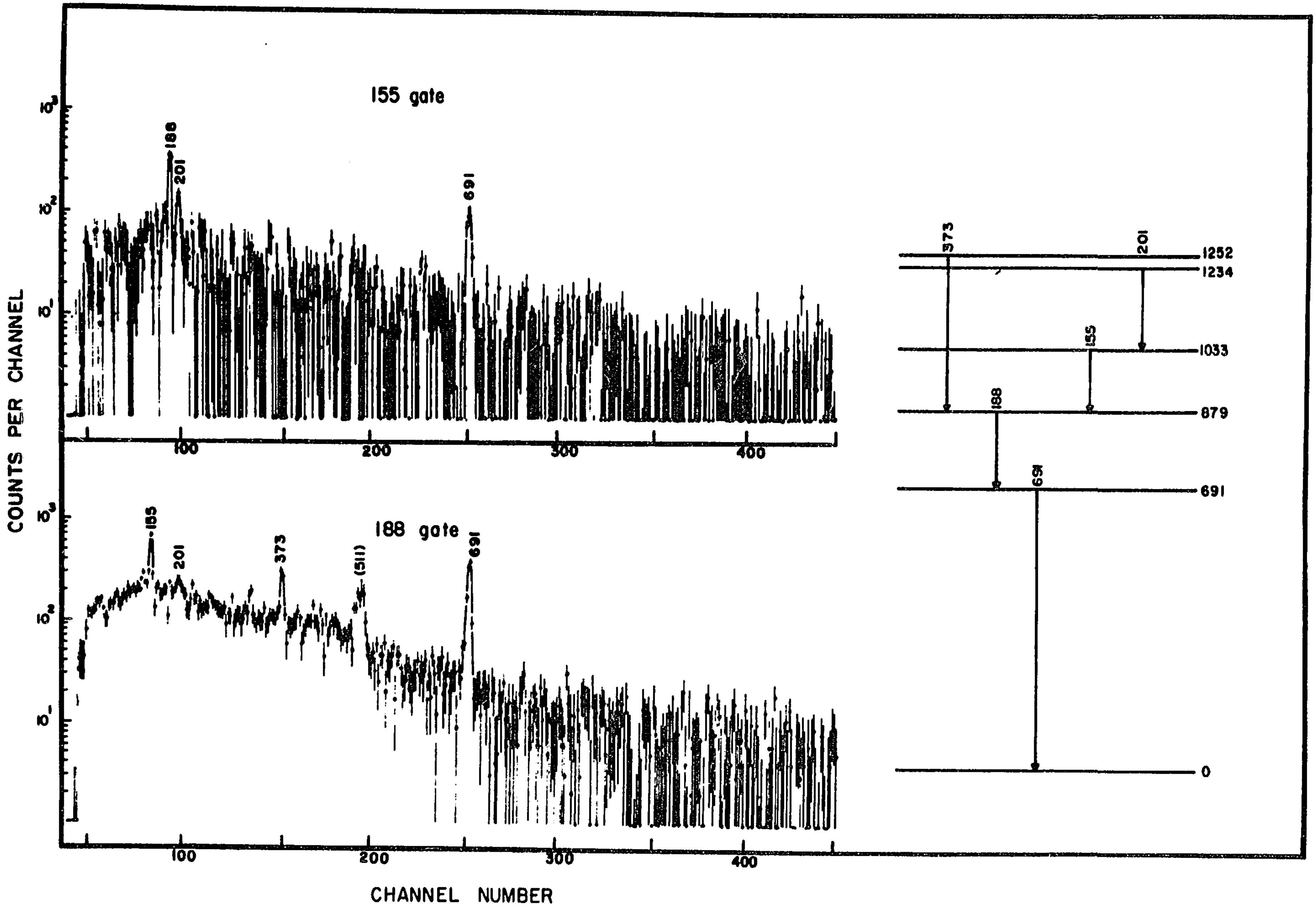

155 gate
188 gate
COUNTS PER CHANNEL
CHANNEL NUMBER
188
201
691
155
373
(511)
1252
1234
1033
879
0

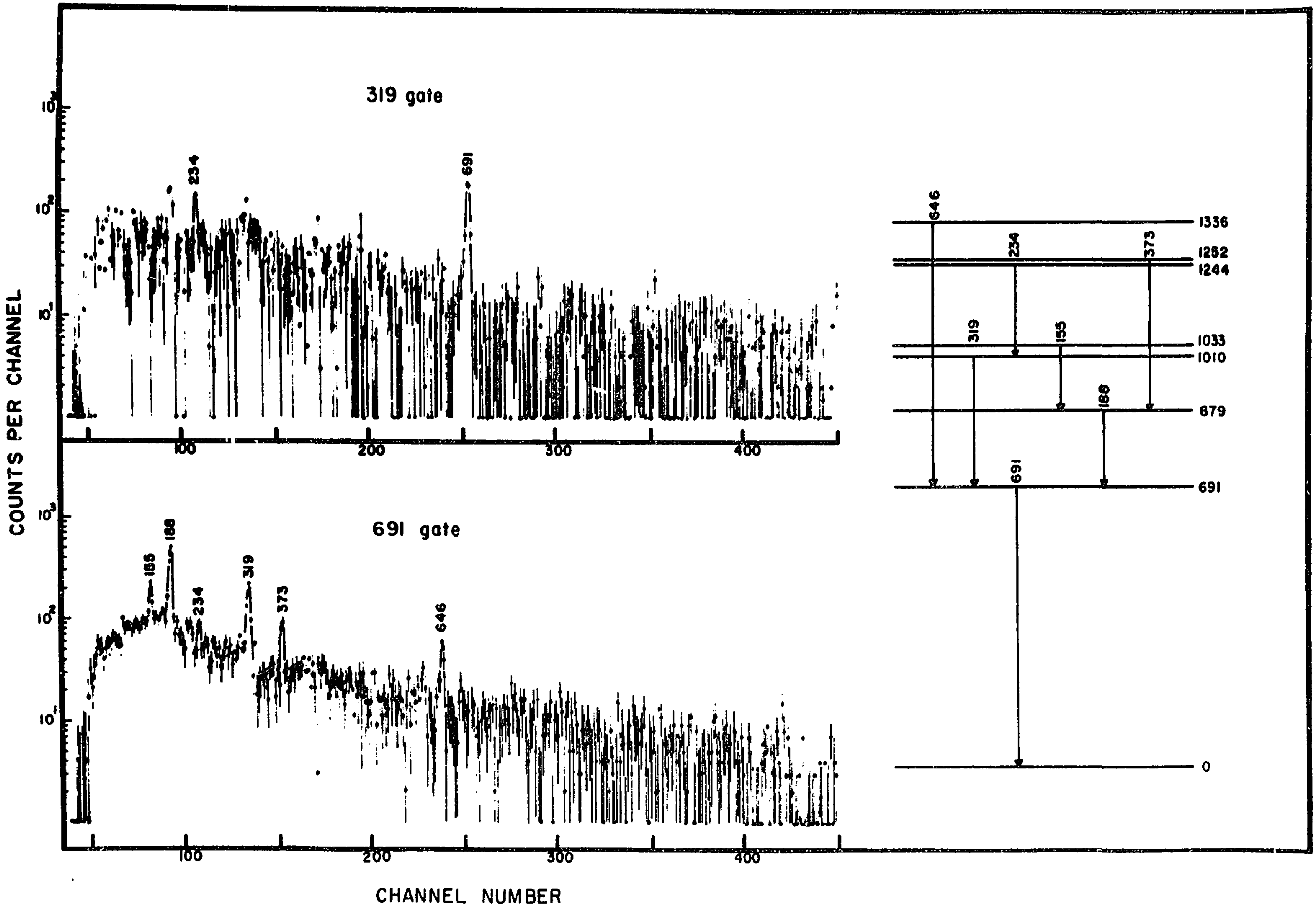

319 gate
691 gate
COUNTS PER CHANNEL
CHANNEL NUMBER
234
691
155
188
319
373
646
1336
1282
1244
1033
1010
879
0

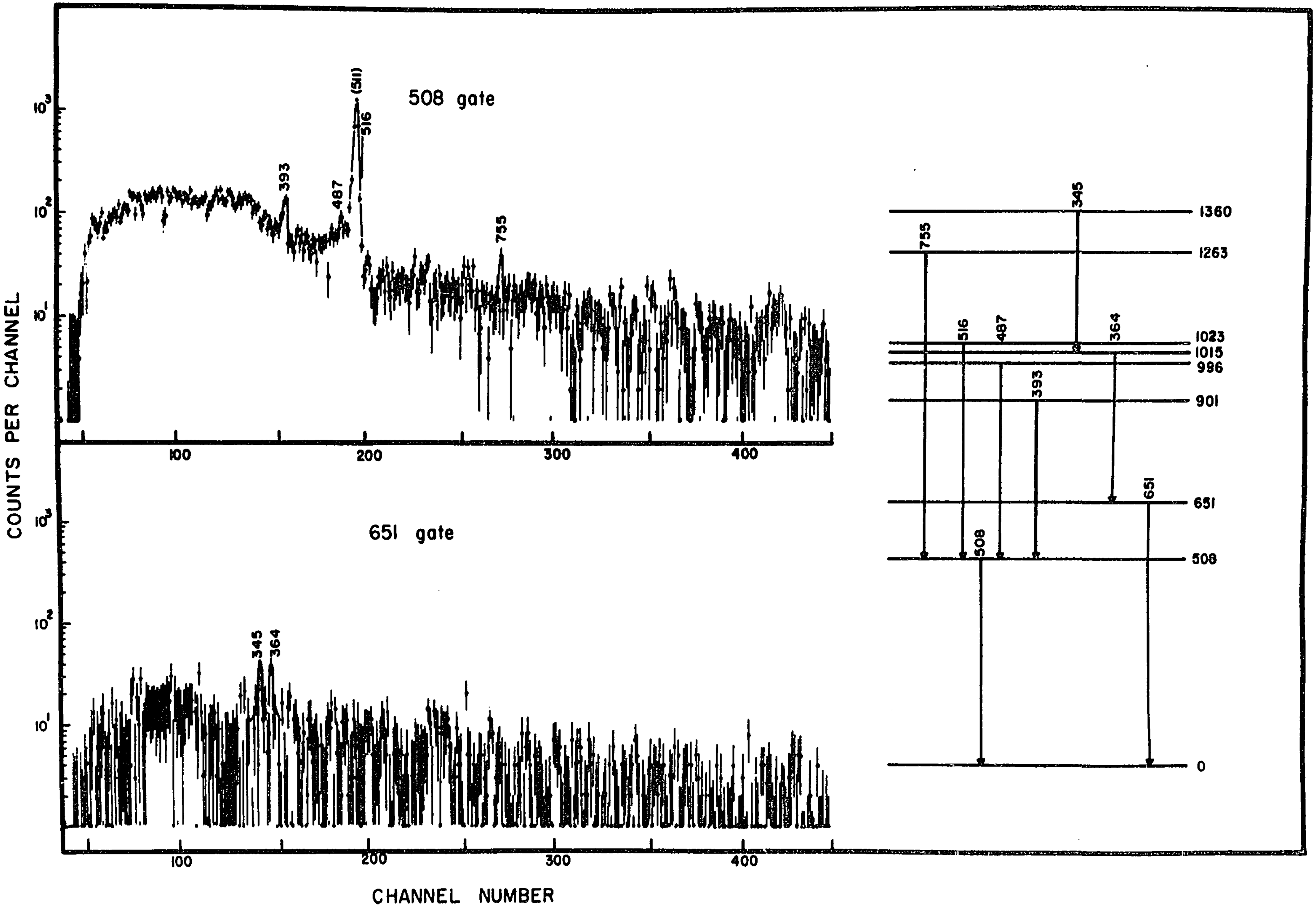

508 gate
(511)
516
393
487
755
651 gate
345
364
COUNTS PER CHANNEL
CHANNEL NUMBER
100
200
300
400
1360
1263
1023
1015
996
901
651
508
0

Table 3.2

Gamma-Gamma Coincidences from $^{70}Zn(p,n\gamma)^{70}Ga$

E_γ \ Gate	154.7	187.6	318.7	364.6	374.3	393.2	487.5	508.1	516.1	632.2	645.7	651.1	690.9
154.7		x											x
187.6	x				x								x
201	x	x											
234.8			x										x
318.7													x
344.6												x	
364.6												x	
374.3		x											x
393.2								x					
487.5								x					
508.1						x	x		x	x			
516.1								x					
632.2													
645.7													x
651.1				x									
690.9	x	x	x		x						x		
755.0								x					

for the 2 MeV protons. Since only the relative excitation functions are necessary the ratio of the number of counts in each peak to the number of Coulomb excitation events (corresponding to Coulomb excitation of the 885 keV state in the target, ^{70}Zn) were obtained as a function of energy. This procedure obviated difficulties of normalization caused by the target deterioration during the run.

Table 3.3 contains the relative yields of γ-rays from ^{70}Ga. Corrections for counter efficiency have not been made on these data. The errors in these measurements are typically of the order of 25% but are occasionally higher for weak peaks.

Cross sections for the (p,n) reactions do not exhibit a strong dependence on the internal properties of the residual state such as the shell model configuration in the case of neutron transfer reactions, or the collectivity of the state in the case of inelastic scattering reactions. Because of this non-selectivity, all the levels in the final nucleus should be populated. According to Hauser-Feshbach statistical theory, however, (p,n) cross sections should depend strongly on the spins of the states (Hauser and Feshbach 1952), and to a lesser extent, on the parities. In a study of the ^{68}Zn(p,n)^{68}Ga reaction, Bass and Stelson (1970) showed that the relative intensities of neutron groups corresponding to excitation of levels in ^{68}Ga are roughly independent of the positions of the levels but do depend on their spins and on the energy available to the neutron, i.e., energy above threshold. In their

Table 3.3

Relative† Intensities of γ-rays from $^{70}Zn(p,n\gamma)^{70}Ga$

E_p	2.1	2.4	2.6	2.8	3.2	3.6	3.8	4.2	4.4	4.6	5.0
E_x(max)	.7	1.0	1.2	1.4	1.8	2.2	2.4	2.8	3.0	3.2	3.6
E_γ(keV)											
139.7						.42	.33	.35	.30	*	*
154.7				.52	1.3	8.2	2.2	3.2	5.1	*	*
170.8										*	*
187.6			1.7	2.6	5.7	22	8.9	14	26	*	*
201											
209.6					.28	.57	.54		1.1	.83	.93
234.8					.93	1.36	1.32	1.14	1.41	1.09	1.34
238.8					.17	.21	.21	.19	.29	.15	.24
245.4						*					
267.6					.13	.23	.28	.20	.31	.25	.27
292.5							.04	.08	.11	.09	.16
316.2					.18	.71	.94	1.0	1.1	1.2	*
318.7		3.3	3.3	4.9	8.1	9.7	9.1	9.2	13	11	17
326.7					.17	.27	.53	.49	.30	*	*
344.6			.39	1.0	1.7	1.4	1.2	.98	1.2	.80	.76
364.0			1.9	3.9	6.0	4.4	3.5	2.6	2.8	1.9	1.8
374.3					1.0	1.8	2.0	2.9	4.7	4.4	7.6
377.6						.37	.46	.41	.97	*	*
389.6	10	1.7	.9	.85	.42	.32	.24	.26	.32	.40	.51
393.2			.24	.36	.91	1.5	1.7	2.6	3.8	4.4	7.6
410.7				.22	.42	.70	.63	.81	1.1	.93	1.3
417.4						.11	.13	.29	.31	.22	*
426.8					.31	.67	.73	.95	1.16	.98	1.3
430.5						.78	.21	.17	.21	.14	.12
444.5					.89	1.04	.90	.98	1.1	.94	.89

(continued next page)

Table 3.3 (continued)

E_p	2.1	2.4	2.6	2.8	3.2	3.6	3.8	4.2	4.4	4.6	5.0
E_x (max)	.7	1.0	1.2	1.4	1.8	2.2	2.4	2.8	3.0	3.2	3.6
E_γ (keV)											
450.0						*					
487.5		3.4	2.3	3.0	2.9	2.8	2.5	2.4	2.6	2.1	2.4
508.1		.35	.32	.33	.34	.33	.33	.35	.43	.40	
516.1				.15	.24	.28	.24	.26	.26	.28	.32
520.4						*		*	*	*	*
527.7						*	.17	.40	.50	.42	
532.6						*			*	*	*
554.3					.57	.96	1.2	1.5	*	1.8	2.3
572.1							.25	.22	.24	*	.22
585.1					.07	.10	.19	.34	.31	.34	.89
596.1						*					
598.6						*					
612.9							.18	.20	.34	.29	.43
617.5			*	*	*	*	*	*	*	*	*
632.2				1.2	2.4	2.1	1.6	1.5	1.6	1.2	1.2
636.7						*		*	*	*	*
645.7											
651.1	13	55	24	24	21	14	12	8.9	10	9.9	7.3
655.8								*	*	*	*
669.3							.08	.10	.14	.10	.11
681.9									.20		
690.9	7.2	14	17	22	23	33	20	22	27		
708.7			*	*							
722.5						*					
755.0				.11	.60	1.0	.85	.88	1.1	.86	1.1
794.8						.19	.21	.17	.21	.20	.26
798.6					.30	.80	.77	.71	.97	.70	.77
803.7			*	*	.05	.26	.19	.18	*	*	*

(continued next page)

Table 3.3 (continued)

E_p	2.1	2.4	2.6	2.8	3.2	3.6	3.8	4.2	4.4	4.6	5.0
E_x(max)	.7	1.0	1.2	1.4	1.8	2.2	2.4	2.8	3.0	3.2	3.6
E_γ(keV)											
827.4		.17	.08	.08	.29	.79	.79	.73	.77	.60	.65
851.0					.48	.82	.98	1.0	.10	.91	1.0
867.1					.13	.34	.30	.35	.43	.29	.22
881.7						*					
904.8							.19	.22	.26	.27	.27
930.8							.10	.19	.11	.07	.03
948.3						.10	.13	.16	.16	.27	.17
962.4		.70	.12	.19	.12	.09	.03	.07	.07	.12	.18
970.1							.05	.09	.11	.09	.10
982.3						.20	.17	.19	.25	.16	.13
995.7			.19	.88	1.3	1.1	1.1	.97	1.1	.79	.86
1000.6						.48	.15	.27	.36	.27	.26
1010.2						1.5	.48	.66	.88	.78	.98
1023.8					.06	.06	.04	.05	.06	.07	.03
1044.6						*	*	*	*	*	*
1047.7						*	*	*	*	*	*
1125.4						.48	.60	.61	.64	.50	1.19
1135.3				13	3.7	3.9	3.5	3.2	3.7	2.9	3.8
1140.4				1.8	3.5	3.1	3.7	2.7	2.5	1.8	2.0
1173.0						.06	.11	.27	.33	.37	.30
1203.5				.40	1.3	1.5	1.4	1.3	1.6	1.2	1.3
1212.1						.05	.10	.17	.29	.20	.27
1227.9							.06	.11	.17	.12	.18
1244.5				2.6	1.8	2.3	2.1	1.8	2.1	1.7	2.0
1286.2						.07	.11	.20	.24	.17	.15
1307.0					.41	.68	.54	.70	.68	.59	.61
1312.0					1.9	2.4	2.4	1.9	2.0	.59	1.6

(continued next page)

Table 3.3 (continued)

E_p	2.1	2.4	2.6	2.8	3.2	3.6	3.8	4.2	4.4	4.6	5.0
E_x (max)	.7	1.0	1.2	1.4	1.8	2.2	2.4	2.8	3.0	3.2	3.6
E_γ (keV)											
1359.7					.47	.89	.82	1.3	1.9	1.2	2.1
1445.9					.68	1.4	1.4	1.3	1.3	*	*
1502.0					.23	.64	.65	.56	.62	.39	.37
1518.3					.27	.67	.77	.91	1.1	.77	.88
1533.1					.04	.30	.38	.39	.55	.43	.56
1552.9					.06	.17	.23	.28	.32	.23	.26
1620.9					.37	.94	1.1	1.2	1.4	1.1	1.3
1725.0						.11	1.7	.28	.43	.34	.57
1794.2						.14	.21	.35	.45	.33	.39
1808.0						.16	.28	.38	.46	.32	.31
1865.3						.07	.17	.50	.70	.62	.79
1905.0						.02	.10	.25	.35	.28	.36
1931.0						.07	.15	.33	.46	.33	.41
1981.9			.14	.10	.06	.07	.07	.11	.09	.07	.07

* There was evidence for the peak but an intensity could not reliably be extracted.

† Ratio of the area for a given γ-ray peak to that for the 885 keV ^{70}Zn Coulomb excitation line. No corrections for the variation of detector efficiency with E_γ have been made. For some of the γ-rays a 0.9 cm^3 counter was used.

paper they assigned spins by comparing cross sections with Hauser-Feshbach calculations. In such an experiment, thin targets are required in order to obtain the energy resolution necessary to separate the individual neutron groups. Since the theory assumes a statistical average over states in the compound nucleus, it is then necessary to average the results of several spectra at closely spaced proton energies. Another source of difficulty in applying the Hauser-Feshbach theory is the presence of isobaric analog resonances in the (p,n) reaction. Cross sections measured at such resonances will not reflect the purely statistical averaging of states required by the theory. Resonances in the $^{70}Zn(p,n)^{70}Ga$ reaction may occur in the range of proton energies used for the yield function measurements.

These difficulties may be solved, in part, by observing the γ-rays produced in the (p,n) reaction. Thick targets may be used to obtain the necessary statistical averaging in the compound nucleus, with no loss in the energy resolution. The superior resolution of Ge(Li) counters enables the measurement of very weakly populated levels. The total γ-ray yield from a level (properly, this must be corrected for indirect feeds from other levels) is proportional to the (p,n) cross section, and may then be related to the spin of the level. This requires, however, that the absolute efficiency of the Ge(Li) counters be known. This difficulty may be overcome by measuring the yield of γ-rays from a level as a function of the beam energy. As shown by Bass and Stelson, the (p,n) yield functions are characteristic of the spin of the level. Effects due to isobaric analog resonances will then appear at isolated points on these yield functions. Since the γ-ray energy is, of course, independent of the beam energy, it is unnecessary to make any efficiency correction as is required when the neutrons are counted.

Examination of the data in Table 3.3 shows that the yield functions, except for minor fluctuations at some of the beam energies, fall into distinct families. In particular, the 508 keV γ-ray from the state at 508 keV (which has spin 2, as will be shown in the next section) follows the Coulomb excitation cross section closely throughout the entire range of energies used, whereas the yield of the 651 keV γ-ray (from the spin 1 state at 651 keV) drops by a factor of $\sim$ 7 in the same energy range. In contrast, the yield of the 393 keV γ-ray from the level at 902 keV (spin 4) rises steeply, gaining a factor of approximately 30 in the same energy range.

The data of Table 3.3 are presented graphically in Fig. 3.5 for the lower lying levels of ^{70}Ga. The curves for the 508, 651 and 691 keV γ-rays are the yield functions after the contributions from indirect feeding have been removed. For this, of course, it is necessary to know the efficiency of the detector at different E_{γ}. The experimental curves are

Figure 3.5

Relative yield functions for γ-rays from $^{70}Zn(p,n\gamma)^{70}Ga$. Shown also are relative yield functions taken from the Hauser-Feshbach calculation of Bass and Stelson (1970) and normalized to the 508 keV yield function for J=2. The yield functions for the 508, 651 and 691 keV levels have been corrected for indirect feeds.

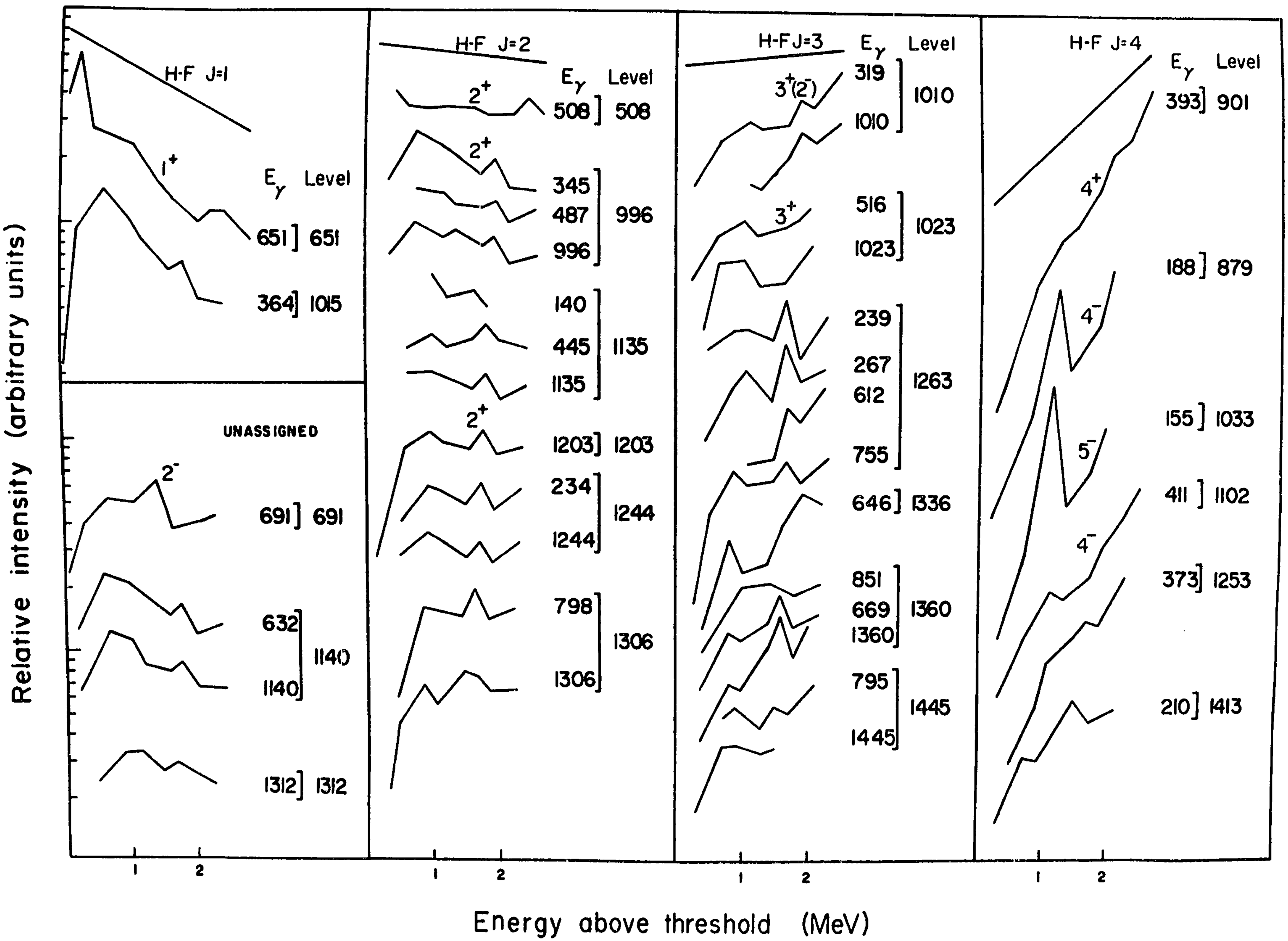
H-F J=1
1+
Eγ Level
651] 651
364] 1015
UNASSIGNED
2-
691] 691
632
1140
1140
1312] 1312
H-F J=2
Eγ Level
2+
508] 508
2+
345
487
996
996
140
445
1135
1135
2+
1203] 1203
234
1244
1244
798
1306
1306
H-F J=3
Eγ Level
3+(2-)
319
1010
1010
3+
516
1023
1023
239
267
612
755
1263
646] 1336
851
669
1360
1360
795
1445
1445
H-F J=4
Eγ Level
393] 901
4+
188] 879
4-
155] 1033
5-
411] 1102
4-
373] 1253
210] 1413
1
2
Relative intensity (arbitrary units)
Energy above threshold (MeV)

grouped into four categories, corresponding to the relative theoretical yield functions for J = 0 or 1, 2, 3 and 4 or greater. These theoretical curves, which are taken from the calculations of Bass and Stelson (1970) for the $^{68}Zn(p,n)^{70}Ga$ reaction, have been readjusted in order to make the spin 2 curve agree with the experimental yield of the 508 keV γ-ray. It is seen that the levels of known or inferred spin (these spin assignments will be discussed in the next two sections) at 651, 691, 879, 902, 996, 1010, 1023, 1033,1102 and 1203 keV support the theoretical predictions. The grouping of the other excitation functions was made on the basis of the general visual appearance of the curves. The classification according to spin should therefore be regarded as only qualitative.

3.5 γ-Ray Angular Distributions

The conditions for alignment of a nucleus described in Chapter I may be met in a reaction such as $^{70}Zn(p,n\gamma)^{70}Ga$, even if the outgoing neutrons are not detected. If the proton beam energy is just above threshold, the emerging neutrons will mainly have orbital angular momentum $\ell=0$. The residual nucleus will then have an angular momentum component along the beam direction due only to the intrinsic spins of the proton and neutron since the target has spin 0. The angular distributions of γ-rays emitted from these aligned nuclei are then sensitive to the initial and final spins and the mixing ratios of the transitions. This section will describe the measurement of angular distributions of γ-rays from ^{70}Ga produced in the $^{70}Zn(p,n\gamma)^{70}Ga$ reaction. Experimentally, "just above" threshold means from $\sim$ 100 keV to several hundred keV above threshold.

For the early angular distribution runs oxide targets were glued onto carbon backings. As these targets appeared to deteriorate under beam conditions, metallic targets for the later experiments were prepared by vacuum evaporation onto aluminum backings. In the latter case, the 511 keV contaminant line was reduced markedly, probably due to the decreased amount of handling.

A special target chamber was constructed to facilitate the measurement of the angular distributions. Figure 3.6 is a schematic of the apparatus, which has the following features. Two sets of beam defining slits were located 18" apart along the beam axis. Each of these consisted of four electrically isolated tantalum sectors to allow individual reading of beam currents, thus facilitating the steering of the beam through the small apertures. The straight line defined by the slit apertures constrained the beam to remain in the same spot of the target throughout the duration of the run. The entire chamber and slit holder was constructed of glass to electrically insulate the target and slits and to provide the desirable feature of allowing the experimenter to

Figure 3.6

Schematic of the target chamber used in the $^{70}Zn(p,n\gamma)^{70}Ga$ angular distribution measurements.

(a) metal "V" seal, with cooling water inlets

(b) removeable target holder

(c) glass chamber and slit container

(d) rear slits, showing isolated sectors

(e) insulating tube and slit current lead retainer

(f) slit current lead

(g) isolated stainless steel guide tube

(h) front slits, showing isolated sectors

(i) composite view of chamber, and slits in supporting frame.

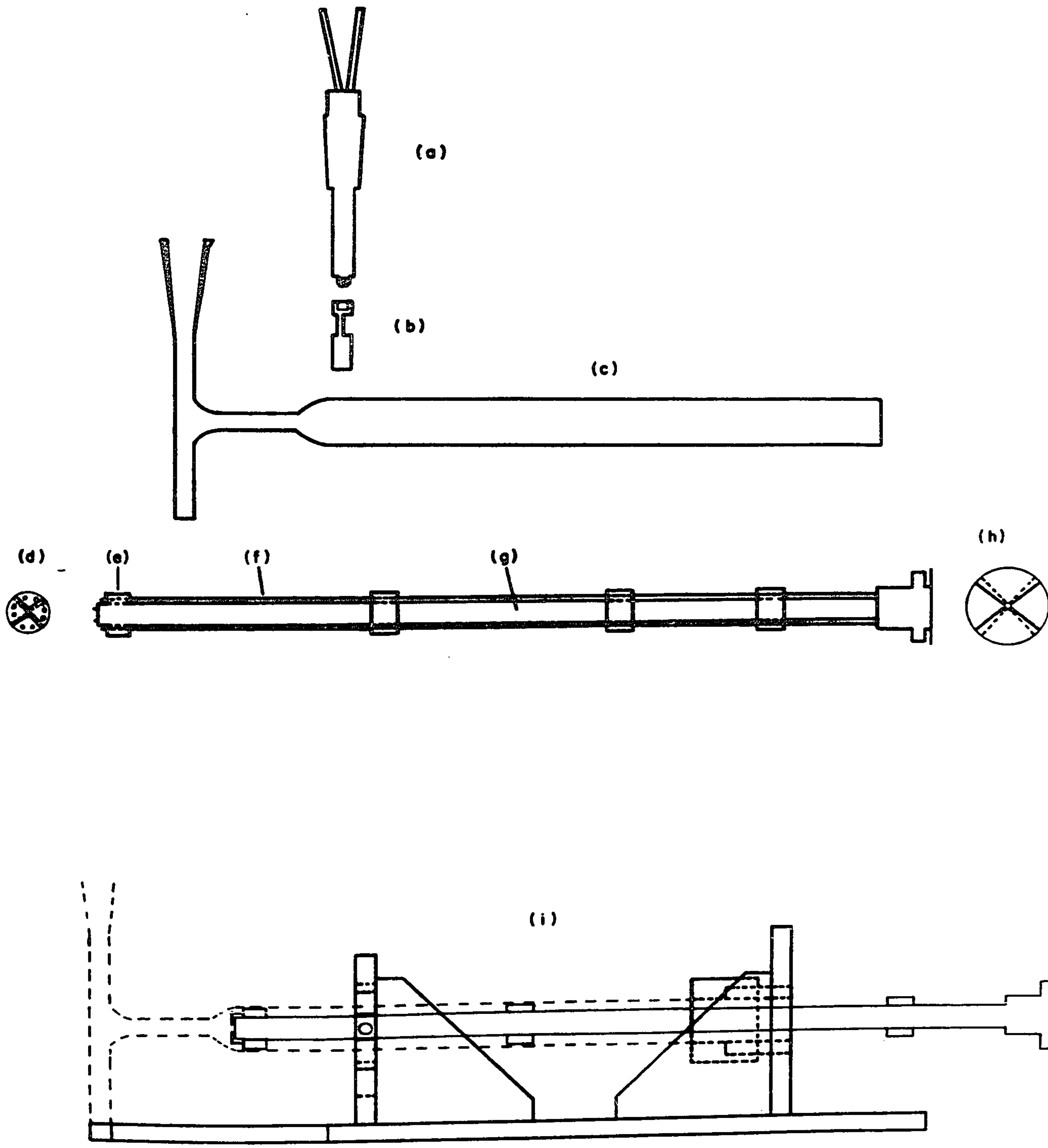
(a)
(b)
(c)
(d)
(e)
(f)
(g)
(h)
(i)

observe the target under experimental conditions. The target chamber is a .43" diameter pyrex tube, with .060" thick walls. The thin walls and low Z material of the chamber combine to permit the detection of very low energy γ-rays with minimum absorption. Because of the small diameter of the chamber, the Ge(Li) counters can be placed so as to subtend large solid angles. This is also an advantage in coincidence experiments where the true-to-chance ratio increases with detector solid angle. The target holder assembly consisted of a ground glass joint, to which is attached the target backing. The target holder could be water cooled if necessary. The target backing consisted of a semi-cylindrical piece (the choice of material depending on the experiment) so that combined with the cylindrical symmetry of the target chamber, absorption effects would then be made isotropic for one quadrant. Only one quadrant is required to measure the angular distribution provided unpolarized targets and beams are used as in this experiment.

The apparatus was tested with the $^{55}Mn(p,n\gamma)^{55}Fe$ reaction using the isotropic γ-ray de-exciting the spin 1/2 state at 440 keV. A small experimental anisotropy was observed due to a slight movement of the detector mounts. When the angular distributions of γ-rays from low-lying levels in ^{70}Ga were measured with the same experimental configuration, it was found that within statistical error the 651 keV line had the same small anisotropy. It is concluded therefore that the 651 keV line is isotropic. This was verified in further experiments on the K N accelerator in which more rigid detector mounts were available. Subsequently, to avoid errors due to possible target deterioration, the intensities of all other lines in ^{70}Ga were measured relative to the 651 keV line in the angular distribution measurements.

Angular distributions were measured at proton energies of 2.26, 2.44 and 2.75 MeV. The data were fitted to the function

$$W(\theta) = A_0 + A_2P_2(\cos\theta) + A_4P_4(\cos\theta)$$

and the coefficients A_0, A_2 and A_4 were extracted by least squares analysis.

The normalized angular distribution coefficients $a_2 = A_2/A_0$ and $a_4 = A_4/A_0$ are given in Table 3.4 for the highest bombarding energy. These have been corrected for the finite size of the counters used in the experiment such that

$$W(\theta) = \sum_{K\ \text{even}} Q_K\, A_K\, P_K\, (\cos\theta).$$

The attenuation coefficients Q_K used in this analysis are

$$Q_2 = .97$$
$$Q_4 = .95$$

as calculated according to the technique of Smith (1962). To obtain the areas of each of the lines in the spectra, the peaks were fitted to a convoluted Gaussian-plus-exponential

Table 3.4

Legendre coefficients, corrected for solid angle effects, fitted to angular distributions of γ-rays de-exciting levels in ^{70}Ga at $E_p = 2.75$ MeV

E_γ (keV)	a_2	a_4
155	-.16±.04	.00±.05
188	.19±.02	-.04±0.2
319	-.12±.01	.00±.01
345	-.19±.02	-.02±.03
364	.00±.01	.00±.01
373	-.15±.04	.01±.04
393	.31±.04	-.10±.04
411	.50±.03	-.13±.04
487	.18±.02	-.04±.02
508	-.11±.01	.00±.01
516	-.25±.04	.04±.04
631	.01±.03	-.03±.04
651[a]	.02±.02	-.01±.02
691[a]	-.24±.03	.07±.03
691[b]	-.17±.02	.02±.02
691	-.11±.01	-.01±.02
996	-.32±.05	.02±.06
1137	-.01±.04	.06±.04
1140	-.02±.03	.03±.04
1203	-.27±.02	-.03±.03

a) $E_p = 2.26$ MeV

b $E_p = 2.44$ MeV

function using the Chalk River computer routine JAGSPOT (Williams and McPherson 1968).

As described in Chapter I, the theoretical angular distributions of γ-rays may be expressed in terms of the population parameters, the mixing ratio δ, and the spin sequence. A linear least squares fit of the theoretical distribution to the experimental data is made for a discrete set of values of δ, and the population parameters $P(m)$, for each spin sequence. The best fit corresponds to the minimum in the value of χ^2 given by

$$\chi^2 = \frac{1}{n} \sum_i \left[W_{exp}(\theta_i) - W(\theta_i)\right]^2 / \Delta^2(\theta_i)$$

in which $\Delta(\theta_i)$ is the uncertainty assigned to the γ-ray yield, $W_{exp}(\theta_i)$, at angle θ_i. $W(\theta_i)$ is the theoretical yield and n is the number of degrees of freedom (number of data points minus the number of free parameters in $W(\theta)$). Since δ varies between $-\infty$ and $+\infty$, it is more convenient to use $\tan^{-1}\delta$ as a parameter.

Estimates for the population parameters were obtained from Hauser-Feshbach calculations for the reaction, using the computer program MANDY (Sheldon et al, 1971). The penetrabilities for the incoming and outgoing particles were calculated with DWUCK which evaluates the partial wave scattering amplitudes

$$\psi_{\ell,m_j} \sim u_{\ell,m_j} + i\, v_{\ell,m_j}$$

in the presence of the Coulomb and optical model potentials of the nucleus. The optical model parameters used in this calculation are listed in Table 3.5 and are due to Perey et al (1968) for the protons and Wilmore et al (1964) for the neutrons. If the optical model potential contains no spin orbit term, then $\psi_{\ell,m_j} = \psi_{\ell,-m_j} = \psi_\ell$. The penetrabilities are obtainable from the relation (Smith 1965)

$$T_\ell = 4(v_\ell - u_\ell^2 - v_\ell^2).$$

The population parameters for spin 2 calculated using these penetrabilities were in complete agreement with the values corresponding to the minimum χ^2 for the observed distribution of the 508 keV γ-ray. The P(m)'s calculated by MANDY were quite insensitive (for $m \leq J$) to the spin and were allowed to vary, in the χ^2 search, over the ranges given in Table 3.6. The parameters in this table correspond to a proton energy between 200 and 600 keV above threshold. P(m) was set equal to zero for $m \geq 4$. It is expected to be very small in any case.

The value for χ^2 is minimized over this range in the population parameters, and this minimum is plotted as a function of $\tan^{-1}(\delta)$. A typical result is shown in Figure 3.7. Spin sequences for which χ^2 falls below the 0.1% confidence limit are accepted as possible solutions. Table 3.7 summarizes the spins and mixing ratios which produced acceptable minima. Not included in this table are spin sequences

Table 3.5

Optical model parameters used in the calculation of the neutron and proton penetrabilities in the reaction $^{70}Zn(p,n\gamma)^{70}Ga$

	V_S	r_{OS}	a_S	r_{OI}	a_I	$4W_D$
Protons	$61.0-.5\ E_p$	1.28	.66	1.30	.51	4.0
Neutrons	$47.0-.3\ E_n$	1.32	.66	1.26	.48	5.0

where

$$V(r) = U_C(r) - V_S(1+e^x)^{-1} + i4W_D \frac{d}{dx'} (1+e^{x'})^{-1}$$

$$x = a_S^{-1}(r-r_{OS}\ A^{1/3})$$

$$x' = a_I^{-1}(r-r_{OI}A^{1/3})$$

Table 3.6

Population parameter limits used in the analysis of γ-ray angular distributions from $^{70}Zn(p,n\gamma)^{70}Ga$

m	Start	Stop
0	.30	.46
1	.20	.28
2	.03	.080
3	.0	.020
4	.0	.0

Figure 3.7

Angular distributions and best fits for γ-rays de-exciting the 996 keV level in ^{70}Ga.

χ^2 vs $\tan^{-1}\delta$ for the γ-rays de-exciting the 996 keV level in ^{70}Ga.

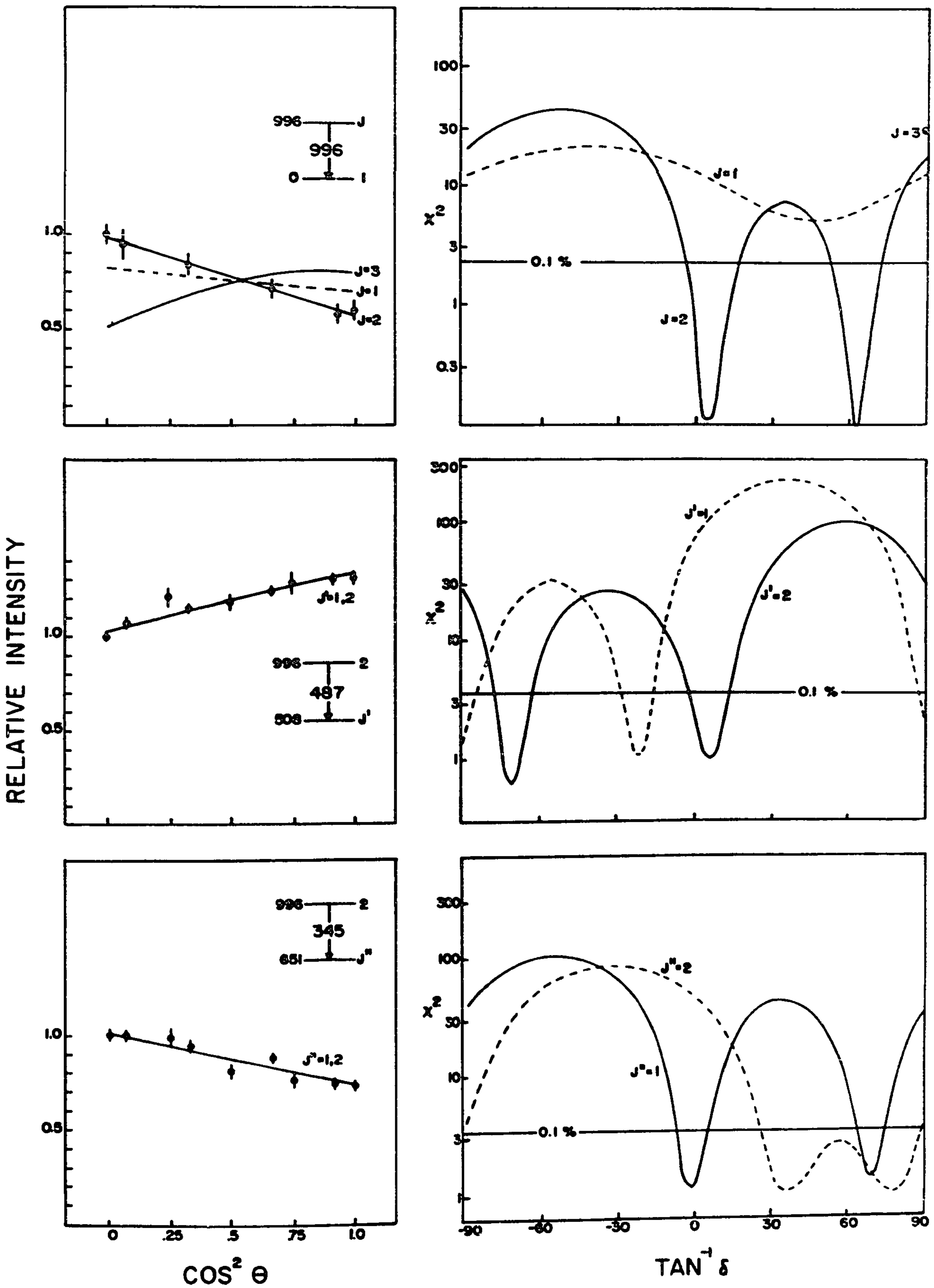
RELATIVE INTENSITY
COS² Θ
TAN⁻¹ δ
χ²
996
0
J
1
J=3
J=1
J=2
0.1 %
J'=1,2
998
2
487
508
J'
J'=1
J'=2
345
651
J"
J"=1,2
J"=2
J"=1

Table 3.7

Values of the mixing ratio and the spin sequences producing acceptable minima in χ^2 for γ-rays in ^{70}Ga

E_γ	E_i-E_f	I_i-I_f	$\tan^{-1}\delta$ (degrees)
155	1033-879	5-4	-4±6
188	879-691	4-2	90
319	1010-691	2-2	28±5
			86±5
		3-2	-6±2
345	996-651	2-1	-2±6
			69±4
		2-2	55±30
364	1015-651	1-1	10±10
			80±10
		2-1	-12±3
			81±3
		1-2	4±20
			70±20
		2-2	18±4
			-84±4
373	1252-879	5-4	-4±6
		4-4	35±10
		3-4	-4±8
393	901-508	4-2	90
		3-2	-21±4
		2-2	-4±10
			-62±10
411	1101-691	4-2	90
487	996-508	2-2	5±7
			-71±7

(continued next page)

Table 3.7 (continued)

E_γ	E_i-E_f	I_i-I_f	$\tan^{-1}\delta$ (degrees)
508	508-0	2-1	-7±3
			75±3
516	1024-508	3-2	-2±6
			74±6
		2-2	36±12
			75±12
		1-2	-50±35
632	1140-508	3-2	-10±5
		2-2	-84±11
			18±10
		1-2	0±90
651	651-0	2-1	-12±3
		1-1	7±6
			84±6
691	691-0	2-1	-6±3
			74±3
		1-1	45±10
996	996-0	2-1	4±8
			63±8
1137	1137-0	2-1	-12±6
			81±6
		1-1	5±30
			85±30
1140	1140-0	2-1	-12±6
			81±6
		1-1	10±22
			80±30
1203	1203-0	2-1	3±5
			64±5

which produce acceptable minima but are eliminated by other considerations (such as neutron transfer ℓ-values, or angular distribution data for other γ-rays).

For some of the γ-rays, more than one spin sequence produces an acceptable minimum. This usually occurs for those angular distributions with $a_2 \approx -0.1$. In this case, all that can usually be said is that $\Delta J = 0$ or 1. If more stringent requirements could be imposed on the population parameters, the ambiguity could be resolved in some cases. Another solution would be to detect coincidences between neutrons emitted at 0° and the γ-rays. In this case $\ell_n = 0$ (and hence $m_{\ell_n} = 0$) and only the $m = 0$ and 1 nuclear substates would be populated leading to larger asymmetries than are observed when the neutron is not detected.

Of particular interest is the 155-188-691 keV cascade, de-exciting levels at 1033, 879 and 691 keV. As described in the previous chapter, ℓ=4 (d,p) strength for the level at 1034 keV requires its spin to be 6^- or at least 5^-. This level decays to the 879 keV state by means of the 155 keV γ-ray whose angular distribution requires that the spin change involved is 1 or less. This forces the spin of the 879 keV level to be 4 or greater, with negative parity. This spin assignment is supported by the yield function data for the 188 keV γ-ray. The angular distribution of the 691 keV γ-ray indicates that the spin of this level is 2 or 1, the parity not being determined from the particle work. The angular distribution of the 188 keV γ-ray could not be fitted satisfactorily for the spin sequence 4 to 2 within the population parameter range given in Table 3.6, although the signs of a_2 and a_4 are consistent with a spin 4 assignment for the 879 keV level. The observed angular distribution appears to be attenuated by comparison with the expected E2 pattern. At the time this thesis was being written, the lifetime of the 879 keV state became known (Carlson 1972). The reported lifetime of 28 nsec is consistent with an E2 assignment for the 188 keV transition. In this case theangular distribution for the 188 keV γ-ray will be attenuated due to extra nuclear perturbation. When the attenuation coefficients G_2 and G_3 (section 1.3f) are allowed to vary, acceptable agreement is obtained for G_2 = .50 and G_4 = .24.

This surprising occurrence of a negative parity J=2 state this low in excitation cannot be explained in terms of the lowest neutron configurations in ^{70}Ga

$$|\pi p_{3/2}{}^3;\ \nu(p_{3/2},\ f_{5/2},\ p_{1/2})^{10}_{v=0}\ g_{9/2}{}^1\rangle .$$

The very weak strength for the 691 keV state in both the (d,p) and (d,t) experiments suggests an excited proton configuration for this level, for example

$$|\pi\ p_{3/2}{}^2\ f_{5/2}\ ;\ \nu\ p_{3/2}{}^4\ f_{5/2}{}^6\ p_{1/2}{}^0\ g_{9/2}{}^1\rangle ,$$

or a higher seniority configuration. The negative parity assignment for the 691 keV level merits further experimental verification as described in the next section.

3.6 γ-Ray Linear Polarizations

The measurement of γ-ray linear polarization in conjunction with γ-ray angular distribution yields, in many cases, unambiguous parity assignments. In addition, measurements of this nature can resolve ambiguities in spin assignments not settled by the angular distribution data alone. Since the population parameters of the excited state can usually be eliminated from the analysis, such a study has the desirable feature that it does not depend on any assumptions about the mechanism of the reaction.

Beams of 2.75 MeV protons from the KN accelerator were used in the $^{70}Zn(p,n\gamma)^{70}Ga$ reaction to excite levels in ^{70}Ga. The target and scattering chamber were identical to those used in the angular distribution measurements.

The resulting γ-rays were detected with two Ge(Li) detectors. Angular distributions were measured with a large (37 cm^3) coaxial detector in the angular range from 0° to 90° to the incoming beam. A small planar crystal of dimensions 6×3.5×.65 cm and resolution 5.4 keV at 1.3 MeV was used as a Compton polarimeter and was placed at 90° opposite the angular distribution detector, 16 cm from the target.

The polarimeter is sensitive to the linear polarization of a γ-ray because of the fact that Compton scattered

γ-rays are emitted preferentially in the plane perpendicular to the incident electric vector. For $E_\gamma \gtrsim 500$ keV the major contribution to the full energy peak of a Ge(Li) detector arises from events where the incident γ-rays are first Compton scattered and then totally absorbed in the crystal. Thus, a thin planar detector will give a larger full energy peak when its plane is perpendicular to the electric vector. Denoting the respective yields as $N_{||}$ and $N_{\perp}$, the experimentally determined asymmetry is given by

$$S = \frac{N_{||} - N_{\perp}}{N_{||} + N_{\perp}} \quad .$$

This is related to the polarization described in section 1.3d,

$$P = \frac{W(\theta,\eta=0°)-W(\theta,\eta=90°)}{W(\theta,\eta=0°)+W(\theta,\eta=90°)}$$

by the relation

$$P = -\frac{S}{R}$$

where R is the asymmetry which would be observed for a γ-ray completely polarized perpendicular ($P = -1$) to the plane containing the γ-ray and the quantization axis. R is thus a measure of the sensitivity of the detector to the linear polarization. The polarimeter is described more fully by Ewan et al (1969) and Litherland et al (1970).

Due to the low efficiency of the polarimeter, measurements could be made only on the two strongest γ-rays from ^{70}Ga, at 651 and 691 keV. The resolution of the polarimeter was not sufficient to resolve the 508 keV peak from the 511 annihilation peak so that the polarization of the 508 keV γ-ray could not reliably be measured.

The sensitivity R of the detector used in these experiments has been measured by Baxter et al (1970) using γ-rays, of known polarization, ranging in energy from 1.2 to 2.1 MeV. The sensitivity may be extrapolated to $E_\gamma \simeq 650$ keV using as a rough guide the energy dependence of R expected from the Klein-Nishina formula (Baxter et al 1970). At lower energies however, photoelectric absorption, which shows no asymmetry, is expected to contribute to the total absorption peak and thus attenuate the observed sensitivity R. The sensitivity adopted in this experiment is $R = -.12$, but this must be regarded as only a rough estimate.

The angular distribution of the 691 keV γ-ray was obtained at the same time as the polarization measurements were taken. Two spectra were taken at each position of the moveable counter, corresponding to the plane of the polarimeter parallel, then perpendicular, to the reaction plane. The 651 and 691 keV peaks in the polarimeter were normalized to the 651 keV peak in the moveable counter.

Table 3.8 gives the experimental results for the 651 and 691 keV γ-rays. Also listed are the theoretical polarizations for each spin and mixing ratio permitted by the angular distribution data. In these calculations errors in

Table 3.8

Theoretical and experimental polarizations for the 651 and 691 keV γ-rays in ^{70}Ga.

E_γ	J_i^π	$\tan^{-1}\delta$ (deg.)	P_{theor}	P_{exp}
651	0^+	0	0	.35±.11
	1^+	7±6	.20±.12	
		84±6	.21±.11	
	2^+	-12±6	-.41±.05	
		81±6	.31±.05	
691	2^+	-6±3	-.28±.04	.23±.05
		74±3	.24±.04	
	2^-	-6±3	.28±.04	
		74±3	-.24±.04	

the polarization sensitivity R are not included. Unfortunately, no absolute assignments are possible. If one accepts the argument that large E2/M1 mixing ratios are unlikely (this will be discussed in greater detail in the next chapter) the conclusions are:

651 keV $1^+ \rightarrow 1^+$ $\delta = .12 \pm .10$

691 keV $2^- \rightarrow 1^+$ $\delta = -.11 \pm .05.$

CHAPTER IV

DISCUSSION

4.1 The Level Scheme of ^{70}Ga

A proposed level scheme based on the experimental work described in Chapters II and III is shown for the low lying levels of ^{70}Ga in Fig. 4.1. Energy levels and gamma ray transitions for excitations up to 2 MeV are given in Tables 2.1 and 3.1 respectively. All levels in the scheme are the result of an observation in at least one of the following reactions*:

^{69}Ga(d,p)^{70}Ga - for at least two angles
^{71}Ga(d,t)^{70}Ga - for at least two angles
^{69}Ga(n,γ)^{70}Ga - observation of capture γ-ray
^{70}Zn(p,n)^{70}Ga - observation of neutrons in time of flight

With the exception of the levels at 1287, 1414, 1598, 1695, 1726, and 1844 keV, all the levels ascribed to ^{70}Ga have been observed in either the (d,p) or (d,t) experiments or both. There is no support for the 188 and 448 keV levels proposed by Rester et al (1966), nor is the 20 ms isomer explained by the scheme.

*The references for the (n,γ) and (p,n) reactions are given in Table 2.1.

Figure 4.1

Level scheme for ^{70}Ga. The levels have been classified with positive parity states on the left and those with negative parity on the right. The parities of the states in the middle column are unknown.

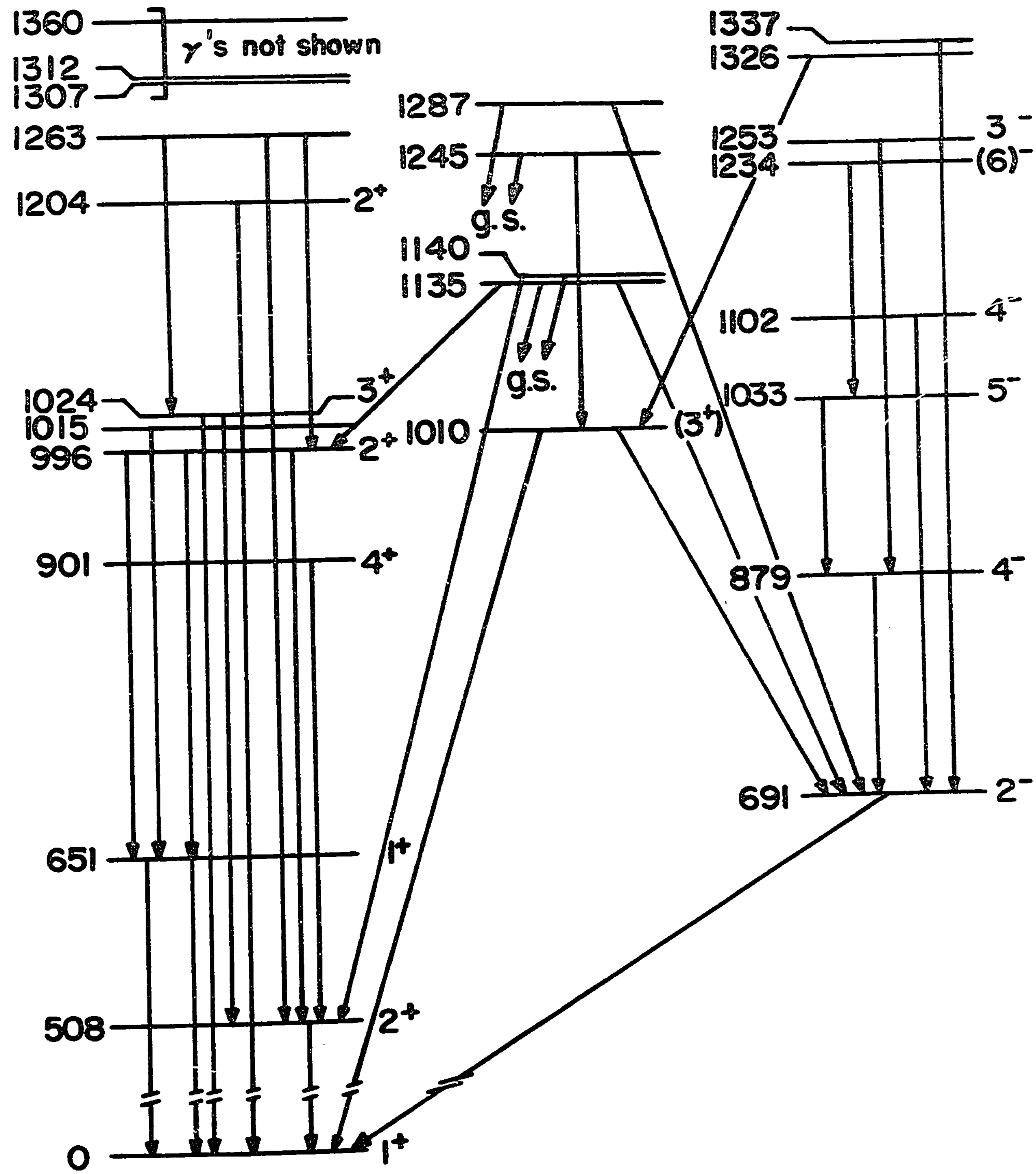
1360
1312
1307
γ's not shown
1263
1204
2+
1024
3+
1015
996
2+
901
4+
651
1+
508
2+
0
1+
1287
1245
g.s.
1140
1135
g.s.
1010
(3+)
1337
1326
1253
3-
1234
(6)-
1102
4-
1033
5-
879
4-
691
2-

$^{70}_{31}Ga_{39}$

Transitions ascribed to ^{70}Ga are listed in Table 3.1. Strong γ-rays have been placed by at least one coincidence observation. Weaker γ-rays not seen in the coincidence spectra have been placed when the energy fit was well within experimental error. In addition, the relative yield functions for all γ-rays emitted from a given level are the same over the range of proton energies used in these experiments, E_p = 2.1 - 5.0 MeV. Two exceptions to this rule are the γ-rays at 319 and 487 keV which appear below the threshold for production in ^{70}Ga. However, both γ-rays have been observed in coincidence, and at higher proton energies, follow the excitation functions of the other γ-rays emitted from the same respective energy levels.

The most striking feature of the energy levels is the large gap of 508 keV between the ground state and the first excited state. From shell model considerations it is expected that the lowest levels of ^{70}Ga would involve the configuration $\pi p_{3/2}{}^{3}\ \nu p_{3/2}{}^{4}\ f_{5/2}{}^{6}\ p_{1/2}{}^{1}$ which gives rise, in the lowest seniority, to levels with spin and parities 1^+ and 2^+. In the zero range approximation for the residual nucleon-nucleon interaction these levels are expected to be degenerate, the degeneracy being removed by perturbations from other levels of the same spins. Splittings of $\sim$ 200 keV are observed in ^{90}Y, for example, (Watson et al 1963).

Another interesting feature of the energy levels is the occurrence of the $J^{\pi} = 2^{-}$ level at 691 keV. As explained in Chapter III, negative parity states with spins from 3 to 6 may be formed by exciting a neutron to the $g_{9/2}$ orbit and coupling it with the $(p_{3/2}{}^{3})_{3/2}$ proton configuration. A $J^{\pi} = 2^{-}$ state requires either the promotion of a proton to the $f_{5/2}$ orbit, or higher seniority in the neutron configuration. Both of these require additional energy and it is surprising therefore that this state is the lowest negative parity state.

4.2 Spin-Parity Assignments

Treating ^{56}Ni as a closed core, the 3 active protons and 11 active neutrons in ^{70}Ga are expected to occupy the $2p_{3/2}$, $1f_{5/2}$, $2p_{1/2}$, $1g_{9/2}$ and $2d_{5/2}$ orbits. By performing either a (d,p) or (d,t) experiment on targets of ^{69}Ga and ^{71}Ga respectively ($J^{\pi} = 3/2^{-}$) and by observing the resultant ℓ transfers, the following restrictions may be placed on the spins and parities of the levels:

ℓ	J_{min}	J_{max}	π
1	0	3	+
3	1	4	+
1 + 3	1	3	+
2	1	4	−
4	3	6	−
2 + 4	3	4	−

The levels in Fig. 4.1 are classified according to parity. Other states, involving proton excitations, will be seen weakly in the neutron transfer reactions. At higher excitation, levels may also be populated with the transfer of $s_{1/2}$ or $g_{7/2}$ neutrons.

From the analysis of the γ-ray angular distribution work, summarized in Table 3.7, it can be seen that for most of the γ-rays, there are several spin sequence - mixing ratio combinations that produce acceptable agreement with theory. The Weisskopf reduced widths may be used to estimate the ratio of E2 and M1 rates. For A = 70 and E_γ = 500 keV this is 1.6×10^{-4}, which is probably reliable only to within an order of magnitude. Thus, E2/M1 transitions with $\delta \gg .13$ ($\tan^{-1}\delta = 8^\circ$) are very improbable in ^{70}Ga below 1 MeV. Above 1 MeV, collective excitations may occur, resulting in enhanced E2 rates. For the M2/E1 case, even smaller mixing ratios are expected. Using this as a rough guideline, many of the previously acceptable possibilities may be removed from Table 3.7.

In thermal neutron capture, primary transitions with dipole character are by far the most probable. The levels observed to be directly populated from the 1^- or 2^- capture states in ^{70}Ga can therefore be assigned spins 0, 1, 2 or 3, and either parity, with positive parity somewhat favoured for the strong transitions (Vervier and Bolotin 1971). The only known negative parity states populated in the (n,γ) are the 691(2^-) and 1253(3^-) states in agreement with this rule. The level at 902 keV is not populated, supporting the 4^+ assignment for this level.

As shown in section 3.4, the yield functions for γ-rays from the (p,n) reaction depend strongly on the spin. It is therefore helpful to examine the yield functions whenever ambiguities in the spin assignments exist, or whenever the γ-ray yield is too low to allow useful angular distribution measurements. Individual cases in which these techniques have been applied to levels in ^{70}Ga are described below.

The ground state - the atomic beam measurement of Ehlers et al (1962) determines the spin of the ground state to be 1. The parity of this state is positive from the ℓ-value assignments in the (d,p) and (d,t) experiments.

The 508.1 keV state - (d,p) and (d,t) spectroscopic factors favour 2^+ for this state. The angular distribution of the 508 keV γ-ray confirms this result.

The 651.1 keV state - this state is populated by mixed $\ell = 1 + 3$, which limits its spin to lie between 1 and 3, with positive parity. The measurements of the circular polarization of neutron capture γ-rays from ^{70}Ga (Stecher-Rasmussen et al 1972) indicates the spin to be 1. This is confirmed by the linear polarization measurements on the 651 keV γ-ray.

The 690.9 keV state - the spin-parity assignment of 2^- for this level has been discussed in sections 3.5 and 3.6.

The 878.5 keV state - the spin-parity assignment of 4^- for this level has been discussed in section 3.5.

The 901.3 keV state - this level was tentatively assigned $J^\pi = 4^+$ on the basis of the $\ell = 3$ strengths in both the (d,p) and (d,t) experiments. It is the only level seen with a pure ℓ=3 pattern and has the largest ℓ=3 strength. This spin assignment is definitely established by the pure E2 angular distribution of the 393 keV γ-ray. This is not a real exception to the adopted view that M1 transition rates should dominate over E2, since this low lying 4^+ state has no other way to decay. It would be interesting to compare the half-life of this state with the 879 keV level.

The 995.7 keV state - the parity of this state is positive, as determined from the mixed ℓ = 1+3 transfer for this state in (d,p) and (d,t). The angular distribution of the 996 keV γ-rays de-exciting this state requires its spin to be 2.

The 1009.7 keV state - the angular distribution data for the 319 keV γ-ray decaying to the 691 keV level ($J^\pi = 2^-$) allows either J = 3 (δ = .11) or J = 2 (δ = .57). The latter case is not favoured in view of the large mixing ratio, particularly for the positive parity case. A 2^- assignment is unlikely in view of the population of the level in both (d,p) and (d,t). The possibility of 3^- is eliminated since the 15% branch to the 1^+ ground state would not be competitive if it were an M2 transition. Thus the 1009.7 keV state is tentatively assigned $J^{\pi} = 3^{+}$.

The 1015.1 keV state - the yield function data, (d,t) strengths, and γ-ray angular distribution data cannot distinguish between 0^{+} or 1^{+} for this level.

The 1024.1 keV state - the angular distribution of the 516 keV γ-ray and the (d,t) strengths for this level determine its spin and parity to be 3^{+}.

The 1033.2 keV state - the spin-parity assignment of 5^{-} for this state has been discussed in section 3.5.

The 1101.6 keV state - the angular distribution of the 411 keV γ-ray from this level determines the spin to be 4. The parity is negative from the $\ell = 2+4$ pattern for this level in the (d,p).

The 1135.4 keV state - this level, one of the most strongly populated in the (p,n) reaction, decays to levels with spins 1^{+}, 2^{-} and 2^{+}. Thus, although the 1135 keV γ-ray is isotropic, it cannot have spin 0. The yield function favours a spin 2 assignment. The parity is not determined from the particle experiments.

The 1140.4 keV state - both of the γ-rays from this level are isotropic and it has a large cross-section in the (p,n) reaction. Thus it could be 0^{+} but if so, then the transition to the 508 keV state would be E2. The yield function for this level does not fit well into any of the four categories, perhaps because of undetected feeding from higher levels. However, its slope, less than that expected for spin 2 suggests a low spin, probably 1 since the level decays to states of spin 1^+ and 2^+.

The 1203.5 keV state - the $\ell = 1$ transfer in the (d,p) and the angular distribution of the 1203.5 keV γ-ray determine the spin and parity of this level to be 2^+.

The 1234 keV state - the tentative spin-parity assignment of 6^- has been discussed in section 3.5.

The 1244.5 keV state - its decay to levels with spins 1^+ and 3^+, and the yield function data favour spin 2. The parity is undetermined.

The 1252.8 keV state - the angular distribution of the 373 keV γ-ray allows spin 3 or 5, with the parity negative from the $\ell = 2+4$ transfer in the (d,p). The $\ell=2$ component in the (d,p), and the strong primary γ-ray to this level in the (n,γ) (Vervier and Bolotin 1971) restrict the spin to 3^-.

The 1263.2 keV state - this level is populated with $\ell = 1$ in the (d,t) and decays to levels with spin-parity 2^+ and 3^+, so the spin-parity is either 1^+,2^+, or 3^+.

Higher lying states - for the many states found above 1263 keV, no spin assignments have been attempted because of the absence of γ-ray angular distribution data for them. The yield function data is unreliable because of the reduced range over which these data exist and because of unknown indirect feeding. The very large fraction of the $\ell=1$ strength in (d,t) for the level at 1555 keV suggests it might be 3^+. The state at 1620.9 keV is populated with pure $\ell = 2$

in the (d,p) and is fed strongly in the (p,n). Its decay to the ground state (1^+), 508(2^+) and 651(1^+) states indicates that its spin is low, either 1^- or 2^-.

From Fig. 4.1, it can be seen that there are remarkably few E1 transitions in the low lying levels in ^{70}Ga. In terms of the simplest configurations, the odd parity levels are probably predominantly of the form $|\pi p_{3/2}\ \nu g_{9/2}\rangle$ (where only the last odd neutron and proton are indicated) whereas the positive parity levels are of the form $|\pi p_{3/2}\ \nu p_{1/2}\rangle$ or $|\pi p_{3/2}\ \nu f_{5/2}\rangle$. Other configurations involving proton excitations will be populated weakly in the neutron transfer experiments (such as the 691 keV state). The lack of E1 transitions can be understood in terms of these configurations. In order for a transition to occur between states of opposite parity, a neutron must be changed from $g_{9/2}$ to $p_{1/2}$, which is ℓ-forbidden, or from $g_{9/2}$ to $f_{5/2}$, which is j-forbidden.

4.3 Spectroscopic Factors

With the knowledge of the spins of the low lying levels in ^{70}Ga, the spectroscopic factors discussed in Chapter II may now be re-examined.

If only lowest seniority components (v=0 or 1) are present in the target wavefunctions, then the spectroscopic factors obey the sum rules

$$\sum_{i,J_N} [S_{\ell j}(i,J_B)\ \frac{2J_B+1}{2J_A+1}] = N_\ell^{\,h} \quad \text{(stripping)}$$

and

$$\sum_{i,J_B} [S_{\ell_j}(i,J_B)] = N_h \qquad \text{(pickup)}$$

where the quantities in the square brackets are the experimentally determined strengths, J_A and J_B are the target and residual nuclear spins and $N_\ell{}^h$ and N_ℓ are the number of holes and particles of type ℓ in the respective targets. In addition , under these assumptions the strength of any one state in the nucleus cannot exceed the 2J+1 limit.

This 2J+1 dependence may be checked if the spins of all the levels that are populated with a given ℓ-transfer are known.

An approximate division of the ℓ=1 strength has been made between $p_{1/2}$ transfer and $p_{3/2}$ transfer by comparing the (d,p) and (d,t) cross-sections,as described in section 2.3. The $p_{1/2}$ spectroscopic strength thus lies mainly below 1100 keV. Fig. 4.2 shows the experimental $p_{1/2}$ spectroscopic factors which were given earlier in Table 2.3, plotted to illustrate the 2J+1 rule. Spin 3 can not be populated by $p_{1/2}$ transfer so that the small amount of ℓ = 1 in the 1023 keV level is from $p_{3/2}$ transfer. As the graph shows, the 2J+1 rule is quite well satisfied, lending credence to the division between $p_{1/2}$ and $p_{3/2}$.

Figure 4.3 shows the $f_{5/2}$ spectroscopic factors plotted as a function of spin. From Table 2.3 it can be seen that most of the ℓ=3 strength is exhausted below 1100 keV. For J = 2 and 3, the (d,p) strength falls below

Figure 4.2

Spectroscopic strengths for $\ell=1$ in $^{69}Ga(d,p)^{70}Ga$ and $^{71}Ga(d,t)^{70}Ga$ plotted as a function of spin.

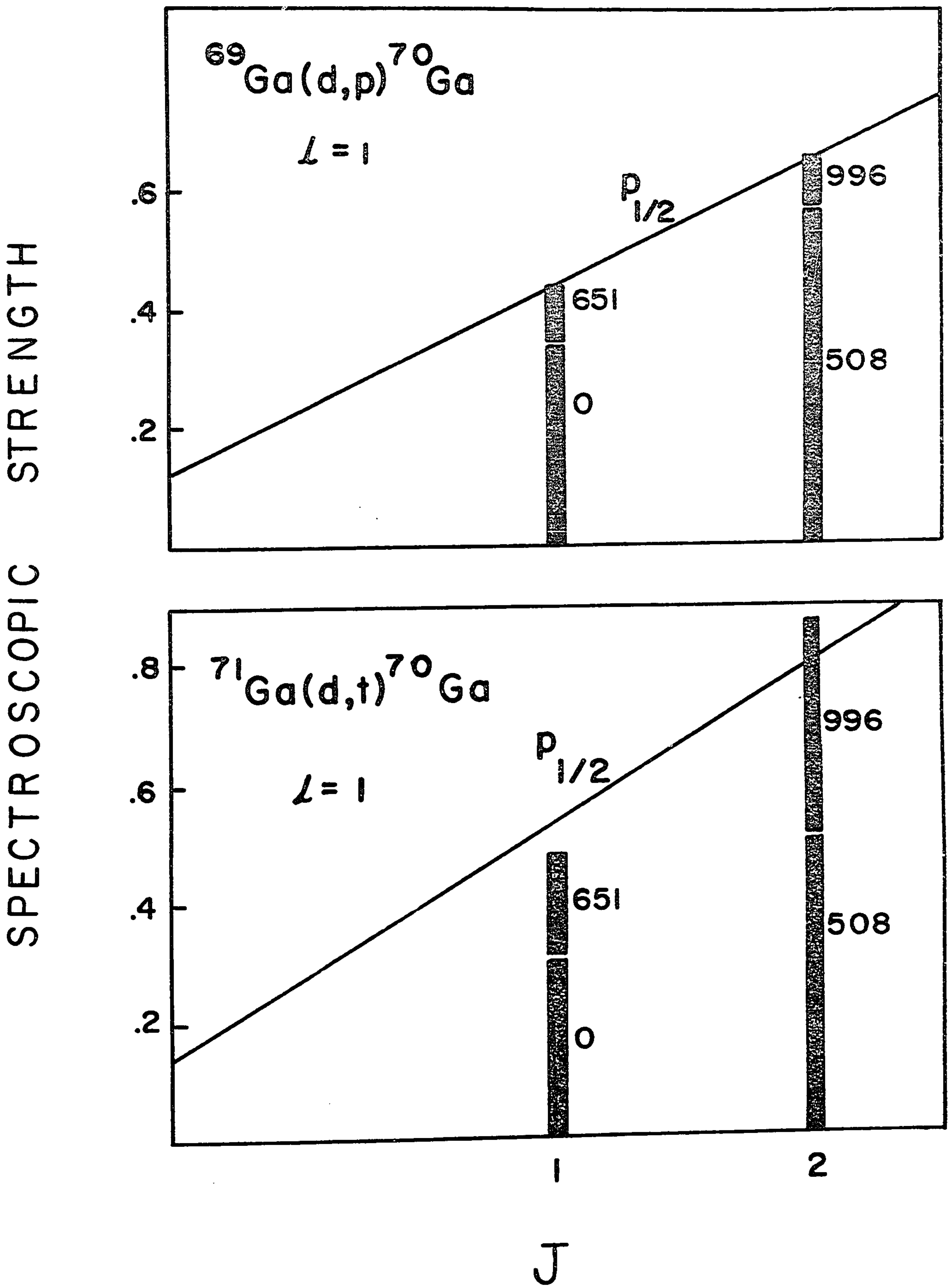

$^{69}Ga(d,p)^{70}Ga$
$\ell = 1$
$p_{1/2}$
996
651
508
0
.6
.4
.2
$^{71}Ga(d,t)^{70}Ga$
$\ell = 1$
$p_{1/2}$
996
651
508
0
.8
.6
.4
.2
1
2
J
SPECTROSCOPIC STRENGTH

Figure 4.3

Spectroscopic strengths for $\ell=3$ in $^{69}Ga(d,p)^{70}Ga$ and $^{71}Ga(d,t)^{70}Ga$ plotted as a function of spin.

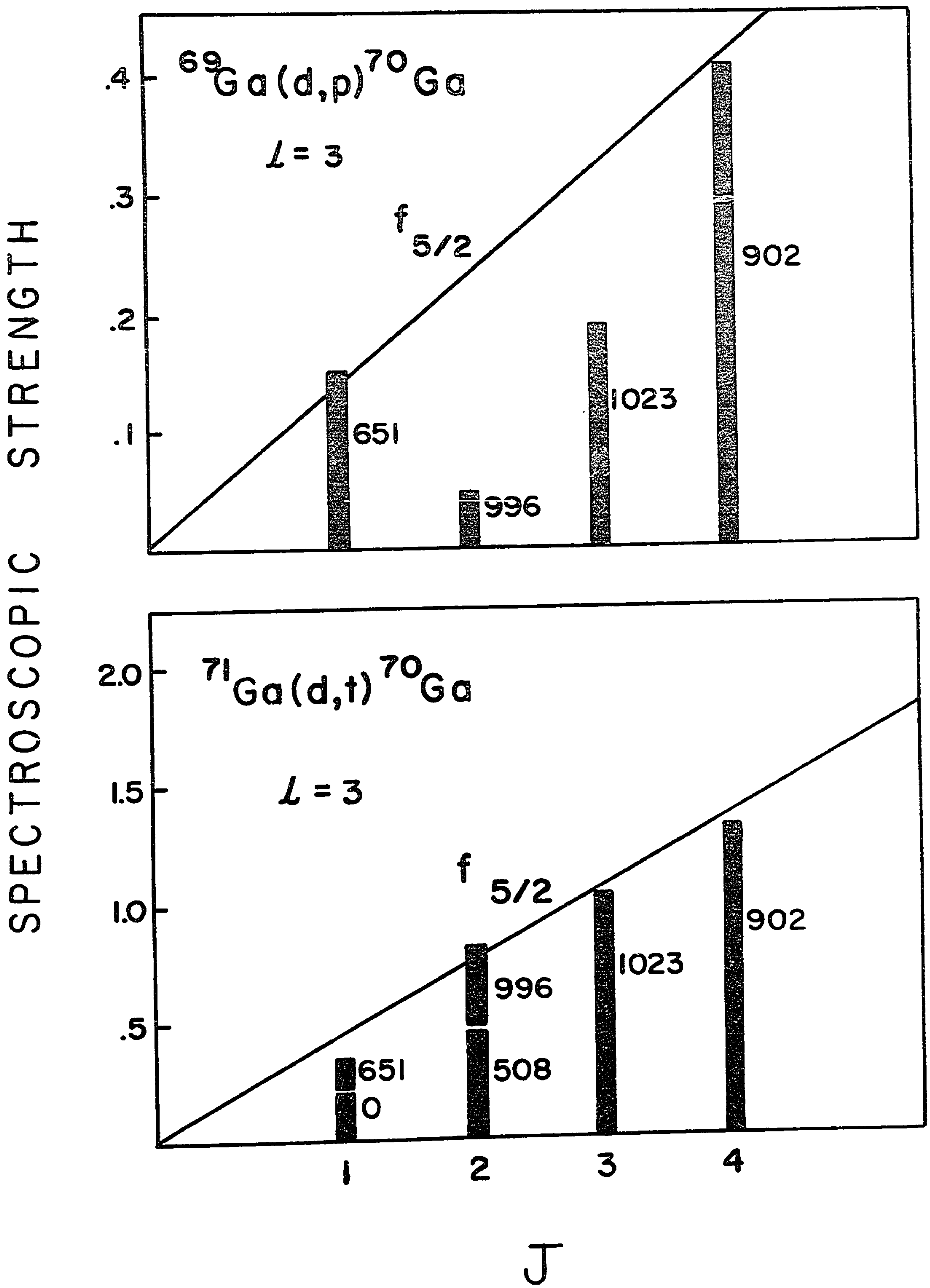

$^{69}Ga(d,p)^{70}Ga$
$\ell = 3$
$f_{5/2}$
651
996
1023
902
.4
.3
.2
.1
SPECTROSCOPIC STRENGTH
$^{71}Ga(d,t)^{70}Ga$
$\ell = 3$
$f_{5/2}$
651
0
996
508
1023
902
2.0
1.5
1.0
.5
1
2
3
4
J

that expected from the 2J+1 rule, but the agreement is acceptable considering the difficulty in extracting reliable ℓ = 3 strengths in the presence of the stronger ℓ = 1 patterns.

The situation in the negative parity levels is not as clear. In the (d,p) experiment the total observed ℓ = 4 strength of 11.3 exceeds the sum rule limit of 10 for $g_{9/2}$. Nevertheless this total may be used to determine the expected individual contributions for each spin. The ℓ = 4 spectroscopic factors are plotted as a function of spin in Fig. 4.4. In this graph, the J = 5 level at 1033 keV has far more strength than expected from the 2J+1 rule in the (d,p). In the (d,t), using the total occupancy of 1.02, the 2J+1 rule is again seen to be disrupted.

There are several possible explanations for this effect:

1) The DWBA calculation of σ^{ℓ}_{DW} is in error for ℓ= 4. In this case, all the ℓ= 4 strengths should be reduced, decreasing in particular the J = 5 component to an acceptable amount. The σ^{ℓ}_{DW} used here agree, relatively well, with those used by von Ehrenstein and Schiffer (1967) for $^{68}Zn(d,p)^{69}Zn$ where the sum rule limit of spectroscopic strength is contained in one state for ℓ=4.

2) The cross sections for (d,p) are in error, so that all the measured strengths should be reduced. This seems unlikely in view of the qualitative agreement between expected and measured occupancies for the $p_{1/2}$, $f_{5/2}$ and $p_{1/2}$ orbits.

3) There is interference between $g_{9/2}$ and $g_{7/2}$ transfers.

Figure 4.4

Spectroscopic strengths for $\ell=4$ in ^{69}Ga(d,p)^{70}Ga and ^{71}Ga(d,t)^{70}Ga plotted as a function of spin.

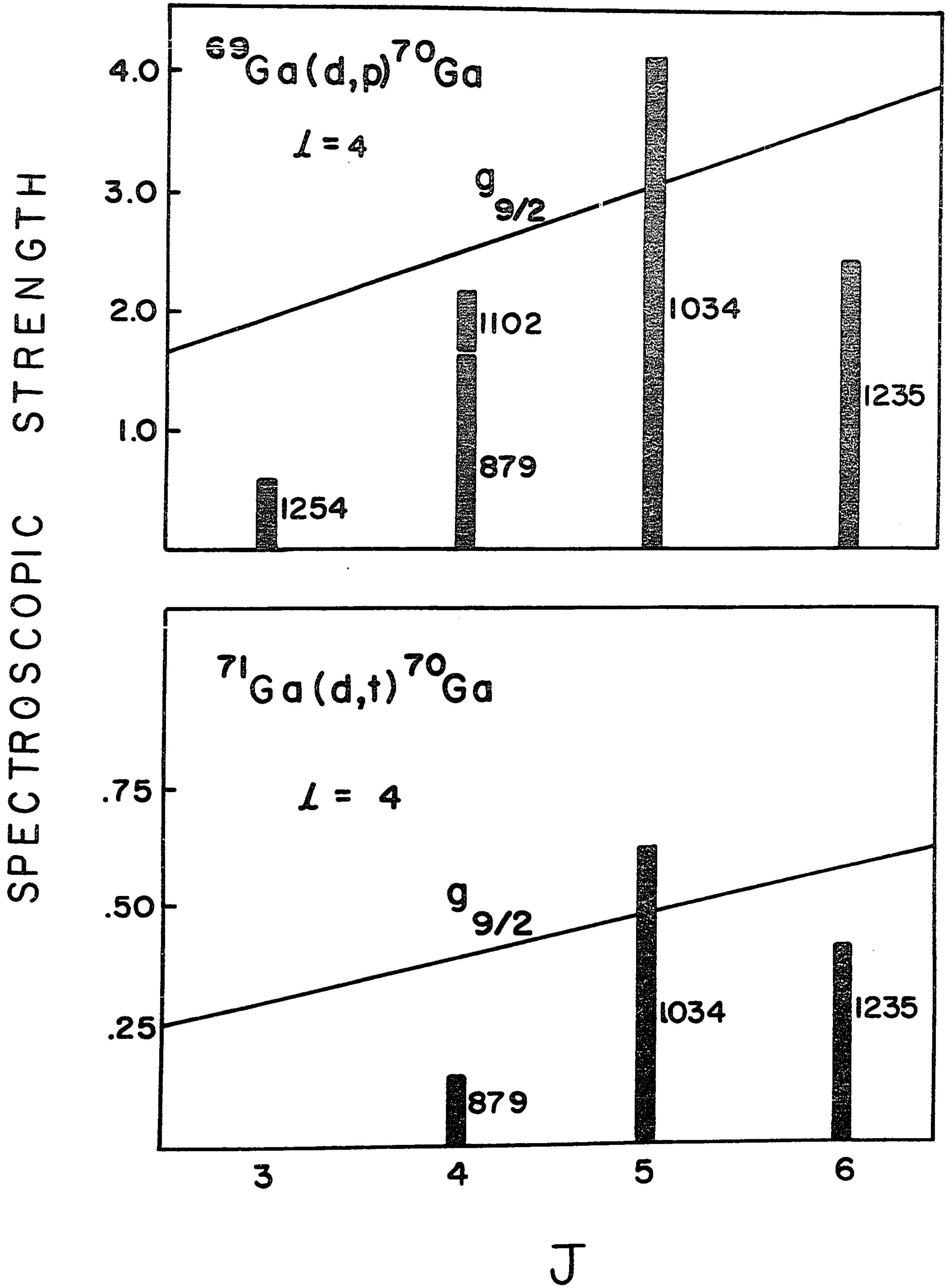

SPECTROSCOPIC STRENGTH
$^{69}Ga(d,p)^{70}Ga$
$\ell = 4$
$g_{9/2}$
4.0
3.0
2.0
1.0
1254
879
1102
1034
1235
$^{71}Ga(d,t)^{70}Ga$
$\ell = 4$
$g_{9/2}$
.75
.50
.25
879
1034
1235
3
4
5
6
J

Interference can arise if one shell-model configuration in the residual state is fed by two different j-transfers. For this to occur, there must be higher seniority configurations in the target wavefunction. If some of the (d,p) strength is from $g_{7/2}$ stripping then this could account for the observed excess of strength for $\ell = 4$. Excitations involving a $g_{7/2}$ neutron are not expected to occur this low in ^{70}Ga, however, and should not be populated in (d,t) where there is also this apparent disruption of the 2J+1-rule.

4) The 1033 keV state is an unresolved doublet. Whereas this hypothesis is difficult to prove or disprove, it is an attractive possibility. Although there is no evidence for a new level in the γ-ray work, this level, if it existed, would be expected to be of high spin (probably $J^{\pi} = 6^{-}$) and so would not be populated strongly in the (p,n) reaction in any case.

The spectroscopic factors can provide a sensitive test of the wavefunctions of both the target and residual nuclei in reactions such as those used here. In view of the complexity of the configurations involved in ^{70}Ga, and the poor agreement between the calculated and experimental energy levels (described in the next section) no detailed calculations of the spectroscopic factors were undertaken.

4.4 Shell Model Calculations for ^{70}Ga

Historically, progress in the theoretical treatment of the odd-odd nuclei has fallen behind that for odd-even and even-even nuclei. The use of models, which is very important in this theoretical treatment, is influenced to a great extent by the properties of neighbouring nuclei. Thus there are regions of "deformed nuclei". while the nuclei near closed shells have traditionally been treated in terms of the shell model.

In the f-p shell, the agreement between theory and experiment has not been very satisfactory. The collective model interpretations suffer from the lack of distinctive rotational and vibrational features in the experimental data. On the other hand the microscopic, individual particle or "shell model" approach has been hampered by the complexity of the problem, in which large numbers of nucleons (typically greater than 10) occupy a considerable valence space (often more than 5 shells).

With the advent of large scale computers, the former limitations on the vector spaces usually encountered in shell model calculations have been extended. Recently, Halbert et al (1971) have performed shell model calculations in the s-d shell using realistic two-body matrix elements derived from the many body theory of the interaction. Their success in predicting a large amount of experimental data, including energy levels, spectroscopic factors, transition rates, electric quadrupole and magnetic dipole moments are a promising indication of the success of this approach in regions where the configuration space may be adequately treated.

Another approach (eg. Wildenthal et al 1971) is to treat the interaction force as a phenomenological quantity and to extract the parameters required to fit the data in regions where the configuration space is computer limited, using the simple two-parameter surface delta interaction. described in Chapter I. This force has been applied successfully by T. Taylor for isotopes of Ni and Co, treating ^{56}Ni as a closed core. The parameters which best fit the energy levels and spectroscopic factors are:

$$A_0 = A_1 = .55 \text{ MeV} .$$

Vervier (1966) has also obtained good agreement with the spectrum of ^{58}Co,using a zero-range force with spin exchange of the form

$$V_{12} = -101(.919+.081\ \vec{\sigma}_1\cdot\vec{\sigma}_2)\delta(\vec{r}_1-\vec{r}_2) \text{ MeV.}$$

In this work,shell model calculations for ^{70}Ga were carried out using both these interactions, with the parameters given above and ^{56}Ni as a closed core. In view of the computer time required no search over the parameters was made.

The low-lying states of ^{70}Ga are formed by coupling the 14 active nucleons (3 protons and 11 neutrons) to T = 4 ($T = \frac{N-Z}{2}$). In this study the $2p_{3/2}$, $1f_{5/2}$, $2p_{1/2}$, and $1g_{9/2}$ shells were treated as active. The single particle energies for these orbits were taken from the spectrum of ^{57}Ni, and are, in MeV,

$p_{3/2}$	0
$f_{5/2}$	.78
$p_{1/2}$	1.08
$g_{9/2}$	2.0

where the principal quantum numbers for the orbits have been dropped for convenience. No J = 9/2 state has been observed in ^{57}Ni so the value of 2 MeV was arbitrily adopted. Calculations in which this single particle energy were varied between .5 and 4 MeV show that the results are fairly insensitive to this quantity.

The lowest seniority* approximation, in which v = 0 for an even number of particles and 1 for an odd number of particles, must be abandoned here, since both neutrons and protons occupy each of the active shells. An even number of nucleons in a shell does not imply an even number of neutrons and protons. Consequently, pairs of nucleons can couple to T = 0, for which J = 0 is not allowed. Therefore, in this treatment, the seniority was allowed to take on the values 0,2 (or 1) for any even (or odd) number of particles within a subshell.

The lowest energy configuration in ^{70}Ga, from considerations of the single particle systematics in this

*The seniority v of an n particle wavefunction denotes the number of particles remaining when all the J=0 pairs are removed.

region is expected to be of the form $p_{3/2}{}^7\ f_{5/2}{}^6\ p_{1/2}{}^1$ corresponding to three $p_{3/2}$ protons, and the 11 neutrons progressively filling the $p_{3/2}$, $f_{5/2}$ and $p_{1/2}$ neutron orbits. Computer costs limited the allowed excitations to within 2 particle excitations from the ground state, where a "particle excitation" corresponds to the excitation of one particle to the next adjacent single particle orbit. The allowed particle number occupations for each of the active subshells were therfore

$p_{3/2}$	5, 6, or 7
$f_{5/2}$	5, 6, 7 or 8
$p_{1/2}$	0, 1,or 2
$g_{9/2}$	0 or 1

taken such that the total number of nucleons is constant at 14.

The multiparticle, multishell basis states constructed in the calculation are of the following form:

$$|[\{f_{5/2}^{n_1}\ (j_1t_1)p_{3/2}^{n_2}\ (j_2t_2)\}_{J_1T_1}\ p_{1/2}^{n_3}\ (j_3t_3)]_{J_2T_2}\ g_{9/2}^{n_4}\ (j_4t_4)\rangle_{JT}$$

where n_i is the number of nucleons in the i^{th} shell. The order of the shells in the calculation was

$$f_{5/2} = 1$$
$$p_{3/2} = 2$$
$$p_{1/2} = 3$$
$$g_{9/2} = 4\ .$$

In this expression,

$j_i(t_i)$ are the resultant angular momenta (isospins) formed by coupling the j's (t's) of the n_i nucleons in the i^{th} shell.

$J_i(T_i)$ is the intermediate angular momentum (isospin) formed by coupling the resultant j's(t's) of the first i shells with the j(t) of the $(i+1)^{th}$ shell.

In terms of the formalism of French et al (1969), the basis wavefunctions are represented by the vector coupling diagram:

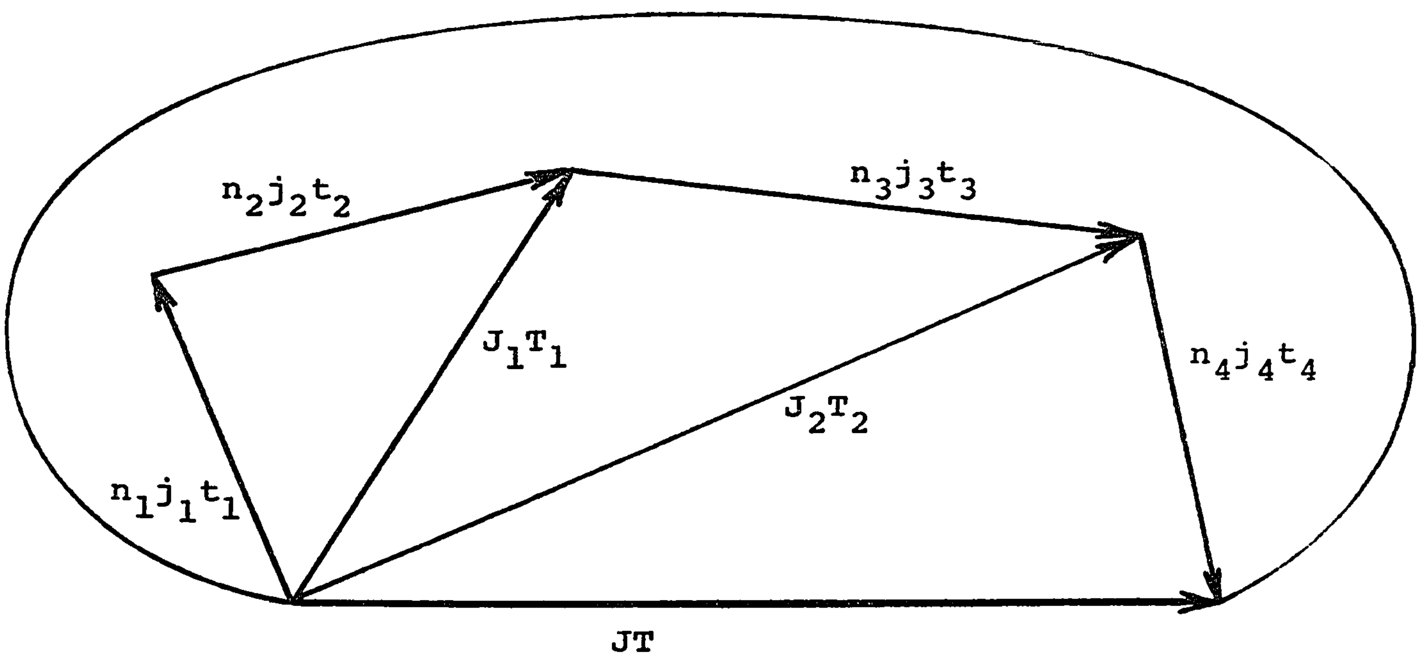

where the arc denotes antisymmetrization over all the active nucleons. For given J and T = 4, wavefunctions for all allowed combinations of the quantum numbers n_i j_i t_i; i = 1, 4 are constructed. The basis wavefunctions which are most important for low lying levels in ^{70}Ga are listed in Table 4.1, using

Table 4.1

Basis Multi-shell Wavefunctions for Low-lying Levels in ^{70}Ga

J^{π}	Configuration	n_1	n_2	n_3	n_4	$2j_1$	$2j_2$	$2j_3$	$2j_4$	$2t_1$	$2t_2$	$2t_3$	$2t_4$	$2J_1$	$2J_2$	$2T_1$	$2T_2$
0^+	A	6	6	2	0	0	0	0	0	6	2	2	0	0	0	6	8
	B	6	6	2	0	0	0	0	0	6	2	2	0	0	0	8	8
	C	6	6	2	0	4	4	0	0	4	2	2	0	0	0	6	8
	D	7	6	1	0	5	4	1	0	5	2	1	0	1	0	7	8
1^+	A	5	7	2	0	5	3	0	0	5	1	2	0	2	2	6	8
	B	6	6	2	0	0	0	2	0	6	2	0	0	0	2	8	8
	C	6	6	2	0	0	2	0	0	6	0	2	0	2	2	6	8
	D	6	6	2	0	0	4	2	0	6	2	0	0	4	2	8	8
	E	6	6	2	0	2	0	0	0	4	2	2	0	2	2	6	8
	F	6	6	2	0	2	4	0	0	4	2	2	0	2	2	6	8
	G	6	6	2	0	4	4	0	0	4	2	2	0	2	2	6	8
	H	6	6	2	0	6	4	0	0	4	2	2	0	2	2	6	8
	I	6	7	1	0	0	3	1	0	6	1	1	0	3	2	7	8
	J	7	6	1	0	5	4	1	0	5	2	1	0	1	2	7	8
	K	7	6	1	0	5	4	1	0	5	2	1	0	3	2	7	8
	L	8	5	1	0	0	3	1	0	4	3	1	0	3	2	7	8
2^+	A	5	7	2	0	5	3	0	0	5	1	2	0	4	4	6	8
	B	6	6	2	0	0	4	0	0	6	2	2	0	4	4	6	8
	C	6	6	2	0	0	4	0	0	6	2	2	0	4	4	8	8
	D	6	6	2	0	0	4	2	0	6	2	0	0	4	4	8	8
	E	6	6	2	0	2	4	0	0	4	2	2	0	4	4	6	8
	F	6	6	2	0	4	0	0	0	4	2	2	0	4	4	6	8
	G	6	6	2	0	4	4	0	0	4	2	2	0	4	4	6	8
	H	6	6	2	0	6	4	0	0	4	2	2	0	4	4	6	8
	I	6	6	2	0	8	4	0	0	4	2	2	0	4	4	6	8
	J	7	6	1	0	5	0	1	0	5	2	1	0	5	4	7	8
	K	7	6	1	0	5	4	1	0	5	2	1	0	3	4	7	8
	L	7	6	1	0	5	4	1	0	5	2	1	0	5	4	7	8
	M	8	5	1	0	0	3	1	0	4	3	1	0	3	4	7	8

(continued next page)

Table 4.1 (continued)

J^{π}	Configuration	n_1	n_2	n_3	n_4	$2j_1$	$2j_2$	$2j_3$	$2j_4$	$2t_1$	$2t_2$	$2t_2$	$2t_4$	$2J_1$	$2J_2$	$2T_1$	$2T_2$
3^+	A	5	7	2	0	5	3	0	0	5	1	2	0	6	6	6	8
	B	6	6	2	0	0	4	2	0	6	2	0	0	4	6	8	8
	C	6	6	2	0	0	6	0	0	6	0	2	0	6	6	8	8
	D	6	6	2	0	2	4	0	0	4	2	2	0	6	6	6	8
	E	6	6	2	0	4	4	0	0	4	2	2	0	6	6	6	8
	F	6	6	2	0	6	0	0	0	4	2	2	0	6	6	6	8
	G	6	6	2	0	6	4	0	0	4	2	2	0	6	6	6	8
	H	6	6	2	0	8	4	0	0	4	2	2	0	6	6	6	8
	I	6	6	2	0	10	4	0	0	4	2	2	0	6	6	6	8
	J	7	6	1	0	5	0	1	0	5	2	1	0	5	6	7	8
	K	7	6	1	0	5	4	1	0	5	2	1	0	5	6	7	8
	L	7	6	1	0	5	4	1	0	5	2	1	0	7	6	7	8
4^+	A	5	7	2	0	5	3	0	0	5	1	2	0	8	8	6	8
	B	6	6	2	0	4	4	0	0	4	2	2	0	8	8	6	8
	C	6	6	2	0	6	4	0	0	4	2	2	0	8	8	6	8
	D	6	6	2	0	8	0	0	0	4	2	2	0	8	8	6	8
	E	6	6	2	0	8	4	0	0	4	2	2	0	8	8	6	8
	F	6	6	2	0	10	4	0	0	4	2	2	0	8	8	6	8
	G	7	6	1	0	5	4	1	0	5	2	1	0	7	8	7	8
	H	7	6	1	0	5	4	1	0	5	2	1	0	9	8	7	8
5^+	A	6	6	2	0	6	4	0	0	4	2	2	0	10	10	6	8
	B	6	6	2	0	8	4	0	0	4	2	2	0	10	10	6	8
	C	6	6	2	0	10	0	0	0	4	2	2	0	10	10	6	8
	D	6	6	2	0	10	4	0	0	4	2	2	0	10	10	6	8
	E	7	6	1	0	5	4	1	0	5	2	1	0	9	10	7	8

(continued next page)

Table 4.1 (continued)

J^{π}	Configuration	n_1	n_2	n_3	n_4	$2j_1$	$2j_2$	$2j_3$	$2j_4$	$2t_1$	$2t_2$	$2t_3$	$2t_4$	$2J_1$	$2J_2$	$2T_1$	$2T_2$
2^-	A	5	7	1	1	5	3	1	9	5	1	1	1	6	5	6	7
	B	7	6	0	1	5	0	0	9	5	2	0	1	5	5	7	7
	C	7	6	0	1	5	4	0	9	5	2	0	1	5	5	7	7
	D	7	6	0	1	5	4	0	9	5	2	0	1	7	7	7	7
	E	7	6	0	1	5	4	0	9	5	2	0	1	9	9	7	7
3^-	A	5	7	1	1	5	3	1	9	5	1	1	1	2	3	6	7
	B	5	7	1	1	5	3	1	9	5	1	1	1	4	3	6	7
	C	5	7	1	1	5	3	1	9	5	1	1	1	6	5	6	7
	D	6	7	0	1	0	3	0	9	6	1	0	1	3	3	7	7
	E	7	6	0	1	5	0	0	9	5	2	0	1	5	5	7	7
	F	7	6	0	1	5	4	0	9	5	2	0	1	3	3	7	7
	G	7	6	0	1	5	4	0	9	5	2	0	1	5	5	7	7
	H	7	6	0	1	5	4	0	9	5	2	0	1	7	7	7	7
4^-	A	5	7	1	1	5	3	1	9	5	1	1	1	2	1	6	7
	B	5	7	1	1	5	3	1	9	5	1	1	1	4	3	6	7
	C	5	7	1	1	5	3	1	9	5	1	1	1	4	5	6	7
	D	5	7	1	1	5	3	1	9	5	1	1	1	6	5	6	7
	E	5	7	1	1	5	3	1	9	5	1	1	1	8	7	6	7
	F	6	7	0	1	0	3	0	9	6	1	0	1	3	3	7	7
	G	7	6	0	1	5	0	0	9	5	2	0	1	5	5	7	7
	H	7	6	0	1	5	4	0	9	5	2	0	1	1	1	7	7
	I	7	6	0	1	5	4	0	9	5	2	0	1	7	7	7	7
	J	7	6	0	1	5	4	0	9	5	2	0	1	9	9	7	7
5^-	A	5	7	1	1	5	3	1	9	5	1	1	1	2	1	6	7
	B	5	7	1	1	5	3	1	9	5	1	1	1	2	3	6	7
	C	5	7	1	1	5	3	1	9	5	1	1	1	4	3	6	7
	D	5	7	1	1	5	3	1	9	5	1	1	1	8	7	6	7
	E	5	7	1	1	5	3	1	9	5	1	1	1	8	9	6	7
	F	6	7	0	1	0	3	0	9	6	1	0	1	3	3	7	7
	G	7	6	0	1	5	4	0	9	5	2	0	1	7	7	7	7
	H	7	6	0	1	5	4	0	9	5	2	0	1	7	7	7	7

Table 4.1 (continued)

J^π	Configu-ration	n_1	n_2	n_3	n_4	$2j_1$	$2j_2$	$2j_3$	$2j_4$	$2t_1$	$2t_2$	$2t_3$	$2t_4$	$2J_1$	$2J_2$	$2T_1$	$2T_2$
6^-	A	5	7	1	1	5	3	1	9	5	1	1	1	2	3	6	7
	B	5	7	1	1	5	3	1	9	5	1	1	1	4	3	6	7
	C	5	7	1	1	5	3	1	9	5	1	1	1	6	5	6	7
	D	5	7	1	1	5	3	1	9	5	1	1	1	6	7	6	7
	E	5	7	1	1	5	3	1	9	5	1	1	1	8	7	6	7
	F	5	7	1	1	5	3	1	9	5	1	1	1	8	9	6	7
	G	6	7	0	1	0	3	0	9	6	1	0	1	3	3	7	7
	H	7	6	0	1	5	4	0	9	5	2	0	1	3	3	7	7
	I	7	6	0	1	5	4	0	9	5	2	0	1	9	9	7	7

the notation described above. The Hamiltonian matrix is then constructed and diagonalized in this basis. Table 4.2 contains the resulting eigenvalues and eigenvectors for all the levels within 1.5 MeV of the lowest eigenvalue for the SDI force. The results for the zero range calculation are presented in Table 4.3.

The results of the two calculations are also shown in Fig. 4.5. The zero range calculation bears no resemblance to the experimental data. Although spin 1 is correctly predicted for the ground state, the calculated wavefunction for this state (and in fact, for the first four states) is purely

$$p_{3/2}^{\;7}\ f_{5/2}^{\;5}\ p_{1/2}^{\;2}$$

contrary to the $\ell = 1$ patterns observed in both (d,p) and (d,t). The predicted 1.7 MeV gap above 1 MeV is not observed experimentally.

The surface delta interaction gives somewhat better agreement with experiment. The most noticeable discrepancy in the calculation is its failure to reproduce the experimentally observed gap of 508 keV between the spin 1^+ ground state and the spin 2^+ first excited state. In fact, the calculated 1^+ and 2^+ states are reversed in order. The theoretical prediction in Fig. 4.5 has been shifted so that the centre of gravity of the lowest 1^+ and 2^+ states agrees with the experimental centre of gravity. The predominant $p_{3/2}^{\;7}\ f_{5/2}^{\;6}\ p_{1/2}^{\;1}$ component predicted for these states is

Table 4.2

Calculated energies and wavefunctions for low lying states in ^{70}Ga, for the SDI residual interaction

E_x (kev)	J^{π}	Basis Wavefunction Components												
		A	B	C	D	E	F	G	H	I	J	K	L	M
0	2^+	.357	-.083	.090	.094	.097	-.139	-.122	-.034	-.014	-.042	.087	.009	-.475
66	1^+	.205	-.056	-.150	-.157	-.031	-.110	-.145	-.008	-.771	-.005	-.091	.520	
363	3^+	.091	-.102	.001	.023	.056	-.558	.181	-.330	-.135	-.670	.228	.074	
385	1^+	.795	-.108	.326	.010	.403	-.008	-.051	-.176	.113	.181	.079	-.038	
401	2^+	-.178	-.043	-.092	.066	-.133	.439	-.308	.281	-.113	.687	-.058	-.217	-.166
629	4^+	.306	-.100	.339	-.795	-.150	.165	.315	.039					
651	5^-	.216	.263	.376	-.333	-.104	-.719	-.137	-.238					
670	0^+	.789	.835	-.180	-.105									
826	1^+	.278	-.694	-.147	-.002	-.513	.147	.133	-.065	.016	-.252	-.114	-.190	
843	4^-	.385	-.440	-.105	-.108	.255	.687	-.102	-.123	.127	.198			
970	3^+	.601	-.088	.153	.288	.383	-.333	-.108	-.075	.176	-.411	-.001	.224	
998	0^+	-.510	.465	.139	-.378									
1003	2^+	-.126	.472	.128	-.171	.337	.576	.030	.079	.140	-.367	-.175	-.051	-.274
1014	4^+	.853	-.136	-.040	.214	-.221	.006	-.386	-.088					
1146	5^+	.220	.338	.668	.141	.609								
1204	6^-	.366	.470	-.174	-.158	-.461	-.189	-.546	-.111	.114				
1301	2^-	-.152	.883	-.323	-.263	-.122								
1307	2^+	-.770	-.178	.160	-.212	-.212	-.260	-.128	-.134	.040	-.128	-.117	.050	-.339
1329	3^-	.196	.315	.214	-.549	-.640	-.125	.119	.269					

Table 4.3

Calculated energies and wavefunctions for low lying states in ^{70}Ga for the zero range calculation

E_x (keV)	J^{π}	Basis Wavefunction Components												
		A	B	C	D	E	F	G	H	I	J	K	L	M
0	1^+	.995	.008	-.015	.000	-.079	-.016	-.018	.042	-.001	.040	-.015	-.000	
506	4^+	.995	.028	-.036	.058	.050	-.007	-.033	.005					
689	2^+	.995	.003	-.003	-.007	-.053	.044	-.033	.023	.039	-.009	.022	-.003	.002
977	3^+	.992	.009	-.005	-.083	-.030	.051	-.012	.030	-.007	.009			

Figure 4.5

Comparison of the experimental ^{70}Ga spectrum with the shell model calculation using the surface delta interaction (SDI) and zero range force (ZR).

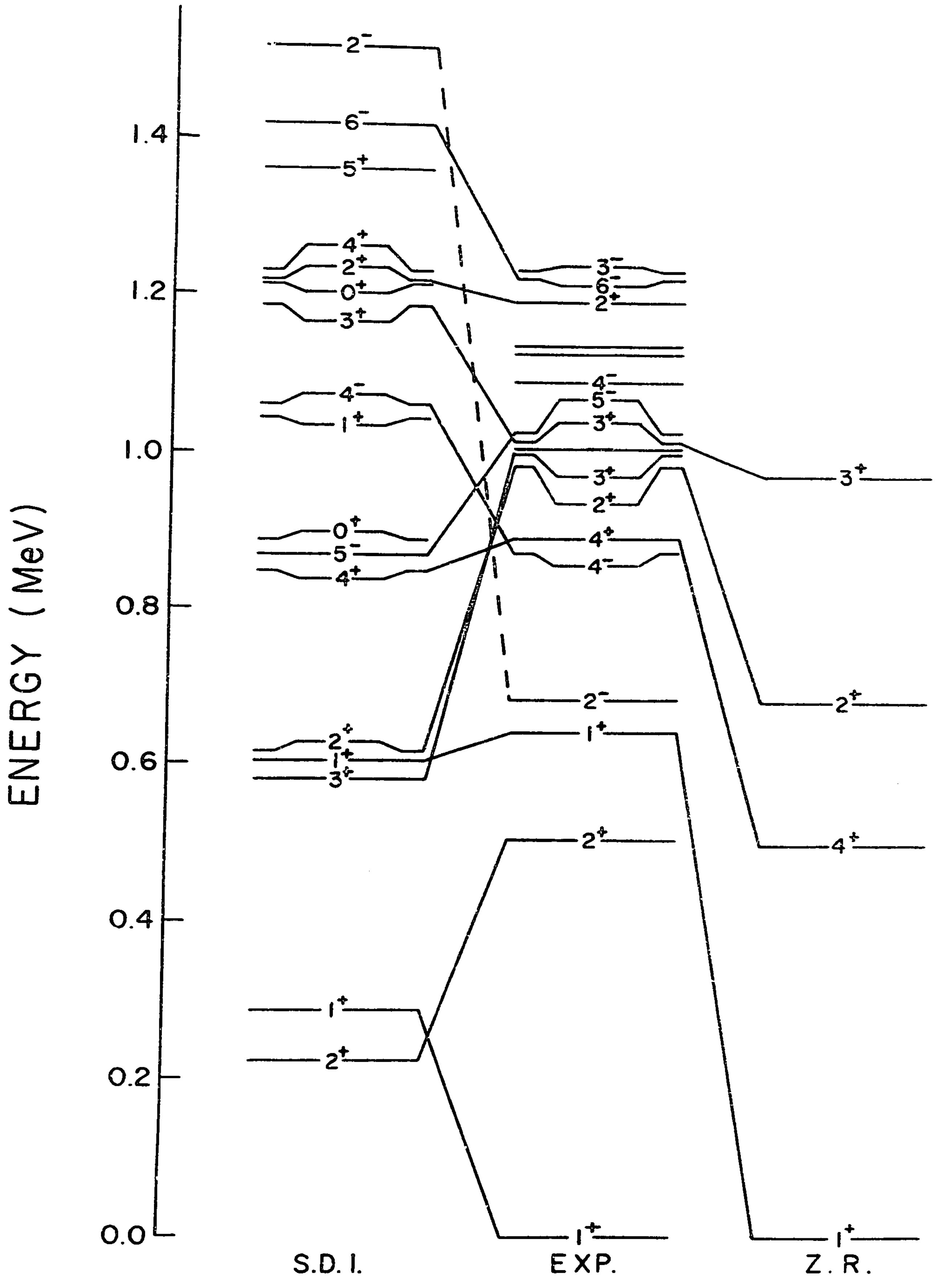

ENERGY (MeV)
0.0
0.2
0.4
0.6
0.8
1.0
1.2
1.4
2⁻
6⁻
5⁺
4⁺
2⁺
0⁺
3⁺
4⁻
1⁺
0⁺
5⁻
4⁺
2⁺
1⁺
3⁺
1⁺
2⁺
3⁻
6⁻
2⁺
4⁻
5⁻
3⁺
3⁺
2⁺
4⁺
4⁻
2⁻
1⁺
2⁺
1⁺
3⁺
2⁺
4⁺
1⁺
S.D.I.
EXP.
Z.R.

^{70}Ga

consistent with the ℓ = 1 patterns observed in (d,p) and (d,t).

Another shortcoming of the calculation is its failure to predict the correct ordering of the negative parity states. In particular, the observed 2^- state at 691 keV, is predicted to lie at 1.3 MeV. The calculated ordering of the 4^- and 5^- states appears reversed to that experimentally observed.

Despite these inconsistencies in the calculation, certain features of the experimental spectrum are adequately described. The calculations predict 12 levels below 1 MeV and 24 between 1 and 2 MeV. This is in acceptable agreement with observed numbers of 7 and 47 respectively, considering the limited configuration space used. This is improved if the theoretical calculation is shifted up to make the centers of gravity of the first two levels agree as in Figure 4.5. The general agreement for the predictions of other levels in ^{70}Ga is shown by the dotted lines in Fig. 4.2, connecting states of the same spin.

The most obvious limitation in the calculation is the truncated configuration space occupied by the valence nucleons, particularly the restriction to one $g_{9/2}$ nucleon. Higher seniority might also be expected to play an important role. The spin 2^- state at 691 keV, describable in simple shell model terms as the coupling of an excited $f_{5/2}$ proton with a $g_{9/2}$ neutron, can also be constructed by coupling a $p_{3/2}$ proton with, for example, a neutron configuration of the form $(g_{9/2})^3_{7/2}$. A configuration of this type would be populated very weakly in neutron transfer reactions. Another obvious shortcoming of the calculation is the omission of the $d_{5/2}$ and $s_{1/2}$ orbits from the configuration space. States with $J^\pi = 2^-$ formed by coupling the $p_{3/2}$ proton with either a $d_{5/2}$ or $s_{1/2}$ neutron would be expected to mix with the calculated 2^- level at 1.3 MeV, thereby pushing it down, in better agreement with the observation at 691 keV excitation.

To extend the configuration space to allow, for example, three $g_{9/2}$ neutrons in general seniority would make the shell model calculation prohibitively long. The present calculation, allowing seniority ≤ 2 in each subshell and up to 2 particle excitations required 504 computer central processor seconds to produce the Hamiltonian matrices, and 16 seconds to diagonalize them. The largest matrix encountered, that for J = 3, was 26×26. A more exact calculation of the energy levels of ^{70}Ga, allowing the treatment of active nucleons up to the $s_{1/2}$ shell in full seniority awaits improved computer technique. The calculation of the wavefunctions should be put to the more stringent tests of predicting the observed spectroscopic factors for ^{70}Ga, as well as electromagnetic transition rates.

SUMMARY

A diversified experimental study of the odd-odd nucleus ^{70}Ga using direct and compound nuclear reactions, and gamma-ray spectroscopy, has been described. The results provide a fairly clear picture of the spins and parities of the low-lying energy levels. Between $\sim$1.3 and 2 MeV excitation energy, less information is available but it is probably safe to say that most, if not all, of the excited states have been observed.

Particularly useful in this work was the (p,n) reaction which is ideally suited for the study of medium mass odd-odd nuclei since an even-even target has spin zero and the proton energy can be kept close to threshold. This produces appreciable alignment of the excited states of the residual nucleus so that spin determinations can be made from measurements of γ-ray angular distributions. Even more definite information could be secured if the outgoing neutron were detected on axis but such coincidence experiments are difficult. In addition, the cross section for this reaction appears to be strongly dependent on the spins of the levels produced. Thus, by measuring the variation with bombarding energy of thick target γ-ray yields much useful information can be obtained.

Many new questions about ^{70}Ga have been raised as a result of this study. It would be interesting to examine the neutron transfer reactions leading to excitations above 2 MeV

to verify the implication that the $2p_{1/2}$, $2p_{3/2}$, $1f_{5/2}$ and $1g_{9/2}$ strengths are virtually exhausted below 2 MeV. At the same time, better statistics in the $^{71}Ga(d,t)$ reaction might clarify the anomaly in the 2J+1 rule for $\ell=4$. Since both potential targets, ^{71}Ge and ^{69}Zn are radioactive, proton transfer spectroscopic factors are unobtainable. However, the measurement of angular distributions for two-nucleon transfer reactions, such as $^{68}Zn(^{3}He,p)^{70}Ga$, would provide a further test of the wave functions for the various excited states.

The electromagnetic properties of the levels also require further study. In this regard, the use of the $^{68}Zn(p,n)$ reaction has been already emphasized but the high spin states should be most readily populated via the reaction $^{67}Zn(\alpha,p)$. Arnell et al (1971) have reported a small effort in this direction. Lifetime measurements in ^{70}Ga would be valuable, all the more so because they would reveal the extent to which collectivity can be safely ignored in the low-lying levels. The determination of the ground state magnetic moment should be feasible (but difficult, because of the 21-minute half life) by the atomic beam method. Also interesting would be perturbed angular correlation study of some of the excited states, for example the 879 keV level.

Theoretically , a thorough shell model study of ^{70}Ga would be enthusiastically welcomed. This should include calculations of the ground state wave functions for ^{69}Ga and ^{71}Ga so that the (d,p) and (d,t) spectroscopic factors can be compared with experiment. The computation of the electromagnetic properties of the levels would provide a test of the observed branching ratios, and would predict lifetimes. Finally, it would be interesting to extend the study to the neighboring odd-odd Ga isotopes in order to see if the truncated space can reproduce the much higher density of low-lying states that is observed in ^{68}Ga and ^{72}Ga.

REFERENCES

Arnell, S.E., Linusson, H., and Sawa, Z. 1971. Nucl. Phys. A166, 241.

Arvieu, R. and Moszkowski, S.A. 1966. Phys. Rev. 145, 830.

Bass, W.T. and Stelson, P.H. 1970. Phys. Rev. C. 6, 2154.

Bassel, R.H. 1966. Phys. Rev. 149, 791.

Baxter, A.M., Gillespie, B.W.J., and Kuehner, J.A. 1970. Can. J. Phys. 48, 2434.

Blatt, J.M. and Weisskopf, V.G. 1952. "Theoretical Nuclear Physics" Wiley.

Burke, D.G. 1969. Private communication.

Carlson, L.E. 1972. Private communication.

Daehnick, W.W. 1969. Phys. Rev. 177, 1763.

de-Shalit, A. and Talmi, I. 1963. "Nuclear Shell Theory" Academic Press.

Dohan, D.A., and Summers-Gill, R.G. 1970. Bull. Amer. Phys. Soc. 15, 782.

Dohan, D.A., and Summers-Gill, R.G. 1972. Physics in Canada 28, No. 4, 27.

Ehlers, V.J., Nierenberg, W.A., and Shugart, H.A. 1962. Phys. Rev. 125, 2008.

Ewan, G.T., Andersson, G.I., Bartholomew, G.A., and Litherland, A.E. 1969. Phys. Lett. B 29, 325.

Finckh, E., Jahnke, U., Schreiber, B., and Weidinger, A. 1970. Nucl. Phys. A144, 67.

Frauenfelder, H. and Steffen, R.M. 1966. Alpha-, Beta- and Gamma-Ray Spectroscopy. Ed. K. Seigbahn. North Holland Publishing Co.

French, J.B., Halbert, E.H., McGrory, J.B., and Wong, S.S.M. 1969. Advances in Nucl. Phys. 3, 193.

Glagolev, V.L., Kavrishnykh, O.M., Makarov, Yu. V. and Yampolskii, P.A. 1959. Soviet Physics JETP. 9, 742.

Glaudemans, P.W.M., Wiechers, G. and Brussard, P.J. 1964. Nuc. Phys. 56, 529 and 548.

Glaudemans, P.W.M., Brussard, P.J., and Wildenthal, B.H. 1967. Nucl. Phys. A102, 593.

Glaudemans, P.W.M. 1970. Nuclear Physics Seminar Notes compiled by Koops, J.E., and Keverling Busman, A.S., Ch. IV.

Goeppert Mayer, M. 1948. Phys. Rev. 74, 235.

__________ 1949. Phys. Rev. 75, 1969.

Halbert, E.C., McGrory, J.B., Wildenthal, B.H., and Pandya, S.P. 1971, Advances in Nucl. Phys. 4, 135.

Hauser, W., and Feshbach, H. 1952. Phys. Rev. 87, 366.

Haxel, O., Jensen, J.H.D., and Suess, H.E. 1948 Naturwiss., 35, 375.

__________ 1949. Phys. Rev. 75, 1766.

Kuo, T.T.S., and Brown, G.E. 1966. Nucl. Phys. 85, 40.

__________ 1967. Nucl. Phys. A103, 71.

Linusson, H., Hardell, R., and Arnell, S.E. 1970. Ark. Fys. 40, 197.

Litherland, A.E., Ewan, G.T., and Lam, S.T. 1970. Can. J. Phys. 48, 2320.

Mattauch, J.M.E., Thiele, W., and Wapstra, A.H. 1965. Nucl. Phys. 67, 1.

Meyers, P. and Schats, J.J.C. 1966. Physica 32, 179.

Morozov, A.M., and Yampolskii, P.A. 1959. Soviet Physics JETP 9, 671.

Perey, C.M., and Perey, F.G. 1963. Phys. Rev. 132, 755.

Perey, C.M., Perey, F.G., Dickens, J.K., and Silva, R.J. 1968. Phys. Rev. 175, 1460.

Poletti, A.R., Warburton, E.K., and Olness, J.W. 1967. Phys. Rev. 164, 1479.

Rester, D.H., Durham, F.E. and Class, C.M. 1966, Nucl. Phys. 80, 1.

Robertson, R.G.H. 1971. Ph.D. Thesis, McMaster University.

Robertson, R.G.H., and Summers-Gill, R.G. 1971 Can. J. Phys. 49, 1186.

Rose, H.J. and Brink, D.M., 1967. Rev. Mod. Phys. 39, 306.

Satchler, G.R. 1964. Nucl. Phys. 55, 1.

Satchler, G.R. 1965. In "Lectures in Theoretical Physics", Vol. VIII C, ed. Kunz, P.D., Lind, D.A. and Brittin, W.T. University of Colorado Press, Boulder (published 1966), p. 73.

Sheldon, E., Mathur, S., and Donati, D. 1971. Comp. Phys. Comm. 2, 272.

Smith, P.B. 1962. Nuclear Reactions, Vol. II, Chap. V. North Holland.

Smith, W.R. 1965. ORNL publication TM-1117.

Soper, H.M. 1969. Isospin in Nuclear Physics. P.H. Wilkinson ed. North Holland Publishing Co.

Spencer, J. and Enge, H.A. 1967. Nucl. Inst. Meth. 49, 181.

Stecher-Rasmussen, F., Kopecky, J., Abrahams, K., and Ratynski, W. 1972. Nucl. Phys. A181, 250.

Talmi, I. 1962. Rev. Mod. Phys. 34, 704.

Tanaka, S., Stelson, P.H., Bass, W.T., and Lin, J. 1970. Phys. Rev. C. 2, 160.

Vervier, J. 1966. Nucl. Phys. 78, 497.

Vervier, J. and Bolotin, H.H. 1971. Phys. Rev. C, 3, 1570.

von Ehrenstein, D. and Schiffer, J.P. 1967. Phys. Rev. 164, 1374.

Watson, C., Moore, C.F. and Sheline, R.K. 1963. Nucl. Phys. 54, 519.

Wildenthal, B.H., McGrory, J.B., Halbert, E.C., and Graber, H.D. 1971. Michigan State University Internal Report MSUCL-30.

Williams, G.N., and McPherson, D. 1968. CRNL report PR-P-76.

Wilmore, D., and Hodgson, P.E. 1964. Nucl. Phys. 55, 673.